Quantum-Mechanical Reaction Dynamics: Method Development and Applications

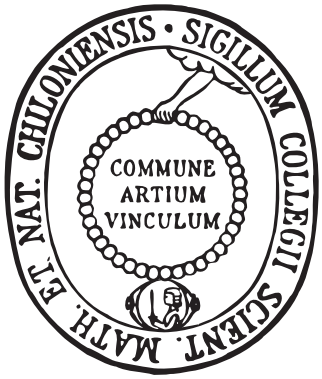

Dissertation

in fulfillment of the requirements
for the degree

Dr. rer. nat.

of the Faculty of Mathematics and Natural Sciences
at Kiel University

submitted by

Jan Sielk

Kiel, July 2010

First referee:	Prof. Dr. B. Hartke
Second referee:	Prof. Dr. F. Temps
Date of the oral examination:	October 21, 2010
Approved for publication:	October 21, 2010
Signed:	Prof. Dr. L. Kipp, Dean

Abstract

In many chemical situations the description of moving nuclei as classically treated particles is sufficient. However, this approximation does not allow for the description of quantum effects such as tunneling, zero point energy or the interference of different reaction paths. In such systems a quantum-mechanical treatment of the nuclei is indispensable. In this work the program suite MrPropa has been used and extended in order to solve the time-dependent nuclear Schrödinger equation.

Traditional grid approaches to exact quantum dynamics suffer from their exponential scaling with dimensionality of the system, which limits the exact treatment to not more than six degrees of freedom. One approach reducing the computational costs for the representation of the wavefunction has been extended to general use within this work. The adaptive basis representation proDG stores the wavefunction only at points where it has a non-negligible contribution. Combined with novel basis functions huge amounts of savings compared to a traditional finite basis representation are demonstrated in two- and three-dimensional calculations.

Potential energy surfaces (PES), on which the nuclei are moving, are a mandatory input for all quantum-dynamical calculations. Their evaluation is time-consuming and, therefore, intelligent algorithms are required in order to reduce the number of quantum-chemical program runs. To achieve this a many-mode expansion of the potential energy surfaces has been linked to the quantum-dynamical propagation program MrPropa. The high-level *ab initio* calculations have been fitted analytically, which offers a fast, yet accurate, way of evaluating PESs. Test calculations of the tunneling splittings of hydrogen-peroxide, its isotopologues and of other systems are provided. The choice of the right coordinate system is always a tedious task when large amplitude motions are considered. Thorough tests revealed internal Z-matrix coordinates to be adequate for these systems.

Two photochemical switching processes have been studied in this thesis: the photochemical ring-opening reaction of cyclohexadiene and the $(E) \rightarrow (Z)$ isomerization of a bridged azobenzene derivative. Quantum-dynamical wavepacket propagations on the relaxed surface of the excited 2A state reproduced experimental finding of retention times on this surface of cyclohexadiene very well. To simulate the wavepacket disappearing through a conical intersection (CI) a new method has been employed. The CI-seam has been modeled by an imaginary potential, which reduces the population on the upper PES in a similar manner. First results of simulating transient absorption spectra of the azobenzene derivative from wavepacket dynamics on quasi-diabatic PESs show encouraging results for further development in this area and demonstrate the validity of the employed methods.

Kurzfassung

Bei der Berechnung chemischer Reaktionsdynamik können die Atomkerne häufig als klassisch-mechanisch zu behandelnde Teilchen beschrieben werden. Mit dieser Näherung ist es allerdings nicht möglich, Quanteneffekte wie Tunneln, Nullpunktsenergie oder die Interferenz z. B. verschiedener Reaktionspfade zu beschreiben. In solchen Situationen ist eine quantenmechanische Beschreibung der Kerne unumgänglich. In dieser Arbeit wurde zur Berechnung der zeitabhängigen Schrödingergleichung das Programm MrPropa verwendet und erweitert.

Traditionelle Gitterdarstellungen der Wellenfunktion skalieren exponentiell mit der Anzahl der Freiheitsgrade, wodurch die exakte Beschreibung auf nicht mehr als sechs Freiheitsgrade begrenzt ist. In dieser Arbeit wurde eine modifizierte Darstellung der Wellenfunktion weiterentwickelt. In der adaptiven Basisdarstellung proDG wird die Wellenfunktion nur an Punkten gespeichert, an denen sie einen signifikant von Null verschiedenen Beitrag hat. In Kombination mit neuartige Basisfunktionen konnten in zwei- und dreidimensionalen Rechnungen große Einsparungen gegenüber der traditionellen *Finite Basis Representation* erzielt werden.

Potentialenergieflächen (PES), auf denen sich die Atomkerne bewegen, sind notwendige Voraussetzungen für alle quantendynamische Rechnungen. Da ihre Ermittlung sehr zeitaufwendig ist, werden intelligente Algorithmen benötigt, die eine Reduzierung der Anzahl quantenchemischer Rechnungen ermöglichen. Zu diesem Zweck wurde in dieser Arbeit eine Mehrkörperentwicklung der PES an das Programm MrPropa gekoppelt. Ein analytischer Fit an hochgenaue *ab-initio*-Rechnungen ermöglicht eine schnelle, aber trotzdem präzise, Ermittlung der potentiellen Energie. Die Bestimmung der Tunnelaufspaltungen in Wasserstoffperoxid, seinen Isotopologen und anderen Systemen dienen hierbei als Testrechnungen. Erstrecken sich Kernbewegungen über einen großen Bereich, ist die Wahl geeigneter Koordinatensysteme für quantendynamische Rechnungen schwierig. Für die hier betrachteten Systeme legten intensive Tests die Benutzung interner Z-Matrix-Koordinaten nahe.

Zwei photochemische Reaktionen wurden in dieser Arbeit untersucht: die photochemische Ringöffnungsreaktion von Cyclohexadien und die *(E)→(Z)*-Isomerisierung in einem verbrückten Azobenzolderivat. Mit Hilfe quantenmechanischer Wellepaketpropagationen auf der relaxierten elektronisch angeregten 2A-PES konnten die experimentell bestimmten Verweilzeiten auf dieser Fläche sehr gut reproduziert werden. Das Verschwinden des Wellenpaketes von der oberen Potentialfläche durch die konische Durchschneidung wird hierbei von einem imaginären Potential simuliert, das die Population auf ähnliche Weise reduziert wie eine explizit berechnete konische Durchschneidung. Erste Simulationen transienter Absorptionsspektren des überbrückten Azobenzolderivates auf der Basis von Wellenpaketpropagationen auf quasi-diabatischen Flächen stellen ermutigende Ergebnisse für zukünftige Anwendungen dar und legen die Gültigkeit der verwendeten Methoden nahe.

Contents

1 Introduction

A new era of physics has been started in the late 19th century when the classical laws of physics failed to describe a number of experiments on the atomic and subatomic scale. At its start Max Planck proposed the quantum hypothesis which claims that energy is only radiated and absorbed in discrete quantities. Albert Einstein explained the emision of electrons upon irradiation of matter with light, the photoelectric effect, by describing light as composed of discrete quanta, rather than in the traditional continuous wave picture. On the other hand, electrons, or more precisely all matter, can also be described by a "matter wave", as found by Louis-Victor de Broglie in 1924. The concept of the wave-particle duality was born.

The central equation of the wavefunction-based description of quantum mechanics is the (molecular) Schrödinger equation. In its general form it describes how a quantum state evolves with time. Chemical processes involve both nuclear and electronic motions. Within the concept of the Born-Oppenheimer (BO) separation these two motions are treated independently as it is assumed that the eletrons respond instantaneously to changes in the nuclear coordinates. Because of the BO-separation different kinds of theory may be applied to treat electronic and nuclear motions.

The first, often referred to as quantum chemistry, is governed by the electronic Schrödinger equation and is commonly used to describe the energy levels of atoms and molecules. This results in potential energy surfaces (PES) on which the motion of the nuclei is described by the nuclear Schrödinger equation. On this basis processes such as vibrational or rotational spectra, rate constants or photochemical reactions can be described. If the electronic states come close to each other the BO-approximation breaks down due to coupled nuclear and electronic motion. That is, even small changes in nuclear motions cause a change in the electronic states, which in return influence the overall nuclear motion. These situations are called non-BO processes and are of great importance for photochemical reactions, which will be described later. Many chemical reactions can be described accurately enough by classical motion of the nuclei (classical molecular dynamics). However, with this approximation the descriptions of quantum effects, such as tunneling, zero-

point energy, interference (e. g. of different reaction channels) or the inherent inclusion of several PESs is not possible and either further approximative models or the quantum-mechanical treatment of the nuclear motions become indispensable.

In principle, the description of a system within the time-dependent and the time-independent picture is equivalent. However, certain preferences of one or the other have been developed depending on the problem under consideration. In quantum chemistry usually stationary electronic states are calculated in the time-independent picture, to describe chemical reactions or other nuclear movements, however, the time-dependent treatment is more intuitive. Especially in photochemical events that involve dissociative potentials the time-dependent view is much more natural because reactions are usually imagined as dynamic processes.

Quantum chemistry has been a very broad and popular area of research for many decades. A large variety of approximative solutions for the electronic Schrödinger equation have been proposed and implemented in easy-to-use computer programs. In 1998, the Nobel prize was awarded to John Pople for the quantum-chemical program GAUSSIAN, highlighting the need for development of methods and programs in theoretical chemistry that can also be used by non-specialists.

On the one hand, for the calculation of classical nuclear motion numerous molecular dynamics (MD) programs are available and widely used, especially for larger molecular systems such as proteins and enzymes. On the other hand, the developement of universal computer programs for solving the nuclear Schrödinger equation lags far behind. Most research groups employ their own codes, which are ususally set up system specifically and require major re-programming if the system under consideration is changed. The most prominent example for a program that is universal at least to some extend is MCTDH. However, the preparation of the calculation is not easy and requiring larger amounts of prior knowledge from the user.

One of the main problems in traditional quantum dynamics is the so-called *curse of dimensionality*. The nuclear wavefunction of a system is described in a basis representation on a complete direct-product grid. The amount of required grid points (and hence the computer memory) scales exponentially with dimensionality of the system, which limits the exact quantum-dynamical treatment to not more than six degrees of freedom. Reducing the memory requirements of the wavefunction representation has been a major task in research for the last years, but no fully satisfying breakthroughs have been made yet. Another challange is closely related to the problems of the representation of the wavefunction caused by the curse of dimensionality. At every grid point the potential energy has to be known, which is determined by quantum-chemical programs. As the numerical effort is tremendously large for high-level calculations there is the need for intelligent interpolation schemes, which reduce the number of required computations.

Another central aspect of quantum dynamics is the choice of appropriate coordinate systems. As easy-to-use cartesian coordinates suffer from using six degress of

freedom too many, namely for rotation and translation, (molecule-) internal coordinate systems are advantageous. However, the use of such curvilinear coordinates entails a severe complication of the Hamiltonian of the system. Nauts and Lauvergnat have solved this problem in a program called TNUM by calculating the kinetic energy operator numerically but exactly for almost all molecular structures.

To overcome the problem of system specific computer programs Frank von Horsten developed a universal, easy-to-use quantum-dynamical computer program, named MRPROPA. This program allows for the input of the molecular structure in internal, e. g. Z-matrix, coordinates, which are widely used in quantum chemistry. An interface to the TNUM-code eliminates the need to setup a complicated Hamiltonian. Different reduced-dimensional models can be employed. With their help it is possible to select certain degrees of freedem to be treated in a quantum-dynamical way explicitly while other degrees of freedom are not included in the explicit dynamics. This approach is justified in many cases as the movement in molecules during reactions can often be reduced to few internal degrees of freedom. So MRPROPA offers a quantum-dynamical treatment of molecular systems without reprogramming major parts of the code and without larger amounts of prior knowledge.

This work includes both method development and applications in quantum-dynamics. The developed methods are implemented in the framework of the MRPROPA-program, which was developed in a previous PhD thesis by Frank von Horsten in this group. The focus of the program extensions is set to preserving the universal and easy-to-use complexion of the program. The remainder of this thesis is organized as follows. Chapter 2 gives a brief introduction to the theoretical principles of quantum dynamics implied in this thesis. At the end of that chapter the objectives of the thesis are given. Chapter 3 presents the extension of a novel method, proposed earlier in this group. The adaptive basis representation has been extended to higher dimensionality and combined with a novel type of basis functions. In chapter 4 the interface to an analytical fit of high-level *ab initio* calculations is demonstrated, which facilitates a fast and efficient, yet accurate evaluation of the potential energy. Finally, chapter 5 deals with two different kind of molecular switches. The ring-opening reaction of cyclohexadiene and the photochemical inversion of a bridged azobenzene derivative are investigated with quantum-dynamical methods. Chapter 6 sums up the results of this thesis and gives an outlook for future work.

2

Theoretical Background

In wavepacket dynamics the motion of nuclei is described in the framework of the nonrelativistic time-dependent Schrödinger equation. Using the Born-Oppenheimer separation and approximation, which will be explained in section 2.1, the theoretical background of wavepacket dynamics is divided into two parts. First, the electronic time-independent Schrödinger equation has to be solved in order to set up the time-dependent nuclear Schrödinger equation. The first is often referred to as quantum chemistry, in which the nuclei are held at fixed positions and the electronic energy of the system is evaluated. However, this chapter will focus on introducing theory of the nuclear problem, as the solution of the electronic Schrödinger equation is thoroughly described in quantum chemistry textbooks (such as Refs. [1–3]) and in this work only well-established standard methods are used.

After solving the electronic problem the focus can be set on the nuclear time-dependent Schrödinger equation. In order to solve it a suitable numerical representation has to be achieved. In section 2.2 the most popular representations of nuclear wavepackets will be presented, followed by section 2.3 in which the most famous methods for their time propagation will be introduced. The theoretical considerations will continue with a general description of the kinetic energy operator in curvilinear coordinates in section 2.6, as the kinetic energy operator in its simplest form is only valid for cartesian coordinates, which, in general, are not suitable for time propagation of larger molecular systems. Three reduced-dimensional models are introduced in section 2.7, which allow for the quantum-dynamical treatment of larger molecules. The chapter will end with a short synopsis of current research related to this work (section 2.9) and the objectives of the thesis (section 2.10).

Note, that this chapter cannot cover theory comprehensively. It is merely meant to give an overview of the used concepts and methods and was created with the help of several different books, reviews and other articles [4–9]. For further reading the previously mentioned texts are advisable. Only few textbooks are covering quantum mechanics from the *time-dependent* view. Namely Tannor's *Introduction to Quantum Mechanics—A time-dependent perspective* [8], is strongly recommended.

2.1 Born-Oppenheimer Separation and Approximation

The molecular *Time-Dependent Schrödinger Equation* (TDSE) is

$$i\hbar\frac{\partial}{\partial t}\Psi(\mathbf{R},\mathbf{r},t) = \hat{H}^{\mathrm{mol}}\Psi(\mathbf{R},\mathbf{r},t) \tag{2.1}$$

with the molecular (time-independent) Hamiltonian $\hat{H}^{\mathrm{mol}}$. Here, $\mathbf{R}$ denotes the coordinates of the nuclei, $\mathbf{r}$ the coordinates of all electrons and t the time. Assuming that the temporal evolution can be seperated from coordinates (separation ansatz) the solution of the molecular TDSE can be written in the form

$$\Psi(\mathbf{R},\mathbf{r},t) = \tilde{\Psi}(\mathbf{R},\mathbf{r})\chi(t). \tag{2.2}$$

Substitution of Eq. (2.2) in Eq. (2.1) and separation of variables yields

$$i\hbar\frac{\frac{\partial}{\partial t}\chi(t)}{\chi(t)} = \frac{\hat{H}^{\mathrm{mol}}\tilde{\Psi}(\mathbf{R})}{\tilde{\Psi}(\mathbf{R})}. \tag{2.3}$$

As both sides contain derivatives with respect to different variables only constant functions lead to equality. Either substituting the left or the right side by E_k for energy results in two different equations

$$i\hbar\frac{\partial}{\partial t}\chi(t) = E_k\chi(t) \tag{2.4}$$

$$\hat{H}^{\mathrm{mol}}\tilde{\Psi}^{(k)}(\mathbf{R},\mathbf{r}) = E_k\tilde{\Psi}^{(k)}(\mathbf{R},\mathbf{r}). \tag{2.5}$$

Eq. (2.5) is an eigenvalue equation, which yields to a set of various solutions, namely the corresponding eigenfunctions $\tilde{\Psi}^{(k)}$ and eigenenergies E_k, where k denotes the quantum state of the stationary state. The solution of the differential Eq. (2.4) is

$$\chi(t) = \chi_0 e^{-iE_k t/\hbar}. \tag{2.6}$$

Substituting Eq. (2.6) in Eq. (2.2) yields the solution of the molecular TDSE for the kth eigenstate

$$\Psi(\mathbf{R},\mathbf{r},t) = \tilde{\Psi}^{(k)}(\mathbf{R},\mathbf{r})\chi_0 e^{-iE_k t/\hbar} \tag{2.7}$$

where the constant factor χ_0 may be absorbed into $\tilde{\Psi}^{(k)}$. It should be stressed again that this is just a special, particular solution. The general solution is rather a linear combination of *all* eigenstates

$$\Psi(\mathbf{R},\mathbf{r},t) = \sum_k c_k e^{-iE_k t/\hbar}\tilde{\Psi}^{(k)}(\mathbf{R},\mathbf{r}) = \sum_k a_k(t)\tilde{\Psi}^{(k)}(\mathbf{R},\mathbf{r}), \tag{2.8}$$

which has explicitly time-dependent coefficients $a_k(t)$. This shows the equivalence of the time-dependent and time-independent picture. If all time-independent eigenstates $\tilde{\Psi}^{(k)}(\mathbf{R},\mathbf{r})$ and eigenenergies E_k are known, the complete temporal evolution of the system can be constructed from Eq. (2.8), arbitrarily far forward and backward in time.

The full molecular Hamiltonian in Eq. (2.1) consists of the following terms:

$$\hat{H}^{\mathrm{mol}} = \hat{T}_{\mathrm{n}}(\mathbf{R}) + \hat{T}_{\mathrm{e}}(\mathbf{r}) - \hat{V}_{\mathrm{ne}}(\mathbf{r},\mathbf{R}) + \hat{V}_{\mathrm{ee}}(\mathbf{r}) + \hat{V}_{\mathrm{nn}}(\mathbf{R}). \tag{2.9}$$

In a molecular system containing N nuclei with masses M_i and charges Z_i and I electrons this includes the kinetic energy of the nuclei and electrons

$$\hat{T}_{\mathrm{n}}(\mathbf{R}) = \sum_{n=1}^{N} -\frac{\hbar^2}{2M_n}\nabla_n^2 \tag{2.10}$$

resp.

$$\hat{T}_{\mathrm{e}}(\mathbf{r}) = \sum_{i=1}^{I} -\frac{\hbar^2}{2m_e}\nabla_i^2, \tag{2.11}$$

the Coulomb interaction of electrons and nuclei

$$\hat{V}_{\mathrm{ne}}(\mathbf{r},\mathbf{R}) = \frac{e^2}{4\pi\varepsilon_0}\sum_{n=1}^{N}\sum_{i=1}^{I}\frac{Z_n}{|r_i - R_n|}, \tag{2.12}$$

as well as the nucleus-nucleus and electron-electron repulsions

$$\hat{V}_{\mathrm{nn}}(\mathbf{R}) = \frac{e^2}{4\pi\varepsilon_0}\sum_{n=1}^{N}\sum_{m>n}^{N}\frac{Z_n Z_m}{|R_n - R_m|} \qquad \text{resp.} \qquad \hat{V}_{\mathrm{ee}}(\mathbf{r}) = \frac{e^2}{4\pi\varepsilon_0}\sum_{i=1}^{I}\sum_{j>i}^{I}\frac{1}{|r_i - r_j|}. \tag{2.13}$$

2.1.1 Adiabatic Separation

In order to find an approximate solution of the molecular *Time-Independent Schrödinger equation* (TISE) Eq. (2.5) a similar ansatz to the one yielding the separation of time in Eq. (2.8) is assumed. In order to separate the nuclear from the electronic coordinates the molecular stationary wavefunction $\Psi^{(k)}$ can be written in a so-called *adiabatic basis* in the framework of the Born-Oppenheimer separation

$$\tilde{\Psi}^{(k)}(\mathbf{r},\mathbf{R}) = \sum_{n=1}^{\infty}\varphi^{(n)}(\mathbf{r};\mathbf{R})\tilde{\psi}^{(n,k)}(\mathbf{R}), \tag{2.14}$$

in which $\varphi^{(n)}(\mathbf{r};\mathbf{R})$ depends on the nuclear coordinates only parametrically. This leads to an electronic TISE at fixed nuclear coordinates

$$\hat{H}^{\mathrm{el}}(\mathbf{r};\mathbf{R})\varphi^{(n)}(\mathbf{r};\mathbf{R}) = V_n^{(a)}(\mathbf{R})\varphi^{(n)}(\mathbf{r};\mathbf{R}) \tag{2.15}$$

with the (adiabatic) eigenenergies $V_n^{(a)}$ that depend only parametrically on the nuclear coordinates and with an electronic Hamiltonian $\hat{H}^{\mathrm{el}}$, which reduces to

$$\hat{H}^{\mathrm{el}} = \hat{T}_{\mathrm{e}}(\mathbf{r}) + \hat{V}_{\mathrm{ee}}(\mathbf{r}) - \hat{V}_{\mathrm{ne}}(\mathbf{r};\mathbf{R}). \tag{2.16}$$

The reason for the missing two terms is that the nuclei are held at fixed positions and therefore $\hat{V}_{\mathrm{nn}}(\mathbf{R})$ becomes a constant. Furthermore, the last part of the molecular Hamiltonian $\hat{T}_{\mathrm{n}}(\mathbf{R})$ only acts on the nuclear wavefunction $\psi^{(n,k)}(\mathbf{R})$. So the full molecular Hamiltonian can be written as

$$\hat{H}^{\mathrm{mol}} = \hat{T}_{\mathrm{n}}(\mathbf{R}) + \hat{H}^{\mathrm{el}}. \tag{2.17}$$

The resulting eigenenergies of the electronic Schrödinger equation (Eq. (2.15)) $V_n^{(a)}$ will be referred to as adiabatic PESs, which are obtained by electronic structure theory calculations.

Using Eq. (2.15), substituting Eq. (2.14) in Eq. (2.5) and projecting from the left with $\langle\varphi^{(m)}|$ leads to a set of coupled equations (for clarity the explicit notation of the dependence on $\mathbf{r}$ and $\mathbf{R}$ is omitted):

$$\left(\hat{T}_N + V_m^{(a)}\right)\tilde{\psi}^{(m,k)} + \sum_{n=1}^{\infty}\left(2\hat{T}'_{mn} + \hat{T}''_{mn}\right)\tilde{\psi}^{(n,k)} = E_k\tilde{\psi}^{(m,k)} \tag{2.18}$$

with the so-called *non-adiabatic coupling elements*

$$T'_{mn} = \sum_i^N -\frac{\hbar^2}{2M_i}\langle\varphi^{(m)}|\nabla_i|\varphi^{(n)}\rangle\cdot\nabla_i = \sum_i^N -\frac{\hbar^2}{2M_i}F_{mn}\cdot\nabla_i, \tag{2.19}$$

$$T''_{mn} = \sum_i^N -\frac{\hbar^2}{2M_i}\langle\varphi^{(m)}|\nabla_i^2|\varphi^{(n)}\rangle. \tag{2.20}$$

The physical interpretation of Eq. (2.18) is that the movement of the nuclei on one electronic surface $V_m^{(a)}$, which is described by the nuclear wavefunction $\tilde{\psi}^{(m,k)}$, is coupled to *all* other electronic surfaces in an infinite set of coupled Schrödinger equations. Practically, the number of coupled equations is limited to a finite number of electronic states as in numerical applications infinite sums like the one in Eq. (2.18) cannot be evaluated. Assuming that couplings are never exactly zero this is already an approximation and numerical implementations can never be completely exact. If the coupling terms are actually large and involve many different PESs it would be advantageous to explicitly treat the electrons dynamically and omit the Born-

Oppenheimer separation. This is technically difficult to achieve, however recent developements have been made (see e. g. Ref. [10] and references therein).

The non-adiabatic coupling terms include derivatives of the electronic wavefunctions with respect to their nuclear coordinates. T'_{mn} typically is more important than T''_{mn} as it contains the first derivatives but usually they are both small compared to the first term in Eq. (2.18). The complete neglect of the non-adiabatic coupling terms is known as the Born-Oppenheimer approximation [11], which leads to nuclear Schrödinger equations of the type

$$(\hat{T}_N + V_m^{(a)})\tilde{\psi}^{(m,k)} = \hat{H}\tilde{\psi}^{(m,k)} = E_k\tilde{\psi}^{(m,k)}, \tag{2.21}$$

which describe the nuclei on isolated, uncoupled electronic PESs $V_m^{(a)}$.

The same ansatz is applicable to the time-dependent Schrödinger equation, which leads to an uncoupled set of equations of the form:

$$i\hbar\frac{\partial}{\partial t}\psi_m^{(a)} = \hat{H}\psi_m^{(a)} = \left(\hat{T}_N + V_m^{(a)}\right)\psi_m^{(a)}, \tag{2.22}$$

which include time-dependent nuclear wavepackets $\psi_m^{(a)} = \psi_m^{(a)}(\mathbf{R}, t)$ for every adiabatic potential energy surface $V_m^{(a)}$.

The next paragraph will answer the question what is happening when two adiabatic PESs come close to each other. Suppose that all but two of the solutions of the electronic Schrödinger equation are known and ϕ_1 and ϕ_2 are two functions which, together with the found solutions, constitute a complete orthonormal set. Then, the two remaining electronic eigenfunctions, whose intersection is of interest here, can be expressed in the form

$$\psi_{1,2} = c_1\phi_1 \pm c_2\phi_2. \tag{2.23}$$

The corresponding two-level Hamiltonian is

$$\hat{H} = \begin{pmatrix} H_{11} & H_{12} \\ H_{21} & H_{22} \end{pmatrix} \tag{2.24}$$

with its elements $H_{ij} = \langle\phi_i|\hat{H}|\phi_j\rangle$ and the corresponding eigenvalues being the electronic energies of interest. They are given by

$$E_{1,2} = \frac{H_{11} + H_{22}}{2} \pm \sqrt{\left(\frac{H_{11} - H_{22}}{2}\right)^2 + H_{21}H_{12}}. \tag{2.25}$$

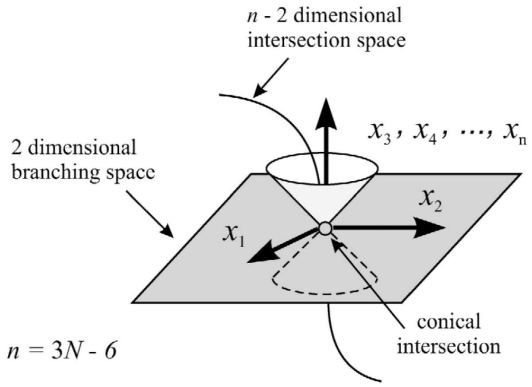

Figure 2.1: Eigenenergies in the branching space.

Figure from [12].

In order to get degenerate solutions, where the two states ψ_1 and ψ_2 are crossing the radicant must vanish. It is necessary to satisfy the two independent conditions

$$H_{11} = H_{22} \tag{2.26}$$

$$H_{12} = H_{21} = 0, \tag{2.27}$$

which requires at least two independently variable nuclear coordinates. So for diatomic molecules that only have one interatomic coordinate the conditions cannot be satisfied and hence the states can not cross[1]. This is often referred to as the non-crossing rule which leads to *avoided crossings*. In polyatomic systems the conditions might be satisfied in a $N-2$-dimensional subspace, which is called the *conical intersection* (CI) seam. So CIs are not isolated points but rather infinite number of points forming a seam. The two-dimensional space orthogonal to the seam where the degeneracy is lifted is called *branching space*. The term conical intersection referes the picture that arises when the energies of the two intersecting states are plotted against the two branching space coordinates (see Fig. 2.1). It shows a double cone with the vertex located at the branching space origin.

The ordering of the adiabatic states is strictly determined by their energies. As a consequence in regions near avoided crossings or conical intersections, where the adiabatic PESs come close to each other, the electronic wavefunctions change their character drastically, and hence the non-adiabatic coupling terms can become quite significant. In such cases the Born-Oppenheimer approximation breaks down and the couplings must be included in the calculation. The phyical interpreation is that even small nuclear motions cause a change in the electronic states, which in return

[1] Strictly, this is only true if the electronic states have the same symmetry. For states with different symmetry the secondary diagonal elements of the Hamiltonian vanish due to symmetry reasons and only one condition is remaining. Hence, two states of different symmetry may cross also for diatomic systems.

effects the overall nuclear motion. The fact that the first derivative matrix elements of the non-adiabatic coupling matrix (F_{mn} in Eq. (2.19)) can also be expressed as [13]

$$F_{mn} = \frac{\langle \varphi^{(m)} | \nabla \hat{H}^{\mathrm{el}}(\mathbf{r}, \mathbf{R}) | \varphi^{(n)} \rangle}{V_m(\mathbf{R}) - V_n(\mathbf{R})}, \tag{2.28}$$

reveals that the non-adiabatic matrix elements diverge at points where the adiabatic PESs come close to each other. Hence, the choice of a different basis than the adiabatic basis may be advantageous. The concept of the *diabatic representation* will briefly be discussed in the next section.

2.1.2 Diabatic Representation

As the adiabatic basis is not always advantageous for numerical applications, an electronic basis which changes smoothly across the region of the avoided crossing is more desirable. From Eq. (2.14) it can be deduced that a change of the electronic basis $\{\varphi^{(n)}\}$ entails also a change of the nuclear wavefunctions $\tilde{\psi}^{(n)}$, which are mathematically just the expansion coefficients. In the so-called *diabatic basis* the diabatic nucluear wavefunctions $\psi^{(d)}$ are constructed such that the electronic coupling matrices $\mathbf{T}'/\mathbf{T}''$ (Eqs. (2.19) and (2.20)) (at least approximately) vanish. The couplings are moved to the off-diagonal elements of the potential energy matrix. This is called *potential coupling* as opposed to *kinetic coupling* in the adiabatic representation, where the couplings occur in the off-diagonal elements of the matrix representation of the kinetic energy operator. With this strategy it is ensured that the diabatic states do not change their electronic character abruptly but stay smooth throughout the nuclear coordinate space. As a direct consequence diabatic states are allowed to cross each other in contrast to the strictly energy ordered adiabatic states.

The adiabatic nuclear wavefunction $\psi^{(a)} = (\psi_1^{(a)}, \ldots, \psi_i^{(a)})^T$ can formally be transformed to a diabatic basis by a unitary transformation

$$\psi^{(d)} = \mathbf{U}^{\dagger} \psi^{(a)}, \tag{2.29}$$

which can also be regarded as an expansion of $\psi^{(d)}$ in the basis of the $\psi_j^{(a)}$. The same transformation can be applied to the adiabatic potential energy surfaces in order to construct diabatic ones:

$$\mathbf{V}^{(d)} = \mathbf{U}^{\dagger} \mathbf{V}^{(a)} \mathbf{U}. \tag{2.30}$$

In case of a two-level system $\mathbf{U}$ is defined as

$$\mathbf{U} = \begin{pmatrix} \cos\theta & -\sin\theta \\ \sin\theta & \cos\theta \end{pmatrix}, \tag{2.31}$$

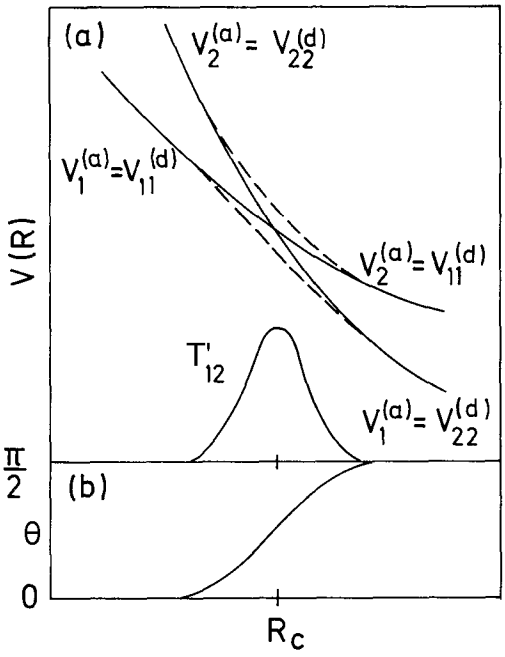

Figure 2.2: (a) Adiabatic potentials, $V_1^{(a)}$ and $V_2^{(a)}$ (dashed curves), and the diagonal elements of the diabatic potential matrix, $V_{11}^{(d)}$ and $V_{22}^{(d)}$ (solid curves). T'_{12} shows schematically how the non-adiabatic couplings change with the coordinate $\mathbf{R}$. (b) Variation of the mixing angle θ in the region of the abvoided crossing.

Drawing taken and adjusted from Ref. [4].

with $\theta(\mathbf{R}, \mathbf{r})$ being the coordinate dependent *mixing angle*. As displayed in Fig. 2.2 it may change between 0 and $\pi/2$ in such manner that at regions far away from the crossing the diabatic potentials match the adiabatic ones and the coupling is exaclty zero. The diabatic potentials obviously are no longer eigenenergies of the electronic Schrödinger equation (Eq. (2.15)) and hence may cross.

For real electronic wavefunctions the diagonal elements of the first derivative matrix elements of the non-adiabatic coupling matrix (F_{mn} in Eq. (2.19)) vanish, while the off-diagonal elements are of the same value but with reversed signs [13,14]. With this the transformed off-diagonal element $F_{12}^{(d)}$ can be derived to be

$$F_{12}^{(d)} = \nabla\theta(\mathbf{R}) + F_{12}. \tag{2.32}$$

The requirement that enforces the off-diagonal coupling elements to vanish in the transformed basis

$$F_{12}^{(d)} = 0 \tag{2.33}$$

leads to a first-order differential equation for the adiabatic to diabatic mixing angle

$$\nabla\theta(\mathbf{R}) = -F_{12} = \langle\varphi^{(2)}|\nabla|\varphi^{(1)}\rangle. \tag{2.34}$$

In general, this could be used to determine the mixing angle from the derivative matrix elements F_{12} in Eq. (2.19), if those are calculated, e. g. by an *ab initio* calculation. However, this can only be carried out easily for one-dimensional, i. e. diatomic, systems. For multi-dimensional systems the so-called *curl-condition*

$$\nabla \times F_{12} \equiv \text{curl } F_{12} = 0 \tag{2.35}$$

applies. It can only be satisfied when the whole space of interacting electronic states is considered in the transformation matrix $\mathbf{U}$, which is contradictory to the spirit of the diabatic basis. Thus, except for adiabatic states in diatomic molecules (with the same symmetry) there is no strictly diabatic basis for which all components of the nuclear momentum coupling vanishes [15]. For larger molecules the non-adiabatic couplings can only partially be transformed away. As a consequence many different transformation schemes are known and thoroughly reviewed in the literature (see e. g. Refs. [13, 14, 16] and references therein). One of these approximate schemes—regularized quasi-diabatic states by Köppel and coworkers [17–19]—will be explained in more detail and applied in chapter 5.

2.1.3 Several Potential Energy Surfaces

In case more electronic surfaces are involved the dynamics can be extended straightforwardly. For two coupled states the adiabatic time-dependent Schrödinger equations for nuclear wavepackets $\psi(\mathbf{R}, t)$ are:

$$i\hbar\frac{\partial}{\partial t}\psi_1^{(a)} = \left(\hat{T}_N + V_1^{(a)}\right)\ \psi_1^{(a)} + \sum_{n=1}^{2}\left[2\hat{T}'_{1n} + \hat{T}''_{1n}\right]\psi_n^{(a)}, \tag{2.36}$$

$$i\hbar\frac{\partial}{\partial t}\psi_2^{(a)} = \left(\hat{T}_N + V_2^{(a)}\right)\ \psi_2^{(a)} + \sum_{n=1}^{2}\left[2\hat{T}'_{2n} + \hat{T}''_{2n}\right]\psi_n^{(a)}, \tag{2.37}$$

or in matrix-vector form

$$i\hbar\frac{\partial}{\partial t}\begin{pmatrix}\psi_1^{(a)}\\ \psi_2^{(a)}\end{pmatrix} = \left[\begin{pmatrix}\hat{T}_N + 2\hat{T}'_{11} + \hat{T}''_{11} & 2\hat{T}'_{12} + \hat{T}''_{12}\\ 2\hat{T}'_{21} + \hat{T}''_{21} & \hat{T}_N + 2\hat{T}'_{22} + \hat{T}''_{22}\end{pmatrix} + \begin{pmatrix}V_1^{(a)} & 0\\ 0 & V_2^{(a)}\end{pmatrix}\right]\cdot\begin{pmatrix}\psi_1^{(a)}\\ \psi_2^{(a)}\end{pmatrix}. \tag{2.38}$$

As already mentioned the couplings occur in the kinetic part of the Hamiltonian. In the diabatic case the couplings are moved to the potential energy matrix with a diagonal kinetic energy

$$i\hbar\frac{\partial}{\partial t}\psi_1^{(d)} = \left(\hat{T}_N + V_{11}^{(d)}\right)\ \psi_1^{(d)} + V_{12}^{(d)}\psi_2^{(d)}, \tag{2.39}$$

$$i\hbar\frac{\partial}{\partial t}\psi_2^{(d)} = \left(\hat{T}_N + V_{22}^{(d)}\right)\ \psi_2^{(d)} + V_{21}^{(d)}\psi_1^{(d)}, \tag{2.40}$$

or again in matrix-vector form

$$i\hbar\frac{\partial}{\partial t}\begin{pmatrix}\psi_1^{(d)}\\ \psi_2^{(d)}\end{pmatrix} = \left[\begin{pmatrix}\hat{T}_N & 0\\ 0 & \hat{T}_N\end{pmatrix} + \begin{pmatrix}V_{11}^{(d)} & V_{12}^{(d)}\\ V_{21}^{(d)} & V_{22}^{(d)}\end{pmatrix}\right]\cdot\begin{pmatrix}\psi_1^{(d)}\\ \psi_2^{(d)}\end{pmatrix}. \tag{2.41}$$

2.2 Numerical Representation of the Wavefunction and Hamiltonian

With the help of the Born-Oppenheimer separation it is possible to divide the molecular Schrödinger equation in two consecutive problems. First, the electronic Schrödinger Eq. (2.15) is calculated, which only depends on the nuclear coordinates parametrically as their positions are held fixed. With the resulting PESs the nuclear Schrödinger Eq. (2.22) can be solved. As a well-known matter of fact the time-dependent and time-independent views are equivalent [20] but advantageous or disadvantageous depending on what quantities are to be calculated.

Considering the uncoupled time-dependent nuclear Schrödinger equation on just one adiabatic electronic surface

$$i\hbar\frac{\partial}{\partial t}\psi(\mathbf{R},t) = \left(\hat{T}_N + V^{(a)}\right)\psi(\mathbf{R},t) \tag{2.42}$$

two tasks arise. First, the nuclear wavefunction ψ needs to be represented numerically and second, it needs to be propagated in time. The remainder of this section will focus on the numerical representation, the next section will introduce methods for time propagation.

For clarity, the following discussion will be restricted to one-dimensional problems with the spacial coordinate x and x_i being the ith gridpoint in this dimension. Extension to higher dimensionality is (formally) straightforward and will shortly be addressed in section 2.2.5.

2.2.1 Finite Basis Representation

In general, in a so-called *spectral representation*, the nuclear wavefunction $\psi(x)$ is expanded in a set of time-independent non-orthogonal basis functions $\{\phi_i\}$ (for which $\langle\phi_i|\phi_j\rangle \neq \delta_{ij}$)

$$\psi(x) = \sum_{i=1}^{\infty} c_i\phi_i(x), \tag{2.43}$$

with the so-called *contravariant* coefficients c_i. The projection

$$c_j^{\mathrm{co}} = \langle\phi_j|\psi\rangle = \int_{-\infty}^{\infty}\phi_j^*(x)\psi(x)\mathrm{d}x \tag{2.44}$$

yields the *covariant* coefficients c_j^{co}, which are related to the contravariant coefficients via the overlap matrix $\mathbf{S}$ (with its elements $S_{ij} = \langle\phi_i|\phi_j\rangle = \int_{-\infty}^{\infty} \phi_i^*(x)\phi_j(x)\ \mathrm{d}x$)

$$c_j^{\mathrm{co}} = \sum_i S_{ji} c_i. \tag{2.45}$$

In the *Finite Basis Representation* (FBR) the sum in Eq. (2.43) is truncated at the finite value N so the ansatz is feasible for numerical applications. Insertion into the time-dependent Schrödinger Eq. (2.42) yields

$$i\hbar \frac{\partial}{\partial t} \sum_i c_i \phi_i = \sum_i c_i \hat{H} \phi_i. \tag{2.46}$$

Projecting from left with $\langle\phi_j|$ yields a matrix-vector equation for the propagation of the wavepacket

$$i\hbar \mathbf{S} \frac{\partial}{\partial t} \mathbf{c} = \mathbf{H}\mathbf{c}, \tag{2.47}$$

with the elements of the Hamiltonian $\mathbf{H} = \mathbf{T} + \mathbf{V}$

$$H_{ij} = \langle\phi_i|\hat{H}|\phi_j\rangle = T_{ij} + V_{ij}, \tag{2.48}$$

with

$$T_{ij} = \langle\phi_i|\hat{T}|\phi_j\rangle = -\frac{\hbar^2}{2M} \int_{-\infty}^{\infty} \phi_i^*(x) \nabla^2 \phi_j(x)\ \mathrm{d}x, \tag{2.49}$$

$$V_{ij} = \langle\phi_i|\hat{V}|\phi_j\rangle = \int_{-\infty}^{\infty} \phi_i^*(x) V(x) \phi_j(x)\ \mathrm{d}x. \tag{2.50}$$

Obviously, the choice of number and functional form of the basis functions is decisive for the quality of this approach but these parameters vary between different systems, which enforces convergence tests. A broad range of different function types has been employed as basis functions. Popular choices are sine/cosine, distributed Gaussians, different types of polynomials (e. g. Legendre, Chebychev, Hermite) and more recently wavelets [21, 22].

2.2.2 Collocation

Closely related to the FBR method is the collocation method, which was first popularized by Friesner [23] and Yang and Peet [24]. In contrast to traditional FBR the numerical effort is drastically reduced due to the fact that no evaluation of any integrals is required. Instead only pointwise evaluations of the basis functions are necessary. In Ref. [24] Yang and Peet derive that the matrix elements are

Table 2.1: Comparison of the FBR and collocation methods.

	FBR	Collocation
Propagation Scheme	$i\hbar\mathbf{S}\frac{\partial}{\partial t}\mathbf{c} = \mathbf{Hc}$	$i\hbar\mathbf{R}\frac{\partial}{\partial t}\mathbf{c} = \mathbf{Hc}$
T_{ij}	$\langle\varphi_i\vert\hat{T}\vert\varphi_j\rangle$	$\hat{T}\varphi_j(x_i)$
V_{ij}	$\langle\varphi_i\vert\hat{V}\vert\varphi_j\rangle$	$V(x_i)\delta_{ij}$
S_{ij} resp. R_{ij}	$\langle\varphi_i\vert\varphi_j\rangle$	$\varphi_j(x_i)$

$$T_{ij} = \hat{T}\varphi_j(x_i) = -\frac{\hbar^2}{2M}\nabla^2\varphi_j(x_i), \tag{2.51}$$

$$V_{ij} = V(x_i)\delta_{ij} \tag{2.52}$$

and

$$R_{ij} = \varphi_j(x_i). \tag{2.53}$$

T now holds simple pointwise evaluations of the second derivatives of the basis function at the grid points, **V** is just a diagonal matrix with the potential values on its diagonal and **R** is the equivalent to the overlap matrix **S** in FBR but now also just a pointwise evaluation of the basis function on the grid. Table 2.1 summarizes the differences between FBR and the collocation method.

Although the method is not variational and not hermitian by construction it can be used for practical purposes with sufficient accuracy, as the non-hermiticity should only be of minor impact [24]. However, some considerations regarding the use of collocation in combination with the Tnum methodology will be done in section 3.4.1.

In analogy to Eq. (2.47) the TDSE with collocation can be written as

$$i\hbar\mathbf{R}\frac{\partial}{\partial t}\mathbf{c} = \mathbf{Hc}, \tag{2.54}$$

which can be propagated in time with the standard methods explained in section 2.3.

As in a regular FBR there is a possibility for the collocation matrix **R** to vanish upon clever choice of the basis functions. In FBR the overlap matrix **S** is identical to the unity matrix if the basis functions are orthonormal ($\langle\phi_i|\phi_j\rangle = \delta_{ij}$). Since the collocation matrix **R** is just a simple pointwise evaluation of the basis functions on the grid it is sufficient to construct functions with roots on all grid points except the one where they are located. Such a basis was constructed by a cooperation partner from the Schneider group (Univ. Kiel, now TU Berlin) and implemented. The so-called *Interpolating Gaussians* are based on regular Gaussian functions and modified in such way that the **R**-matrix becomes the unity matrix. Also a brief

review of the collocation method, its numerical advantages and the derivation of the basis functions will be given in the publication of chapter 3.

2.2.3 Discrete Variable Representation

The idea of the *Discrete Variable Representation* (DVR) is to modify the spectral representation, so that the evaluation of the integrals is simplified. Its basic concepts were developed already in the 1960s [25, 26] but it was first popularized for use in quantum dynamics in the 1980s by Light *et al.* [27, 28]. As usually no analytical integration of the FBR matrix elements (Eq. (2.48)) is available they are determined with any numerical integration method. If a Gaussian quadrature rule is used to compute the matrix elements, there is an isomorphism between FBR and DVR. For any quantum system, for which a basis set expansion exists and a Gaussian quadrature rule can be used to compute the matrix elements, the DVR is applicable.

By approximating the usual FBR expansion coefficients Eq. (2.44) via discretization on a grid with the Gaussian quadrature rule (with the weights ω_α and quadrature grid points x_α) one obtains (for an orthogonal basis where $c_i = c_i^{\mathrm{co}}$)

$$c_i = \sum_\alpha \omega_\alpha \phi_i^*(x_\alpha)\psi(x_\alpha). \tag{2.55}$$

Inserting this in the FBR ansatz (Eq. (2.43)) yields

$$\psi(x) = \sum_i \sum_\alpha \omega_\alpha \phi_i^*(x_\alpha)\psi(x_\alpha)\phi_i(x) \tag{2.56}$$

$$= \sum_\alpha \psi_\alpha \delta_\alpha(x), \tag{2.57}$$

which again can be regarded as a linear combination of DVR basis functions

$$\delta_\alpha(x) = \sqrt{\omega_\alpha} \sum_i \phi_i^*(x_\alpha)\phi_i(x), \tag{2.58}$$

with its expansion coefficients

$$\psi_\alpha = \sqrt{\omega_\alpha}\psi(x_\alpha). \tag{2.59}$$

They are given by evaluation of the wavefunction ψ on the quadrature grid points x_α. $\delta_\alpha(x)$ is a function which acts on the continuous space variable x and defines a basis in the discrete representation in analogy to Eq. (2.43). With the definition of

$$\mathbf{T}^\dagger_{i\alpha} = \sqrt{\omega_\alpha}\phi_i^*(x_\alpha) \tag{2.60}$$

Eq. (2.58) simplifies to

$$\delta_\alpha(x) = \sum_i \phi_i(x)\mathbf{T}^\dagger_{i\alpha}. \tag{2.61}$$

This shows that the DVR basis functions $\delta_\alpha(x)$ can be obtained by transformation of the (spectral) FBR basis functions $\phi_i(x)$ with the transformation matrix $\mathbf{T}^\dagger_{i\alpha}$. Furthermore, it can be shown that $\mathbf{T}^\dagger_{i\alpha}$ is unitary, which also causes the DVR basis functions $\{\delta_\alpha(x)\}$ to be orthonormal.

The matrix elements of the potential operator can again be obtained with Gaussian quadrature

$$\langle\phi_i|\hat{V}|\phi_j\rangle = \int_{-\infty}^{\infty} \phi_i^*(x)V(x)\phi_j(x)\mathrm{d}x \tag{2.62}$$

$$\approx \sum_\alpha \omega_\alpha \phi_i^*(x_\alpha)V(x_\alpha)\phi_j(x_\alpha). \tag{2.63}$$

Introducing another summation over β in combination with $\delta_{\alpha\beta}$ does not change the value of the matrix element

$$\langle\phi_i|\hat{V}|\phi_j\rangle = \sum_{\alpha\beta} \omega_\alpha \phi_i^*(x_\alpha)V(x_\alpha)\delta_{\alpha\beta}\phi_j(x_\beta), \tag{2.64}$$

but enables the definition of a diagonal potential matrix

$$\mathbf{V}^{\mathrm{DVR}}_{\alpha\beta} = V(x_\alpha)\delta_{\alpha\beta}. \tag{2.65}$$

With this and Eq. (2.60) the potential matrix element can be written as

$$\langle\phi_i|\hat{V}|\phi_j\rangle = \sum_{\alpha\beta} \mathbf{T}^\dagger_{i\alpha}\mathbf{V}^{\mathrm{DVR}}_{\alpha\beta}\mathbf{T}_{\beta j} \tag{2.66}$$

$$= (\mathbf{T}^\dagger\mathbf{V}^{\mathrm{DVR}}\mathbf{T})_{ij} \tag{2.67}$$

The full Hamiltonian in DVR representation then is

$$\mathbf{H}^{\mathrm{DVR}} = \mathbf{T}\mathbf{H}^{\mathrm{FBR}}\mathbf{T}^\dagger \tag{2.68}$$

$$= \mathbf{T}\mathbf{T}^{\mathrm{FBR}}_N\mathbf{T}^\dagger + \mathbf{T}\mathbf{V}^{\mathrm{FBR}}\mathbf{T}^\dagger \tag{2.69}$$

$$= \mathbf{T}\mathbf{T}^{\mathrm{FBR}}_N\mathbf{T}^\dagger + \mathbf{T}(\mathbf{T}^\dagger\mathbf{V}^{\mathrm{DVR}}\mathbf{T})\mathbf{T}^\dagger \tag{2.70}$$

$$= \mathbf{T}\mathbf{T}^{\mathrm{FBR}}_N\mathbf{T}^\dagger + \mathbf{V}^{\mathrm{DVR}}. \tag{2.71}$$

There are several favorite choices for basis functions in DVR. Most common are sine/cosine and Legendre, Hermite or Chebychev polynomials.

2.2.4 Fast Fourier Transform Method

The *Fast Fourier Transform* (FFT) method was developed and popularized by Feit and Fleck [29–31] and Kosloff and Kosloff [32–35] and is probably the most widely used method to calculate the action of the Hamiltonian on the wavefunction in time-dependent calculations.

Its basic idea is to perform the operations $\hat{T}\psi$ and $\hat{V}\psi$ in the representation where each of the operators is local. So the action of the potential operator $\hat{V}$ is calculated in coordinate space, since it is local in this representation. Then, it is simply a multiplication of $V(x_i)$ with $\psi(x_i)$, where x_i are the grid points. To calculate the action of $\hat{T}$ on ψ the wavefunction is transformed into momentum space (Fourier space) by a backward Fourier Transformation (FT). In this representation $\hat{T}$ is local and its action becomes again a simple multiplication by the kinetic energy discrete spectrum $T(k) = -\hbar^2 k^2/2M$.

In order to calculate $\hat{H}\psi = \hat{T}\psi + \hat{V}\psi$ one can use the following strategy:

1. Transform to momentum space, calculate $\hat{T}\psi$ and transform back to coordinate space:

$$\psi(x) \xrightarrow{\mathrm{FT}^{-1}} \tilde{\psi}(k) \longrightarrow -\frac{\hbar^2 k^2}{2m}\tilde{\psi}(k) \xrightarrow{\mathrm{FT}} \frac{\hat{p}^2}{2m}\psi(x) = \hat{T}\psi. \tag{2.72}$$

2. Calculate $\hat{V}\psi$ in coordinate space:

$$V(x)\psi(x) = \hat{V}\psi. \tag{2.73}$$

Practically the transformation between coordinate and momentum space is carried out with *Discrete Fourier Transformations* (DFT), which are widely used in numerical applications and therefore exist in highly efficient implementations. While a simple DFT algorithm would scale as N^2 (with N being the number of grid points) modern and highly efficient DFT routines scale as good as $N \log N$, which makes the FFT method very fast compared to other methods. Also the memory requirements are reduced drastically as the FFT method avoids ever constructing and storing the full Hamiltonian.

2.2.5 Curse of Dimensionality

A central problem of all grid-based methods in quantum dynamics is the exponential scaling with dimensionality of the problem. So far all explanations have been focused on one-dimensional problems. The extension to the general multi-dimensional case is formally straightforward. Every DOF is represented by a (fixed) number of grid points. Because every grid point of one DOF has to be combined with *every* point of *all* remaining DOFs the number of grid points is scaling exponentially with the number of (active) DOFs. For example, a two-dimensional Hamiltonian matrix element according to Eq. (2.48) is

$$H_{nmkl} = \langle \Phi_{nm}|\hat{H}|\Phi_{kl}\rangle = \langle \phi_n \otimes \varphi_m| \left(\hat{T}(\hat{p}_x, \hat{p}_y) + \hat{V}(x, y)\right) |\phi_k \otimes \varphi_l\rangle \,, \tag{2.74}$$

which requires a two-dimensional, numerical integration for *every* matrix element. The required two-dimensional basis functions Φ_{nm} are constructed as a *direct product* of two one-dimensional basis functions ϕ, φ

$$\begin{aligned}\Phi_{nm}(\mathbf{x},\mathbf{y}) &= \phi_n(\mathbf{x}) \otimes \varphi_m(\mathbf{y}) \\ &= \begin{pmatrix} \phi_n(x_1)\varphi_m(y_1) & \phi_n(x_1)\varphi_m(y_2) & \cdots & \phi_n(x_1)\varphi_m(y_L) \\ \phi_n(x_2)\varphi_m(y_1) & \phi_n(x_2)\varphi_m(y_2) & \cdots & \phi_n(x_2)\varphi_m(y_L) \\ \vdots & \vdots & \ddots & \vdots \\ \phi_n(x_K)\varphi_m(y_1) & \phi_n(x_K)\varphi_m(y_2) & \cdots & \phi_n(x_K)\varphi_m(y_L) \end{pmatrix}, \end{aligned} \quad (2.75)$$

which emphazises that the number of grid points is scaling exponentially with dimensionality (here $K \times L$ grid points).

For the full-dimensional treatment of a molecule $3N-6$ internal DOFs ($3N-5$ for linear molecules) have to be included in the calculation. So a four atom molecule already has 6 DOFs, which induces 10^6 basis functions if a minimum of 10 basis functions per dimension is assumed. In this case for every of the 10^{12} Hamiltonian elements six-dimensional numerical integrations have to be performed, which is not a problem in principle, but causes very high numerical effort. Note, that in many cases the numerical integration requires even denser grids than the grid of basis functions. Additionally, the value of the wavefunction needs to be stored in the computer memory at every grid point. As a consequence a full-dimensional, exact treatment of larger molecules (more than 4–5 atoms) is impossible, and will probably always be[2]. This is called the *Curse of Dimensionality*.

In this sense the FFT method is the most economical method introduced here, because the Hamiltonian matrix is never stored completely. Thus, "only" the value of the wavefunction has to be saved on the grid.

There exist some approaches to overcome the exponential scaling, or, at least, reduce its prefactor (also see section 2.9). One of the main important techniques is the *Multi-Configurational Time-Dependent Hartree* (MCTDH) method [36–38]. Here, the wavefunction at a given time is expanded into a series of so-called *single particle functions*, which are time-dependent themselves. However, boiling down the n-dimensional representation to basically n one-dimensional ones is a good approximation for weakly coupled DOFs only. Also the Hamiltonian needs to be separable into a sum of lower-dimensional operators, which is not necessarily easy nor possible, especially for strongly coupled DOFs.

Another ansatz to reduce the numerical effort was investigated in the framework of this work. Based on the fact that the wavepacket is never spread out all over the

[2] For the assumption that the earth purely consists of iron (which is a good approximation at least for its core) it can be estimated that it has $6 \cdot 10^{49}$ atoms. So even if every atom of the earth could store one value of a wavefunction, not more than a molecule with about 18 atoms, hence 48 DOFs, could be saved. [9]

configuration space in real chemical applications, major parts of the direct-product grid do not have contributions to the total wavefunction. So at any given time the wavefunction only needs to be stored at grid points where it is significantly different from zero. As the wavefunction is moving with time this induces a dynamically adapted grid. Test applications and implementation details will be given in chapter 3. The effect of wasted grid was already shown by Kosloff [35] for multi-dimensional FFT. He demonstrates that the momentum space is inherently too large by argueing that (for a multi-dimensional harmonic oscillator) the required phase space would be spherical, however, technically a cubic grid is constructed. That entails wasted momentum space, whose amount increases drastically with dimensionality. This argumentation even holds up for wavepackets, which are spread out over the complete configuration space.

2.3 Time Propagation of the Wavefunction

The second major task besides the numerical representation of the wavepacket is its propagation in time. Formally a propagator

$$\hat{U}(t, t_0) = e^{-i\hat{H}(t-t_0)/\hbar} \tag{2.76}$$

can be defined, which yields the formal solution of the TDSE

$$\psi(t) = e^{-i\hat{H}(t-t_0)/\hbar}\psi(t_0) = \hat{U}(t, t_0)\psi(t_0). \tag{2.77}$$

As the Hamilton operator appears in the exponent of the propagator it cannot be applied to the wavefunction without further modification and more sophisticated schemes have to be developed in order to propagate it in time. The most straightforward approach would arise if all eigenfunctions and eigenvalues (including unbound states) of the Hamiltonian were known. In this case the propagation is simple (cf. Eq. (2.8) after separation of $\mathbf{r}$), but the prize to pay is the diagonalization of the Hamiltonian which can even be impossible for higher-dimensional cases. The most popular propagation schemes *Second Order Differencing* (SOD), *Split Operator* (SPO), *Short Iterative Lanczos* (SIL) and *Chebychev* propagation are reviewed in Ref. [39]. In addition to the above mentioned ones the *Symplectic Integrators* (SI) and the *Taylor expansion* will be briefly discussed in the following sections.

2.3.1 Second Order Differencing

As mentioned above the main problem is that the Hamiltonian $\hat{H}$ appears in the exponent of the time evolution operator $\hat{U}$ and therefore cannot be applied to a

wavefunction directly. The easiest way to propagate a wavefunction in time would be to expand the *discrete* time evolution operator in a Taylor series

$$\hat{U}(t+\Delta t,t) = e^{-i\hat{H}\Delta t/\hbar} = \hat{1} - \frac{i}{\hbar}\Delta t\hat{H} + \dots \quad . \tag{2.78}$$

However, in this simple form the scheme is not stable. Lauvergnat *et al.* developed an implementation which overcomes the instabilities [40] and which will be explained in more detail in section 2.3.4. Another intuitive way to overcome the difficulties is to use the symmetric relation

$$\psi(t+\Delta t) - \psi(t-\Delta t) = (e^{-i\hat{H}\Delta t/\hbar} - e^{-i\hat{H}\Delta t/\hbar})\psi(t) \tag{2.79}$$

which, taking into account the Taylor expansion up to the second order term, results in

$$\psi(t+\Delta t) = \psi(t-\Delta t) - \frac{2i}{\hbar}\Delta t\hat{H}\psi(t). \tag{2.80}$$

So the wavefunction at the next time step $t+\Delta t$ can be calculated by the means of the last wavefunction (at time $t-\Delta t$) and the action of $\hat{H}$ on $\psi(t)$, which was explained in the previous section.

As the Taylor series is truncated after the second term this method is called *Second Order Differencing* (SOD) [41]. Obviously, higher order terms of the Taylor expansion could be included, which should minimize the truncation error (*Third Order Differencing, Fourth Order Differencing, etc.*). Although those schemes have been reported [42] they are not widely used because better time propagators have been developed.

2.3.2 Split Operator

The *Split Operator* method is another very simple way to calculate the action of the time evolution operator on the wavefunction. In this method the Hamiltonian is split up into a kinetic part $\hat{T}$ and a potential part $\hat{V}$. Both are applied to the wavefunction independently. In the simplest form (first order splitting) this yields

$$\hat{U}(t+\Delta t,t) = e^{-i\hat{H}\Delta t/\hbar} \approx e^{-i\hat{T}\Delta t/\hbar}e^{-i\hat{V}\Delta t/\hbar} + \mathcal{O}(\Delta t^2), \tag{2.81}$$

which would be exact if $\hat{T}$ and $\hat{V}$ commuted. As they do not the error can be expected to be proportional to the commutator $[T,V]$. It can be reduced by one order of magnitude by introducing a symmetrized product of the kinetic and potential factors (second order splitting)

$$e^{-i\hat{H}\Delta t/\hbar} \approx e^{-i\hat{V}\Delta t/2\hbar}e^{-i\hat{T}\Delta t\hbar}e^{-i\hat{V}\Delta t/2\hbar} + \mathcal{O}(\Delta t^3). \tag{2.82}$$

The action of the propagator on the wavefunction ψ is carried out in a representation in which the operator is local, because then the action is just a simple multiplication. In order to achieve this, easy transformations between coordinate and momentum space are required at every time step, which may best be carried out using FFT. The SPO method is unitary by construction.

The main drawback of this method is that it requires a representation of the Hamiltonian which is diagonal either in coordinate or in momentum space. This, however, can usually not be achieved for operators of the form $\hat{x}\hat{p}_x$. In such cases the Split Operator Method fails and cannot be used. As presented in section 2.6.2, in this work Hamiltonians are evaluated numerically with the program TNUM. Unfortunately, the TNUM-form of the Hamiltonian contains mixed operators of this form, which bans the use of SPO.

Additionally, the SPO method entails problems in the case that more than one electronic surface is involved in the propagation. In this case the potential is represented as a matrix which is not diagonal itself. Thus, an additional transformation of the potential energy matrix from adiabatic (diagonal kinetic energy operator) to diabatic representation (diagonal potential energy matrix) and back is needed at every time step.

2.3.3 Symplectic Integrators

Symplectic Integrators (SI) are numerical integration schemes specially designed for the numerical solution of (the classical) Hamilton's equations. They respect the symplectic symmetry properties of a dynamical system which means that they preserve the canonical relationship of the phase space variables q and p (coordinate and momentum). They are widely used in classical mechanics, but have been tailored to the needs of quantum-dynamical systems in 1996 by Gray *et al.* [43].

The discrete form of the TDSE is

$$i\hbar\frac{\partial}{\partial t}\mathbf{c}(t) = \mathbf{H}\cdot\mathbf{c}(t), \tag{2.83}$$

where $\mathbf{c}(t)$ is a complex vector. Thus, these expansion coefficients can be divided into a real and imaginary part, i. e.

$$\mathbf{q}(t) = \sqrt{2}\ \mathrm{Re}(\mathbf{c}(t)), \qquad \mathbf{p}(t) = \sqrt{2}\ \mathrm{Im}(\mathbf{c}(t)) \tag{2.84}$$

and a Hamiltonian function

$$h(\mathbf{q},\mathbf{p}) = \frac{1}{2}\sum_{i,j=1}^{N} H_{ij}(p_i p_j + q_i q_j) \tag{2.85}$$

is defined. The classical Hamilton's equation of motion,

$$\frac{\mathrm{d}}{\mathrm{d}t}\mathbf{q}(t) = \frac{\partial}{\partial \mathbf{p}}\, h(\mathbf{q},\mathbf{p}) = \mathbf{H}\cdot\mathbf{p} \tag{2.86}$$

$$\frac{\mathrm{d}}{\mathrm{d}t}\mathbf{p}(t) = -\frac{\partial}{\partial \mathbf{q}}\, h(\mathbf{q},\mathbf{p}) = -\mathbf{H}\cdot\mathbf{q}, \tag{2.87}$$

are then equivalent to the Schrödinger Eq. (2.83). So the quantum dynamics can be regarded as classical mechanics for a large set of quadratically coupled harmonic oscillators and $h(q,p)$ can be interpreted as mean energy of the wavepacket. The procedure for integrating these equations is

$$\mathbf{p}_k = \mathbf{p}_{k-1} - b_k \Delta t\ \mathbf{H}\cdot\mathbf{q}_{k-1} \tag{2.88}$$

$$\mathbf{q}_k = \mathbf{q}_{k-1} + a_k \Delta t\ \mathbf{H}\cdot\mathbf{p}_k \tag{2.89}$$

for $k = 1,\ldots,m$, with m being the order of the SI scheme. The above system of equations involves numerical work equivalent to $2m$ evaluations of the Hamiltonian on a real vector. After that new expansion coefficients are obtained

$$\mathbf{c}(t+\Delta t) \approx (\mathbf{q}(t+\Delta t), \mathbf{p}(t+\Delta t))^{\mathsf{T}}. \tag{2.90}$$

Explicit values for a_k and b_k, with $m = 4, 6, 8, 10, 12$, are given in Ref. [43]. For $m = 2$ the particular choice of $a_1 = a_2 = 1/2$ and $b_1 = 0$, $b_2 = 1$ yields the popular "leapfrog"-algorithm.

This propagation scheme is not only applicable to FBR (as presented above), but also to other representations of the wavepacket such as FFT and DVR.

2.3.4 Taylor expansion

As mentioned in the beginning of the section a Taylor expansion of the time evolution operator would be an intuitive yet unstable way of propagating a wavepacket in time. Lauvergnat *et al.* [40] have developed a propagation scheme that is based on a simple Taylor expansion and is applicable to both time-dependent and time-independent Hamiltonians. As this work only deals with time-independent Hamiltonians the first advantage is of no consequence in this context. The propagation scheme will briefly be discussed in the next paragraphs. For a detailed description one should refer to Ref. [40].

A simple Taylor expansion of $\hat{U}(t,t_0)$ in t about t_0 is

$$\hat{U}(t,t_0) = \sum_{k=0}^{\infty} \frac{(t-t_0)^k}{k!}\hat{U}^{(k)}(t_0,t_0), \tag{2.91}$$

with $\hat{U}^{(k)}$ being the kth derivative of $\hat{U}(t,t_0)$ with respect to time. Insertion of Eq. (2.77) into the TDSE (Eq. (2.42)) yields a different form of the TDSE

$$i\hbar\frac{\partial}{\partial t}\hat{U}(t,t_0) = \hat{H}(t)\hat{U}(t,t_0), \tag{2.92}$$

which, in this context, simply defines $\hat{U}^{(1)} = \frac{\partial}{\partial t}\hat{U}(t,t_0) = \frac{-i}{\hbar}\hat{H}(t)\hat{U}(t,t_0)$. Using this and the fact that $\hat{U}^{(0)}$ is just the identity operator by applying the product rule the second derivative $\hat{U}^{(2)}$ can be obtained as a function of $\hat{H}$ and its first derivate $\hat{H}^{(1)}$

$$\hat{U}^{(2)}(t,t_0) = \frac{-i}{\hbar}\hat{H}^{(1)}(t) + \left(\frac{-i}{\hbar}\hat{H}(t)\right)^2, \tag{2.93}$$

which, of course, can also easily be extended to higher orders of $\hat{U}^{(k)}$.

In the case of time-independent Hamiltonians all derivatives of $\hat{H}$ vanish and one simply gets

$$\hat{U}(t,t_0) = \sum_{k=0}^{\infty}\frac{\Delta t^k}{k!}\left(\frac{-i}{\hbar}\hat{H}\right)^k, \tag{2.94}$$

which is just the Taylor expansion of $U(t,t_0) = e^{-i\hat{H}\Delta t/\hbar}$. Though the convergence radius is infinite numerical instabilities arise, which causes it to be seldomly used in practical applications.

For practical implementations, which also employ time-dependent Hamiltonians, a Taylor expansion of $\psi(t)$ around t_0 instead of $U(t,t_0)$ is more efficient. The expansion is

$$\psi(t) = \sum_{k=0}^{\infty}\frac{(t-t_0)^k}{k!}\psi^{(k)}(t_0) \tag{2.95}$$

with the general derivatives

$$\psi^{(k)}(t_0) = \frac{-i}{\hbar}\sum_{m=0}^{k-1}[C_m^{k-1}\mathbf{H}^{(k-1-m)}(t_0)\psi^{(m)}(t_0)]. \tag{2.96}$$

By introducing $\phi(k) = (\Delta t^k/k!)\psi^{(k)}(t_0)$ the relations between between the different $\phi(m)$ $(m<k)$ can be derived to be:

$$\phi(k) = \frac{-i}{\hbar}\sum_{m=0}^{k-1}\frac{1}{km!}\Delta t^{m+1}\mathbf{H}^{(m)}(t_0)\phi(k-1-m). \tag{2.97}$$

With this the Taylor series of $\psi(t)$, which has to be truncated at k_{conv}, simply reads

$$\psi(t) = \sum_{k=0}^{k_{\mathrm{conv}}}\phi(k). \tag{2.98}$$

Table 2.2: Comparison of favorite time propagator schemes. Adapted and extended from Ref. [39].

	SOD	SPO	SI	Taylor	SIL	Cheby.
Norm unitary	✗	✓	✗	✗	✓	✗
Energy conservation	✗	✗	✗	✗	✓	✗
Unconditionally stable	✗	✓	✗	✗	✗	✗
Error scaling	quadratic	quadratic	nth order	variable	high order	exp.
Hamiltonian	arbitrary	no mixed terms	arbitrary	arbitrary	arbitrary	time-indep.
Storage arrays	3	2	2	$m_{\max}+1$	order $+1$	4

The convergence order k_{conv} is numerically determined from a convergence criterion (norm of $\phi(k)$) and is dependent on the specific Hamiltonian. The differing convergence order troughout a propagation also makes the error scaling of the method variable. A main drawback of the method is, that all $\phi(k)$ have to be stored (and all have the size of the full wavepacket) and thus the memory requirements are large. However, if a maximum number of derivatives of the Hamiltonian $m_{\max}$ is introduced, it can be reduced to $m_{\max}+1$ vectors.

The Taylor expansion scheme was originally designed for the propagation with time-dependent Hamiltonians, as present for simulations that involve interactions of a molecule with an oscillating electric field, e. g. a laser. As it is easy to implement and numerically stable it is also a good alternative for time-independent Hamiltonians, although many other propagator schemes exist.

2.3.5 Other Propagators

There are many other time propagation schemes reported in the literature. Two of the more important ones, which were not yet described here, are the *Chebychev* [44] and *Short Iterative Lanczos* [45] propagation schemes. Both of them are based on an expansion of the time evolution operator into a finite series of polynomials, where the Chebychev propagation method allows unusually large time steps. The two methods will not be described here in more detail as they were not used in this work. A more detailed overview can be found in Tannor's textbook [8] or to the review by Leforestier *et al.* [39].

2.3.6 Comparison

In general, there is no superior method for all types of calculations. Table 2.2 compares the different time propagator schemes, which were mentioned in this work. While some propagation schemes perserve the norm by construction (SPO, SIL), it is necessary for other propagators to check the unitarity throughout the propaga-

tion. The same applies for energy, which can be constant by construction or not. Unconditionally stable schemes do not have an upper limit for the time step, while the other schemes may suffer from exponential overflow, if the time step is chosen to be too large. It should be mentioned that this stability does not necessarily yield to accurate results, so even for unconditionally stable propagation schemes there is a practical limit for the time step. Also some of the schemes do not work with certain types of Hamiltonians, as for example the SPO method cannot deal with mixed terms x and $\hat{p}_x$. Also time-dependent Hamiltonians may restrict the choice of propagation schemes. Among the presented schemes only the Taylor expansion scheme offers the ability to treat truely time-dependent Hamiltonians. Other propagation schemes rely on the approximation that for one given time-step the Hamiltonian can be considered time-independent, but it may change from time step to time step. Also error scaling and memory requirements differ between the methods.

2.4 Eigenstates through Propagation in Imaginary Time

Eigenstates and eigenenenergies of a system can be found (time-independently) by diagonalization of the Hamilton matrix. Since the size of the Hamilton matrix scales quadratically with the number of basis functions this approach might be numerically limited by the memory of the computer. A different way to obtain eigenstates of a system is the propagation of a wavepacket in imaginary time, which was first introduced by Kosloff *et al.* [46].

As shown before, the formal solution $\psi(x,t) = e^{-i\hat{H}t/\hbar}\psi(x,t_0)$ (Eq. (2.77)) of the TDSE in real time (Eq. (2.42)) can be expanded in the set of stationary eigenstates ψ_n, i. e.

$$\psi(x,t) = \sum_n c_n e^{-iE_n t/\hbar}\psi_n(x). \tag{2.99}$$

Purely as a mathematical trick the real time can be exchanged by an imaginary time $\tau = i \cdot t$ thus

$$\hat{H}\psi(x,\tau) = \hbar\frac{\partial}{\partial\tau}\psi(x,\tau) \tag{2.100}$$

and

$$\psi(x,\tau) = e^{-\hat{H}\tau/\hbar}\psi(x,\tau_0). \tag{2.101}$$

From the expansion in eigenstates

$$\psi(x,\tau) = \sum_n c_n e^{-E_n\tau/\hbar}\psi_n(x) \tag{2.102}$$

it can be seen that propagation in imaginary time τ (which can be carried out with the usual propagation schemes) causes an exponential decay ($\exp[-(E_i - E_0)\Delta\tau/\hbar]$) of the ith eigenfunction with respect to the ground state ψ_0, which decays the slowest itself as its energy is the lowest. Because of this, the method is also called relaxation method. Renormalization of the wavefunction after each time step causes ψ_0 to "survive" the last. Through subtraction of the formerly determined lower eigenfunctions at every time step this procedure also enables the calculation of the next higher eigenfunction. Interestingly, the initial wavefunction may be completely arbitrary.

Especially, if the dimensionality of the problem is high and only few lower eigenfunctions are needed this method is advantageous. A main drawback is that higher eigenfunctions are not accessible directly but only if *all* lower ones are calculated previously. Additionally, the numerical error of the lower eigenstates accumulate in the higher ones.

2.5 Absorbing Potentials

As quantum-dynamical calculations are traditionally carried out on (rectangular) fixed grids it is possible that parts of the wavepacket come close to the border of the grid. Due to the symmetry properties of the basis functions this might cause unphysical reflections. Especially for dissociative processes, which in general have an infinite range, problems occur as infinity cannot be covered numerically. An *Absorbing Potential* can be used to delete the parts of a wavepacket, which come close to the border of the grid. There are different kinds reported in the literature. Some only consist of purely imaginary potentials, while others additionally use real parts. The imaginary part of the absorbing potential is responsible for the actual deletion of the wavepacket. As (counterintuitively) the slow parts of the wavepacket are most difficult to absorb the real part of the absorbing potential is solely accelerating the wavepacket, which improves the ability to absorb the formerly slower parts. The behavior can be explained with the corresponding de-Broglie wavelength, which is longer for slower parts of the wavepacket. Due to the limited width of the absorbing potential itself, long ranging parts of the wavepacket are harder to absorb.

Ref. [47] gives a comprehensive overview on construction and use of so-called *Complex Absorbing Potentials* (CAP). A popular version is the modification of Manolopoulos [48] and Zhang [49], which has been used in most of the calculations of this work. The CAP is defined as

$$V_{\mathrm{cap}}(\mathbf{q}) = \sum_j V_{R,j} \exp(-\alpha_{R,j}\,\kappa_j) + iV_{I,j} \exp(-\alpha_{I,j}\,\kappa_j), \tag{2.103}$$

where

$$\kappa_j = \frac{q_j^{\max} - q_j}{q_j - q_j^0}. \tag{2.104}$$

In Eq. (2.104) $q_j^{\max}$, denotes the end of the grid in the jth coordinate. The amplitudes of the real and imaginary parts are $\alpha_R = 0.739$ and $\alpha_I = 3.071$ and the corresponding coefficients are set to $V_R = -1.27 \cdot E_T^{\max}$ and $V_I = -0.994 \cdot E_T^{\max}$ for a maximal kinetic energy $E_T^{\max}$ in the original publication, but can be adjusted to the actual problem. This last parameter is the main advantage of this form of the CAP, as it enables easy parameter choices in practical applications.

As a second choice the MrPropa program supplies the imaginary potential in a Woods-Saxon form [50]:

$$V_{\text{cap}}(\mathbf{q}) = \sum_j \frac{2\lambda_j}{1 + \exp\frac{q_j^{\max} - q_j}{\eta_j}}, \tag{2.105}$$

which will not be used for calculations of this work, however. It has been applied, for example, in Ref. [51].

In chapter 5 absorbing potentials are proposed as a new "tool" for modeling the effects of a conical intersection in case not both the participating PESs are included with explicit couplings. The publication will demonstrate that the main effects of a conical intersection on a wavepacket on one PES are well represented by an (imaginary) absorbing potential.

2.6 The Kinetic Energy Operator

As stated earlier, the molecular Hamiltonian consists of the potential and kinetic energy operator. While from the dynamical point of view the potential is a "simple" input, the kinetic energy operator (KEO) has to be evaluated system specifically. This is easy in case the system is described in cartesian coordinates, but as discussed later for quantum-dynamical caluclations it is usually essential to change the coordinate system to a more suitable coordinate system. However, this complicates the analytical expression of the KEO drastically. As the potential energy operator does not contain any differential operators with respect to the coordinates a change of coordinate systems does not influence the value of the potential energy. It solely depends on the molecular geometry. So the next section will focus on the effects on the kinetic energy operator upon coordinate system change.

2.6.1 Coordinate Systems

Up to this point most of the explanations were performed for just one particle moving in one-dimensional cartesian coordinates. Of course, this lets theory appear simple

and elegant, but real-life applications are more complicated. Extension to higher dimensionality, meaning to include more DOFs in the calculation, is straightforward for cartesian coordinates. The Laplacian in Eq. (2.10) is very simple, as there are only constant coefficients in front of the second derivatives.

$$T_N = \sum_{n=1}^{N} -\frac{\hbar^2}{2M_n}\nabla_n^2 = \sum_{n=1}^{N} -\frac{\hbar^2}{2M_n}\left(\frac{\partial}{\partial x_n^2} + \frac{\partial}{\partial y_n^2} + \frac{\partial}{\partial z_n^2}\right). \tag{2.106}$$

For a system with N atoms there are obviously $3N$ DOFs involved. Despite the simplicity of the KEO there are two main drawbacks which make cartesian coordinates usually not the best choice for quantum-dynamical calculations. First, as mentioned above, $3N$ DOFs are necessary for a complete description of the dynamics, which is a substantial problem caused by the exponential scaling with dimensionality (Curse of Dimensionality, section 2.2.5). As a molecular geometry is completely described by $3N-6$ *internal* coordinates it is possible to save six DOFs when changing coordinate system to any kind of internal coordinates. These saved six DOFs describe the translational and rotational DOFs for the molecule. Translational DOFs are completely irrelevant for the dynamics, whereas with the neglect of the rotational DOFs a restriction to systems with a total angular momentum of zero ($J = 0$) is introduced. There are possibilities to include $J > 0$, for example the approximate J-shifting [52], which are, however, not used in this work as all calculations are restricted to $J = 0$ here. Second, cartesian coordinates are disadvantageous to describe chemical or physical processes as they are not tuned to the system specific properties such as symmetry.

Internal Z-matrix coordinates, which include bond lengths, angles and dihedrals, are very broadly used in quantum chemistry. Coordinates used for electronic structure theory, where the nuclei are kept at fixed positions, are not necessarily also a good choice for nuclar dynamics. However, as geometry optimizations or PES scans, which relate to moving nuclei are often carried out with Z-matrix coordinates they are also plausible for dynamics. Those coordinates can reduce the numerical effort (especially reduce the dimensionality of the problem) as e. g. a dissociation process might be described by only one or two internal DOFs, whereas cartesian coordinates usually require more. Cleverly chosen, this only one coordinate yields to the separation of whole fragments and hence the remaining internal coordinates are also a good choice for describing the internal motion of these well separated fragments. Also parts of a wavefunction travelling into those "dissociative channels" can easily be identified with absorbing potentials in just this one coordinate as all parts eliminated by the absorbing potential contribute to the dissociation process. Due to the fact that less coordinates are required to describe a basic internal motion than with cartesian coordinates the internal coordinates are less coupled to each other. This is essential in order to apply any kind of decoupled treatment such as

any reduced-dimensional model (section 2.7) or MCTDH, as all these schemes rely on weakly coupled DOFs.

However, the prize to pay for the advantages of using internal coordinate systems is that the KEO is much more complicated for most curvilinear coordinates. Its analytical expression can become awfully complicated even in systems with no more than 4 atoms (see e. g. Ref. [53]). In this work an approach, which was developed by Chapuisat and coworkers [54–56], which has been implemented by Lauvergnat and Nauts [57] in a program called TNUM, has been used to overcome this difficulty. It will be described very briefly in the next section.

Of course other coordinates could also be used. In spectroscopic issues normal mode coordinates are very popular as they represent the molecular vibrations around a minimum structure. The KEO would remain simple for mass-weighted normal coordinates, but other disadvantages occur. Mainly the physical interpretation of the coordinates only holds for small elongations from the molecular minimum structure. Normal coordinates will be discussed in chapter 4. Analytical expressions for other coordinates systems as Jacobi coordinates for three atom molecules (e. g. Ref. [58]) or hyperspherical coordinates [59, 60] have been reported, but will not be a topic of this work.

2.6.2 Tnum, a Numerical KEO

The general expression for the kinetic energy operator $\hat{T}_N$ of an N-atom molecule in internal coordinates $\mathbf{q} = (q_1, \ldots, q_{3N-6})$ can be written as (Podolsky method [56])

$$\hat{T}_N(\mathbf{q}, \partial_{\mathbf{q}}) = \frac{1}{2} \sum_{i,j=1}^{3N-6} \hat{p}_i^{\dagger}\, g^{ij}(\mathbf{q})\, \hat{p}_j \tag{2.107}$$

$$= \sum_{i,j=1}^{3N-6} f_2^{ij}(\mathbf{q}) \frac{\partial^2}{\partial q_i \partial q_j} + \sum_{i=1}^{3N-6} f_1^i(\mathbf{q}) \frac{\partial}{\partial q_i}\,, \tag{2.108}$$

where g^{ij} denote the contravariant elements of the metric tensor and $\hat{p}_i$ the conjugate momentum operators. The functions f_2^{ij} and f_1^i are given by

$$f_2^{ij}(\mathbf{q}) = -\frac{\hbar^2}{2} g^{ij}(\mathbf{q})\,, \tag{2.109}$$

$$f_1^i(\mathbf{q}) = -\frac{\hbar^2}{2} \sum_{j=1}^{3N-6} \left[J^{-1}(\mathbf{q}) \frac{\partial}{\partial q_j} J(\mathbf{q}) \right] g^{ij}(\mathbf{q}) + \left[\frac{\partial}{\partial q_j} g^{ij}(\mathbf{q}) \right]\,, \tag{2.110}$$

with the J denoting the Jacobian determinant of the transformation matrix from cartesian to curvilinear coordinates. Lauvergnat *et al.* [57] have developed the Fortran code TNUM to *numerically* but *exactly* calculate the *kinetic functions* $f_2^{ij}(\mathbf{q})$ and $f_1^i(\mathbf{q})$ as functions of the current geometry for molecules of arbitrary size and

the Jacobian determinant and their derivative. This code has been interfaced to the quantum-dynamical propagation program MrPropa, which was developed in this group [9,61].

The above stated equations are only valid if the so-called Euclidian normalization of the wavefunction is used. Here, the volume element $\mathrm{d}\tau$, which is used for all integrals, particularly all matrix elements, is

$$\mathrm{d}\tau = J(\mathbf{q})\mathrm{d}q_1 \dots q_{3N-6}. \tag{2.111}$$

However, especially if curvilinear coordinates are used for the representation of the wavepacket, the Euclidian normalization is not the most advantageous. Another commonly used normalization is

$$\mathrm{d}\tau = \rho(\mathbf{q})\mathrm{d}q_1 \dots q_{3N-6}, \tag{2.112}$$

which is referred to as Wilson normalization [62] for the particular choice of the weight function $\rho(\mathbf{q}) = 1$. In this case a purely multiplicative so-called *extra potential* term [55] appears in Eq. (2.107) and Eqs. (2.110) and (2.109) are modified.

2.7 Reduced-Dimensional Models

The numerical demands are scaling exponentially with the degrees of freedom of a system. This prohibits the exact full-dimensional treatment of larger molecular systems. In order to deal with such systems some approximations have to be made, concerning both the potential and kinetic part of the Hamiltonian. Most chemical reactions or physical processes are dominated by few internal DOFs. If it is possible to characterize those, e. g. with the help of physical or chemical intuition, it is possible to separate the $3N-6$ DOFs $\mathbf{q}$ into n *active* $\mathbf{q}'$ and $m = 3N-6-n$ *inactive* $\mathbf{q}''$ coordinates

$$\mathbf{q} = (\underbrace{q_1, \dots, q_n}_{n \text{ active} \equiv \mathbf{q}'}, \underbrace{q_{n+1}, \dots, q_{3N-6}}_{m \text{ inactive} \equiv \mathbf{q}''}). \tag{2.113}$$

While the active coordinates are treated explicitly within the framework of the above explained methods the inactive coordinates have to be treated approximatively or have to be constrained in some manner. The three most popular reduced-dimensional models are

- the *rigid constraints*,
- the *adiabatic model* (also called *flexible or relaxed constraints*),
- the *(harmonic) adiabatic approximation*, called (H)ADA,

which will briefly be explained in the next sections.

2.7.1 Rigid Constraint Model

The probably simplest way of dealing with inactive coordinates is to "freeze" them at some fixed values, i. e. $\mathbf{q}'' = \mathbf{q}''_0$. From the quantum-chemical point of view things are easy in this case. The PESs just have to be calculated for the active coordinates, while the values for the inactive coordinates are given, so

$$V_0(\mathbf{q}') = V(\mathbf{q}'; \mathbf{q}''_0). \tag{2.114}$$

In other words for a given set of active coordinates quantum-chemical *single point* calculations have to be carried out for every grid point. Besides the choice of active coordinates the main difficulty is that there is no obvious and unambiguous choice of the fixed values. Mostly, critical points of the PES such as the geometry of reactants, products or transition states are used for this approach. As the inactive coordinates are not allowed to "react" to the changes in the active coordinates the approximation to keep them fixed will only be valid if the inactive coordinates do not change drastically during a reaction. The physical interpretation of rigid constraints is the movement of the active coordinates being much faster than the movement of the inactive ones. Actually, they do not adjust to changes in the active coordinates *at all*.

The same approach can be applied to the kinetic energy operator. Its equations are derived in Refs. [63–66], which is much more complicated than derivations for unconstrained systems. This is mainly caused by a changed metric of the configuration space and therefore the different Jacobi determinant. As a consequence, the kinetic energy operator changes due to equations (2.109) and (2.110). The rigid constraint model is also included in the Tnum program package, which is interfaced to MrPropa.

2.7.2 Adiabatically Constrained / Flexibe Model

The other physical extreme of the rigid constraint model is the *flexible model*. Here the inactive coordinates react *instantaneously* to changes in the active set of coordinates. This is achieved by so-called *relaxed* PESs, which means that a (constrained) geometry optimization is carried out at every grid point of the space of active coordinates. This is, of course, computationally more demanding, but on the other hand the inactive coordinates are treated in a well-defined manner. The inactive coordinates thus are a function of the active coordinates, $\mathbf{q}'' = \mathbf{q}''_{\mathrm{eq}}(\mathbf{q}')$, so the PES is

$$V_{\mathrm{relax}}(\mathbf{q}') = V(\mathbf{q}'; \mathbf{q}''_{\mathrm{eq}}(\mathbf{q}')). \tag{2.115}$$

The Tnum package also includes flexible constraints for the kinetic energy operator, which are derived in Refs. [63, 66–68]. The kinetic functions (Eqs. (2.109)

and (2.110)) are adjusted adiabatically to the variations of the active coordinates: $f_{2,1}^{\text{adiab.}}(\mathbf{q}';\mathbf{q}''_{\text{eq}}(\mathbf{q}'))$. As the derivatives of the inactive coordinates with respect to the active ones are part of the adjusted kinetic functions this approximation is valid only if the inactive coordinates do not vary strongly from the reference geometry due to the otherwise large derivatives. In these cases an explicit treatment of the coordinates should be considered.

It should be mentioned that a combination of different reduced-dimensional models has been presented in the literature. Taking a relaxed PES (adiabatic model) together with the rigid kinetic energy operator (rigid constraint model) is quite common and avoids numerical instabilities due to the complicated form of the kinetic energy operator in the adiabatic model. Furthermore, modelling the KEO analytically in the adiabatic model will hardly be possible for larger molecules at all, which restricts the use of the flexible constraints to the PES.

2.7.3 (Harmonic) Adiabatic Approximation

The (harmonic) adiabatic approximation (H)ADA [9, 69–71] will be presented as a third reduced-dimensional model, which is implemented in the MrPropa package. The approximation is similar to the Born-Oppenheimer approximation in which the movement of the slow nuclei was separated from the movement of the faster electrons. Here the PES is expanded in a Taylor series

$$V(\mathbf{q}) = V_{\text{relax}}(\mathbf{q}') + V_2(\mathbf{q}'';\mathbf{q}') + R(\mathbf{q}). \tag{2.116}$$

Additionally to the relaxed PES $V_{\text{relax}}(\mathbf{q}')$, which is calculated in the same way as for the flexible model, the potential includes $V_2(\mathbf{q}'';\mathbf{q}')$, which is the harmonic (quadratic) expansion of the PES around the region of minimal energy. Quantum-chemical programs calculate this in freqency calculations, which make use of the Hessian matrix containing the second derivatives of the potential with respect to all DOFs. The nuclear wavefunction is written in an adiabatic separation ansatz (analogously to the Born-Oppenheimer separation, Eq. (2.18))

$$\psi(\mathbf{q}',\mathbf{q}'') = \sum_{i=1}^{\infty}\sum_{u=1}^{\infty} \phi_u(\mathbf{q}'';\mathbf{q}')\varphi_i(\mathbf{q}'). \tag{2.117}$$

It can be shown that in order to construct the KEO this ansatz requires the full PES for all coordinates (active and inactive), which can be avoided by omitting all anharmonicities, i. e. the remainder R of the Taylor series. For a HADA calculation this practically means, that frequency calculations have to be performed at all grid point of the active space. As the (H)ADA method was not used in this work for further derivations and explanations the reader can refer to the cited literature.

2.8 The MrPropa Program: Feature List

All calculations in this work have been carried out with the MrPropa program package [61], which was started to be developed in the framework of Frank von Horsten's PhD thesis [9] in the Hartke group and is extended continously by him. The focus was set to generality and user friendly inputs. Most calculations can be carried out with a minimum of expert knowledge. To set up a calculation little more than the molecular geometry and the active degrees of freedom have to be specified. During this work the program has not only been used for all calculations but some extensions were implemented. The following list shows the main features of the MrPropa program package:

Basic Program

- No restriction on number and type of DOFs
- Interface to the Tnum program to calculate the Kinetic Energy Operator numerically
- Five most important wavepacket time propagators (SPO, SIL, SI, Chebyshev, Taylor)
- Various possibilities for the representation of the Hamiltonian and the wavefunction (FBR, Collocation, DVR, FFT)
- Three reduced-dimensional models (rigid, flexible, HADA)
- Interface to popular Quantum Chemistry programs: Gaussian, Molpro, Turbomole, Mopac
- Calculation of physical data, such as IR-spectra, cumulative reaction probabilities and rate constants
- Propagation on several electronic PESs
- Calculate eigenstates with different methods (Full Hamiltonial diagonalization, Filter diagonalization for higher vibr. states, Propagation in imaginary time)
- Complex absorbing potentials
- Classical Molecular Dynamics by solving Hamilton's equations of motion (Verlet and Runge-Kutta)
- Time-independent scattering via R-matrix propagation
- Calculation of state resolved differential and total cross sections
- Laser fields (Pump-dump-probe, Optimization of laser pulses)

Extensions within this Work

- Adaptive FBR representation with collocation (chapter 3)
- New FBR basis functions: Interpolating Gaussians (chapter 3)
- Evaluation of the PES in a polynomial expansion (chapter 4)
- Representation of the Hamiltonian in normal mode coordinates (chapter 4)

- Complex absorbing potentials with functional form (chapter 5)
- MOPAC interface (chapter 5)
- Calculation of quasi-diabatic PESs (chapter 5)
- Simulation of transient absorption spectra (chapter 5)

2.9 State of the Art

The scientific area of quantum dynamics is a very broad and complex field, which consists of many different and independent research areas. This section cannot give a comprehensive overview on the complete research of quantum dynamics but rather concentrates on mainly three central interlinked research fields, which are related to this work. These are the choice of coordinates, the correct representation of the PES and of the wavefunction, respectively.

Choice of Coordinates First, the choice of the right coordinates is essential for quantum dynamics as due to the exponential scaling with the active DOFs there is a need to find coordinates which describe the nature of the specific problem the best. This mostly prohibits the use of *cartesian coordinates* at least for larger molecules. *Normal mode coordinates* are only good for small elongations around a critical point on the PES, whereas they do not give a reasonable description for higher vibrational excitations [72, 73]. They are, however, widely used for the description of low-vibrational (or rovibrational) stationary states (e. g. [74, 75]). *Z-matrix coordinates* offer an intuitive way of specifying the molecular structure which even holds up for dissociative processes. Their advantegous role in quantum dynamics has been described in section 2.6.1. Some examples for their application can e. g. be found in Refs. [76, 77]. Dissociative processes of three atom molecules are often described in *Jacobi coordinates* (as applied e. g. in Refs. [58, 78]), however they have the disadvantage of describing only one dissociation asymptote correctly, either reactants or products. They are also adjustable to larger molecules [79, 80]. *Hyperspherical coordinates* are basically mass-weighted polar coordinates, which have the advantage of allowing a smooth description of the reaction system as it traverses along the reaction path. They were used and compared to other coordinate systems for triatomic reactions by Pack and Parker [59] and Shi and Tannor [60].

As explained in section 2.6 the mathematical form of the KEO is directly related to the choice of the coordinate system. While it is simple for cartesian coordinates its structure gets very complicated and lengthy for other coordinates. Even nowadays it is still possible to publish analytical derivations of the KEO for small (4/5-atom) molecules [53] or how to find the analytical KEO in a simpler way [77, 81]. As numerical schemes such as the TNUM [57] code exist, analytical expressions can be checked against the numerical ones, as, for example, Vendrell *et al.* [82, 83] did for the protonated water dimer.

Representation of the Wavepacket The representation of the wavepacket also constitutes a large field of research. The major breakthrough until now was certainly the fast Fourier transform approach by Kosloff and Kosloff [32,33], which still is the fastest and hence the standard representation for exact low-dimensional quantum-dynamical problems. As this traditional approach is limited by the exponential scaling due to the direct product basis it has been tried to avoid the direct product basis. Carrington and coworkers are using a DVR with pruned basis sets, which are not in the direct product form [84,85] (and references therein). With this they were recently able to carry out calculations with test Hamiltonians as big as 32D [86]. In order to circumvent too large numerical grids Wyatt and coworkers developed schemes which prune and move the grid along with the propagated wavepacket [87–90]. This, however, leads to the need to monitor the movement of the wavepacket. It can be achieved with so-called quantum trajectories, but is not necessarily trivial.

Another promising representation is the *Multi-Configuration Time-Dependent Hartree* (MCTDH) method, which was originally published by Meyer *et al.* in 1990 [36] and is thoroughly discussed and reviewed in Refs. [37, 38, 91]. The wavefunction is expanded into a series of dynamically adapted product representations, the so-called *single particle functions*. In this sense the n-dimensional propagation is boiled down to n one-dimensional ones. This entails the need to setup both the kinetic and the potential part of the Hamiltonian in 1D terms, which is not necessarily possible in both cases, especially for strongly coupled DOFs. Opposed to a regular FBR (and to the standard Time-Dependent Hartree (TDH) ansatz e. g. by Gerber and coworkers [92, 93]), where only the expansion coefficients are time-dependent, here also the basis, i. e. the single particle functions, is time-dependent. Also many different configurations, namely different sets of single particle functions, are included in the complete description of the wavefunction. This is a close analogy to the extension of a SCF electronic structure calculation to MCSCF to include couplings of different states. The MCTDH approach enables quantum-dynamical wavepacket propagations for a few dozen DOFs, however, the original MCTDH approach does not beat the exponential scaling with dimensionality either [37]. An encouraging extension of the original idea is cascading or multilayer MCTDH [94,95] which even makes many dozens of DOFs feasible. It should be kept in mind that all these approaches are not exact but approximate.

Of course, if a full quantum-mechanical description of the nuclei is not necessary other molecular dynamics methods are available, namely semiclassical and classical MD variants. Besides classical MD with force fields especially Carr-Parinello MD [96] and direct *ab initio* MD are to be mentioned here. As in all classical trajectory MD simulations the PES only has to be evaluated at points where the system really goes. Semiclassical approaches combine classical elements of a molecular dynamics simulation, such as deterministic classical trajectories, which follow Newton's equation of motion with the non-local character of a wavepacket, represented e. g. by a

Gaussian centered at the trajectory. A prominent historical method in this context are Heller's moving Gaussians [97] or as a more recent extension the Full Multiple Spawning method by Martinez [98, 99]. Here moving Gaussians are propagated on several PESs and may appear and disappear in the region of a conical intersection. However, the correct description of quantum effects like tunneling needs some extra effort in this method [100]. Moving Gaussians are also combined with the MCTDH framework [101], known as G-MCTDH.

There are also methods proposed, which combine low-dimensional exact quantum dynamics with traditional QM/MM schemes, e. g. the one-dimensional movement of a proton in an embedded protein surrounding [102, 103]. Here, the potential for the quantum-dynamical part is recalculated at every time step and may adjust to the changed physical situation.

Representation of the PES A third major research topic is the evaluation of PESs, which are needed for quantum-dynamical calculations. As the potential energy has to be available throughout the complete configuration space for the active coordinates it is essential to develop schemes which avoid performing quantum-chemical calculations on regular rectangular grids, as even for a limited number of DOFs this is not affordable. The *High-Dimensional Model Representation* (HDMR) by Rabitz *et al.* [104] or similarly the n-mode expansion by Bowman and coworkers [105, 106] limit the number of electronic structure calculations as the PES is decomposed to n-body terms with (usually) decreasing significance with higher order, which enables truncation at a certain level of accuracy. Other schemes employ a (modified) Shepard interpolation [107, 108], especially the GROW method by Collins (see the review Ref. [109] and references therein), which has recently been extended to the use of several (diabatic) PESs [110].

Approximately Diabatic States As stated in section 2.1.2 a strictly diabatic basis is only available for diatomic molecules. Hence, many schemes to find approximately diabatic states for larger molecules have been reported in the literature. The most straightforward way to calculate such states is to use the derivative coupling elements. By solving an approximate Poisson equation, the kinetic coupling can be transformed away [111, 112]. Simpler construction schemes have been proposed, as the *ab initio* calculation of all derivative coupling terms is computationally very demanding, e. g. the block diagonalization method [113]. As one of the schemes, which only requires the knowledge of the adiabatic PESs alone, thus avoiding the use of the non-adiabatic coupling elements at all, the regularized quasi-diabatic states of Köppel and coworkers [17–19] are especially mentioned, as they were applied in this work, chapter 5). The calculation of the approximate diabatic sates relies solely on the difference of the two involved adiabatic sates and its derivates. This already simple scheme, however, is somehow sophisticated compared to some model systems

used in the literature (e. g. Refs. [114, 115]), where mixing angles have simply been constructed and expressed analytically.

2.10 General Objectives

The traditional representation of the wavepacket suffers from the exponential scaling with the DOFs. One idea to overcome the exponential scaling, or at least reduce its prefactor significantly, was published by Hartke [116] and is based on the fact that grid representations always use more grid points than actually are needed to represent a wavepacket at a certain time. If the wavefunction was only stored at places where it actually has a non-negligible contribution to the total wavepacket, huge amounts of memory and computational time should be saved. This idea was published in a proof-of-principle paper with a very elementary 1D-implementation. To extend this implementation to higher dimensionality and combine it with the existing MrPropa code was a task of this thesis. Additionally, more advanced basis functions (interpolating Gaussians) in combination with the collocation method were implemented and tested in close collaboration with the Schneider group (Univ. Kiel, now TU Berlin) within the Computational Science Center (CSC) at the University of Kiel. The results of this method development project will be stated and discussed in chapter 3.

The "Collaborative Research Center (SFB) 677—Function by Switching" at the University of Kiel deals with molecular switching processes. As a part of this research chapter 5 deals with the quantum dynamics of photochemical switching processes. The photochemical ring-opening of cyclohexadiene will be investigated by comparing measured retention times on the experimentally relevant 2A surface with quantum-dynamical wavepacket calculations. With the use of the flexible model (section 2.7) for the PES evaluation, which is a novel perspective on the process, experimental retention times could semi-quantitatively be reproduced. As cyclohexadiene may serve as a possible model system for fulgide switches, which are experimentally accessible and investigated in the Temps group for the SFB, the quality of this model will critically be judged. Also experimentally accessible and measured by the Temps group is the *(E)* $\rightarrow$ *(Z)*-isomerization of bridged azobenzenes, which is a very promising class of photoswitches. Chapter 5 will present first results of quantum-dynamical calculations on quasi-diabatic semi-empirical PESs. The most important internal DOFs for this photo-reaction were characterized by surface-hopping molecular dynamic simulations, which were performed in a diploma thesis in our group [117, 118]. Those coordinates were used for the reduced-dimensional quantum dynamics to calculate transient absorption spectra.

As for all such applications one of the bottlenecks is the generation of the PES. In chapter 4 an automated PES generation scheme will be presented. The Rauhut group (Univ. Stuttgart) developed efficient schemes to calculate many-coordinate

representations of potentials, even for high order terms [119, 120]. Z-matrix coordinates have been found to be more suitable for dynamical calculations of systems with double minimum potentials than the formerly used normal mode coordinates. Because of this the n-mode PES expansion is performed in Z-matrix coordinates. Polynomial fits of this PES representation are interfaced to our quantum-dynamical wavepacket propagation program MrPropa, which offers the fast analytical evaluation of highly-accurate PESs. Here, model calculations to test the automatic implementation have been performed. The tunneling splittings of hydrogen-peroxide, its isotopologues and cumulative reactions probabilities for the inversion of PHDCl were evaluated.

3 Adaptive Basis Representation

3.1 Scope of the Project

An essential drawback of traditional quantum-dynamical methods is the exponential scaling with dimensionality of the system. Reduced-dimensional models are a first mandatory step to decrease numerical effort, but the *curse of dimensionality* still prohibits the inclusion of many *active*, i. e. explicitly and exactly treated, DOFs. Based on the fact that a quantum wavepacket in real chemical situations remains spatially compact and does not spread over the whole configuration space, Hartke [116] published the *proof-of-principle* of the following idea: It should be sufficient to store the wavepacket only on grid points where it has a non-negligible contribution, while other grid points can be omitted. This goes in line with former ideas, which move the grid representation along with the propagated wavepacket [89, 90, 121]. However, monitoring of the wavepacket's movement is required, which can be achieved by so-called Quantum Trajectories or different approaches, but is not trivial in general. Other difficulties might occur if the wavepacket bifurcates in certain chemical situations.

The present scheme combines advantages of fixed and moving grids in such way that basis functions of the FBR wavepacket representation are placed at fixed positions on an imagined grid of basis functions, but still only covering the region where the wavefunction actually is. The basis functions themselves, however, are not moving around. As the wavepacket travels along the coordinate space basis functions become activated and disabled depending simply on the size of the expansion coefficients on the outermost grid points. This leads to actual savings only if disabled points and their coefficients are not stored in memory, which, in turn, requires that the corresponding entries in the wavefunction vector and Hamiltonian matrix have to be added and deleted continually throughout the propagation. As a consequence the actually stored wavefunction may be arbitrarily shaped avoiding direct product grids. It may also split up into sub pieces and recombine without further restraints. Technical difficulties arising from the non-orthogonality of a Gaussian basis are min-

imized as the Gaussians are placed on an imagined fixed grid. This ensures that the overlap matrix is always well-defined (non-singular) and does not suffer from near linear dependencies, which may arise in approaches with moving Gaussians when the basis functions are almost lying on top of one another. Another advantage of the imagined fixed grid of basis functions is that for spatially fixed basis functions the expansion of the wavefunction is unique, which is not necessarily the case for a set of moving basis functions.

In the original publication it was shown that the idea produced good results for one-dimensional artificial test cases. If the wavepacket stays compact while propagated the set of active grid points also stays compact and mirrors the wavepacket movement without any further information. Even in situations where the wavepacket is splitting into two sub pieces and/or is rejoining the presented simple criterion, which only checks for the size of the wavefunction expansion coefficients, is sufficient in order to decide which grid points have to be present and which are not required. The most chellenging situation for such an adaptive approach is tunneling. Here the coefficients are very small in regions where the actual tunneling takes place. However, it could be demonstrated that upon correct choice of the coefficient threshold tunneling situations can be described without significant loss of accuracy compared to traditional representations.

This first elementary work contained several deficiencies, though. First, the one-dimensionality is adequate for test cases only, not for real chemical applications. Second, as the basis functions need to be spatially compact the obvious choice is to employ distributed Gaussians. However, this choice is not optimal, as Gaussians entail the disadvantage of nonorthogonality. This is not a problem in principle, but forces numerically demanding operations as for the propagation the overlap matrix needs to be inverted at *every* time step, or equivalently, a linear system of equations with the overlap matrix needs to be solved. Also memory requirements are enlarged as in addition to the Hamiltonian matrix also the overlap matrix has to be stored. Even if known technical ways to avoid storing the complete overlap matrix are used still its inversion has to be carried out. A third drawback of the initial implementation is that the Hamiltonian matrix elements are determined with a simple numerical integration scheme, which requires a much denser grid than the grid of basis functions. Thus, two grids have to be adjusted during the resizing process, which causes not only numerical but also implementational overhead of the size adjustments. Of course, analytical integrations could be performed in a Gaussian basis, but this would restrict the generality of the approach. The kinetic energy operator needs to be present in an analytical form, which is only possible for simple molecules. In order to integrate the matrix elements of the potential energy matrix analytically the potential has to be expanded in a Taylor series of finite length (which could be done since quantum-chemical programs often supply the information of first or second derivatives by performing costly frequency calculations) or fitted

to another suitable analytical form. This, however, is practically quite problematic, especially for higher dimensional potentials.

3.2 Project Objectives

For all the above mentioned aspects improvements can be proposed and are dealt with in the following publication. The extension to higher dimensionality is straightforward in principle and is integrated in the MrPropa program, which offers not only the "infrastructure" for quantum-dynamical calculations of arbitrary dimensionality, but also brings along the benefits of the exact, but numerical evaluation of the KEO with Tnum.

In order to dispose of the numerical integration grid the collocation method is introduced in combination with a new choice of basis functions. So-called Interpolating Gaussians were developed by R. Schneider (Univ. Kiel, now TU Berlin, member of DFG research center Matheon) and his coworker F. Krüger and implemented in this work in the MrPropa program for arbitrary dimensionality. These novel basis functions offer the advantage of orthogonality on the collocation grid, so no overlap matrix (or more precisely its analog for collocation) is required anymore. Furthermore, due to their interpolating property (and due to the fact that the basis is normalized) the usual FBR expansion coefficients in Eq. (2.43) are determined just by the value of the wavefunction on the grid. Using the collocation method in combination with Interpolating Gaussians gives rise to avoiding two numerical integration problems: First, the Hamilton matrix elements and second, the projection of the FBR expansion coefficients.

In this work 2D and 3D calculations are presented, both test cases and real-life applications. Both examples demonstrate the successful upgrade of former work [116] from 1D to higher-dimensional cases and the integration of the adaptive basis representation in the MrPropa framework in combination with a new type of basis function. The 2D example, a double minimum potential combined with a harmonic oscillator, was chosen for two reasons. While the wavepacket is oscillating back and forth in the harmonic coordinate, which results in the need of permanent coefficient checks and resizing of arrays and therefore is a tedious task for the adaptive approach, it is spreading out and tunneling in the double minimum coordinate. Hence, this example also demonstrates the ability to sucessfully describe tunneling situations. The 3D example is a real-life application with a more complicated KEO and a different wavepacket behavior. Besides illustrating that non-constant kinetic functions do not interfere with the adaptive basis representation, the ability to scale up the approach to higher dimensionality is shown. Furthermore, not only the extension to higher dimensionality in principle but the the computational expenses are of great importance. For this 3D example they unexpectably do not exeed the cost for the famous FFT method, which is an encouringing result for future applications.

3.3 Quantum-Mechanical Wavepacket Propagation in a Sparse, Adaptive Basis of Interpolating Gaussians with Collocation

Own contributions presented in the paper:

- Implementation of novel multidimensional basis functions (Interpolating Gaussians) in MrPropa program
- Implementation and extension of the one-dimensional preliminary work to arbitrary dimensions.
- Two propagation algorithms implemented for adaptive basis representation
- Continual resizing of the Hamiltonian matrix and corresponding wavefunction vectors
- Complex absorbing potentials for adaptive basis representation
- Performing 2D and 3D calculations: 2D test case and 3D real-life application including comparison to traditional (FFT/DVR) representations

Additional work within this project, not presented in the paper:

- Checked different frequencies for coefficient checks
- Propagation in imaginary time for calculation of stationary states

Abstract

We present an extension of our earlier work on adaptive quantum wavepacket dynamics [B. Hartke, Phys. Chem. Chem. Phys., 2006, 8, 3627]. In this dynamically pruned basis representation the wavepacket is only stored at places where it has non-negligible contributions. Here we enhance the former 1D proof-of-principle implementation to higher dimensions and optimize it by a new basis set, interpolating Gaussians with collocation. As a further improvement the TNUM approach from Lauvergnat and Nauts [J. Chem. Phys., 2002, 116, 8560] was implemented, which in combination with our adaptive representation offers the possibility of calculating the whole Hamiltonian on-the-fly. For a two-dimensional artificial benchmark and a three-dimensional real-life test case, we show that a sparse matrix implementation of this approach saves memory compared to traditional basis representations and comes even close to the efficiency of the fast Fourier transform method. Thus we arrive at a quantum wavepacket dynamics implementation featuring several important black-box characteristics: it can treat arbitrary systems without code changes, it calculates the kinetic and potential part of the Hamiltonian on-the-fly, and it employs a basis that is automatically optimized for the ongoing wavepacket dynamics.

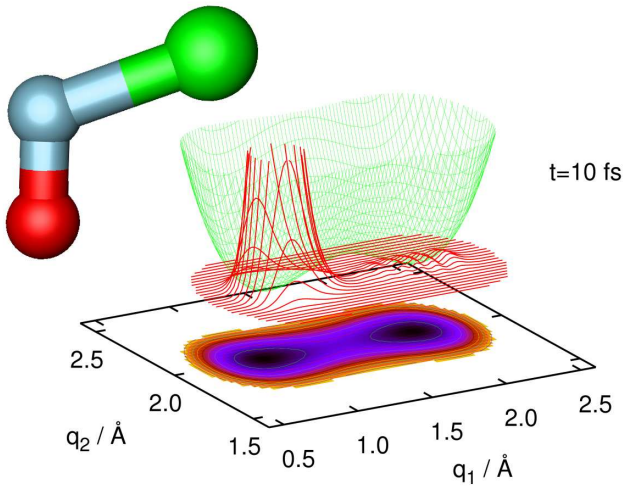

published in Phys. Chem. Chem. Phys., **2009**, *11*, 463-475

Received August 19, 2008, Accepted September 30, 2008
First published as an Advance Article on the web November 17, 2008
DOI: 10.1039/b814315c

3.4 Additional Information

3.4.1 Note on Hermiticity of Hamiltonian with Collocation

The collocation method was first used and implemented in MrPropa in combination with the adaptive basis representation. The following remarks are however not limited to this representation, but also apply to traditional basis representations whenever the collocation method is used with non-constant kinetic functions.

As already stated by Yang and Peet [24] the collocation method does not necessarily preserve hermiticity, i. e. the (complex conjugated) symmetry of the Hamiltonian matrix. According to these authors this should only be of marginal interest, though. This can change, however, for time-dependent calculations where the action of the Hamiltonian is usually performed many thousands of times in contrast to time-independent calculations. Due to the usually preferable curvilinear coordinate systems with more complicated KEOs involving non-constant kinetic functions the non-hermiticity may also increase. This will be illustrated in the next paragraphs.

The kinetic functions in a certain coordinate system (eq. (2.110) and (2.109)) are solely dependent on the molecular geometry. In other words each of them may have different values on different grid points, which are used for the wavepacket representation. Table 2.1 sums up the different ways of obtaining the kinetic energy matrix elements T_{ij}. In the following the kinetic energy matrix elements are compared in more detail with the following notation: With M being the total number of grid points the discrete indexed grid is denoted as the set $\{\mathbf{Q_1}, \ldots, \mathbf{Q_M}\}$ with each element $\mathbf{Q}_i$ beeing a point within the $(3N-6)$-dimensional configuration space $\mathbf{q} = (q_1, ..., q_{3N-6})$. $\frac{\partial}{\partial q^{(k)}}$ is the (first) derivative with respect to the kth dimension of $\mathbf{q}$. φ_i is denoting the ith basis function on the grid. In an actual implementation a matrix element in a *regular FBR* is

$$
\begin{aligned}
T_{ij} &= \langle \varphi_i | \hat{T} | \varphi_j \rangle && (3.1)\\
&= \int_{-\infty}^{\infty} \varphi_i^*(\mathbf{q}) \left(\sum_{k,l=1}^{3N-6} f_2^{kl}(\mathbf{q}) \frac{\partial^2}{\partial q^{(k)} \partial q^{(l)}} + \sum_{k=1}^{3N-6} f_1^k(\mathbf{q}) \frac{\partial}{\partial q^{(k)}} \right) \varphi_j(\mathbf{q}) \, \mathrm{d}\mathbf{q} && (3.2)\\
&= \sum_{k,l=1}^{3N-6} \int_{-\infty}^{\infty} \varphi_i^*(\mathbf{q}) f_2^{kl}(\mathbf{q}) \frac{\partial^2}{\partial q^{(k)} \partial q^{(l)}} \varphi_j(\mathbf{q}) \, \mathrm{d}\mathbf{q} + \\
&\quad \sum_{k=1}^{3N-6} \int_{-\infty}^{\infty} \varphi_i^*(\mathbf{q}) f_1^k(\mathbf{q}) \frac{\partial}{\partial q^{(k)}} \varphi_j(\mathbf{q}) \, \mathrm{d}\mathbf{q}. && (3.3)
\end{aligned}
$$

In the *collocation* method a matrix element becomes

$$T_{ij} = \hat{T}\varphi_j(\mathbf{Q}_i) \tag{3.4}$$

$$= \sum_{k,l=1}^{3N-6} f_2^{kl}(\mathbf{Q_i}) \frac{\partial^2}{\partial q^{(k)} \partial q^{(l)}} \varphi_j(\mathbf{Q_i}) + \sum_{k=1}^{3N-6} f_1^{k}(\mathbf{Q_i}) \frac{\partial}{\partial q^{(k)}} \varphi_j(\mathbf{Q_i}). \tag{3.5}$$

What does this mean in the context of hermiticity, for which $T_{ij}^* = T_{ji}$ is required?

In regular FBR, hermiticity is ensured as the the complete grid $\mathbf{q}$ is integrated. Because basis function φ_i differs from φ_j only at the position on the grid but not in its functional form (and therefore not in its derivatives) the definite integrals in the limits of $\pm\infty$ upon exchange of the indices i and j can be written as

$$\int_{-\infty}^{\infty} f_2^{kl}(\mathbf{q}) \varphi_i^*(\mathbf{q}) \frac{\partial^2}{\partial q^{(k)} \partial q^{(l)}} \varphi_j(\mathbf{q}) \, \mathrm{d}\mathbf{q} = \int_{-\infty}^{\infty} f_2^{kl}(\mathbf{q}) \varphi_j^*(\mathbf{q}) \frac{\partial^2}{\partial q^{(k)} \partial q^{(l)}} \varphi_i(\mathbf{q}) \, \mathrm{d}\mathbf{q}, \tag{3.6}$$

which is exactly the hermiticity condition $T_{ij}^* = T_{ji}$ for every integral of the sum in Eq. (3.3).

However, the situation is different when collocation is used. Since no integrals have to be evaluated anymore, the condition for hermiticity of one summand with real basis functions can be written as (considering that all summands of the sum in (3.5) have to be equal independently):

$$f_2^{kl}(\mathbf{Q_i}) \varphi_j^{(kl)}(\mathbf{Q_i}) = f_2^{kl}(\mathbf{Q_j}) \varphi_i^{(kl)}(\mathbf{Q_j}), \quad \text{with} \quad \varphi_j^{(kl)}(\mathbf{Q_i}) = \frac{\partial^2}{\partial q^{(k)} \partial q^{(l)}} \varphi_j(\mathbf{Q_i}), \tag{3.7}$$

resp. for the first derivative terms

$$f_1^{k}(\mathbf{Q_i}) \varphi_j^{(k)}(\mathbf{Q_i}) = f_1^{k}(\mathbf{Q_j}) \varphi_i^{(k)}(\mathbf{Q_j}), \quad \text{with} \quad \varphi_j^{(k)}(\mathbf{Q_i}) = \frac{\partial}{\partial q^{(k)}} \varphi_j(\mathbf{Q_i}). \tag{3.8}$$

With the same argumentation as above the index change for a basis function does not change its functional form, but only its position on the grid. The meaning of an index change for the pointwise basis function evaluation is illustrated in Fig. 3.1, from which is deduced that for a set of mirror symmetric functions the condition $\varphi_i(Q_j) = \varphi_j(Q_i)$ is always true, while for point symmetric functions the condition $\varphi_i(Q_j) = -\varphi_j(Q_i)$ is fulfilled (not shown). Assuming any kind of symmetry for the basis functions and their derivatives with respect to their center, the products in Eqs. (3.7) and (3.8) can only be equal if the kinetic functions fulfill the condition $f_2^{kl}(\mathbf{Q_i}) = f_2^{kl}(\mathbf{Q_j})$ in case of symmetric second derivatives or $f_2^{kl}(\mathbf{Q_i}) = -f_2^{kl}(\mathbf{Q_j})$ in case of antisymmetric second derivatives. The same applies for $f_1^{k}(\mathbf{Q_i})$. Since these conditions have to hold for *all* pairs of i and j hermiticity can only be present if the kinetic functions have a constant absolute value on the grid, which is only true in special cases. The first derivatives of the used Interpolating Gaussians have

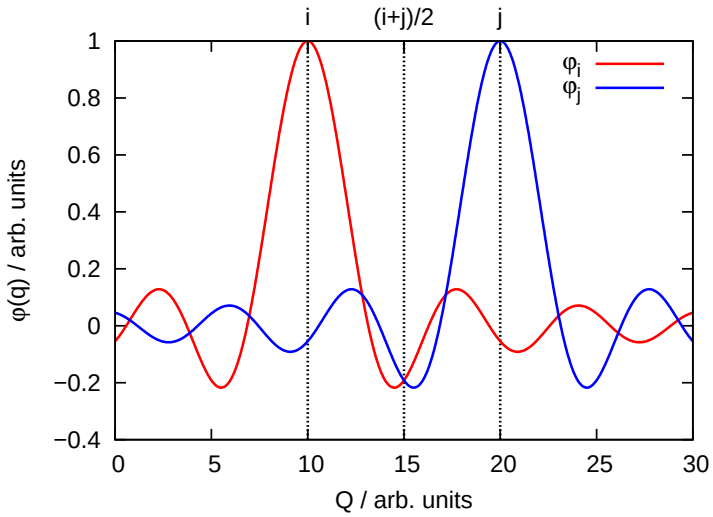

Figure 3.1: Effect of an index change for a symmetric basis function. Here two identical (arbitrary) symmetric functions are shown (φ_i and φ_j), which are shifted with respect to each other on the q-axis by 10 units. Due to their mirror symmetry the two functions φ_i and φ_j are not only shifted but also mirror images with respect to the line half way between i and j (which is located at $Q = (i+j)/2$). From this can be followed that also the value of the function remains unchanged upon index change ($\varphi_j(Q_i) = \varphi_i(Q_j)$), since this is just a special pointwise interpreation of the formerly stated mirror symmetry at two given points Q_i and Q_j.

point symmetry, while the second derivatives show a mirror symmetry with respect to their center.

First, the simplest possible KEO will be considered. For example, in cartesian coordinates all f_2^{kl} with $k \neq l$ and f_1^k are zero and all f_2^{kk} are constant on the grid. Since the second derivatives of interpolating Gaussians $\varphi^{(kk)}$ are symmetric it can be concluded that $\varphi_i^{(kk)}(\mathbf{Q_j}) = \varphi_j^{(kk)}(\mathbf{Q_i})$. So in this very simple case eq. (3.7) is true and hermiticity is preserved.

For arbitrary systems the symmetry of the basis functions does not change, but the kinetic functions are more complicated. They do not have a constant value on the grid in general and the terms for mixed second derivatives f_2^{kl} with $k \neq l$ and for first derivatives f_1^k may not be neglected. As stated above, due to the symmetry of the basis functions, hermiticity can only be present in general if the kinetic functions have a constant absolute value. So the collocation method destroys the hermitian properties of the kinetic energy matrix.

In our numerical applications non-hermiticity did not lead to substantial problems as the numerical differences of T_{ij} and T_{ji}^* were not very large. However, this could change if different systems are under investigation. Especially for systems with strongly varying kinetic functions $f_1^k(\mathbf{q})$ and $f_2^{kl}(\mathbf{q})$, collocation has to be handled with caution. A possible way to avoid difficulties with non-hermitian Hamiltonians (i. e. complex eigenvalues) is to apply the approximation of simply symmetrizing the

Table 3.1: Sparsity of Hamiltonian for H_2O test system. For the Z-Matrix calculation all kinetic functions have to be included, while in the cartesian coordinate system all f_2^{kl} with $k \neq l$ and f_1^k are negligible, which increases sparsity. For more detailed information refer to the text.

	Cartesian	Z-Matrix
2D	89.20 %	0.00 %
3D	99.11 %	84.24 %

Hamiltonian matrix after construction by averaging, which is a drastic procedure, if the values of T_{ij} and T_{ji}^* differ significantly.

3.4.2 The Benchmark System

The photodissociation dynamics of NOCl as a benchmark application for the adaptive basis representation has some advantages compared to general applications. As the system is described in Jacobi coordinates (with the three DOFs (R, r, γ)) all kinetic functions f_2^{kl} with $k \neq l$ and f_1^k are zero (which can also be seen in the analytical form of the Hamiltonian in Jacobi coordinates, e.g in Ref. [58] for this particular system). As furthermore the coefficients f_2^{11} and f_2^{22} are constant and f_2^{33} only varies slightly on the grid, the Hamiltonian is numerically perfectly hermitian. More essential is the fact that the sparsity of the Hamiltonian increases the more kinetic functions vanish on the grid. The number of non-zero elements may increase drastically in the general case, where all f_2^{kl} with $k \neq l$ and f_1^k are actually present, which would decrease the numerical savings, both memory and speed. Nevertheless, the basic assumption that in general sparsity increases with higher dimensionality is unaffected.

Table 3.1 illustrates the different degree of sparsity for a simple example. The sparsity of Hamiltonian matrices for 2D and 3D calculations is analyzed, comparing cartesian coordinates, where all f_2^{kl} with $k = l$ are constant and all f_2^{kl} with $k \neq l$ and f_1^k are zero, with the same system in Z-matrix coordinates where all kinetic functions have to be included. Reduced masses for H_2O are used in combination with two Morse potentials in case of the 2D calculations. For the 3D systems a harmonic oscillator is added in the third coordinate, which is the angle in case of Z-matrix coordinates. 18 grid points and basis functions (Interpolating Gaussians with Collocation) are used. Hamiltonian elements are considered to be negligible if they are smaller than $1 \cdot 10^{-8}$ a.u. The calculations show a significantly increased sparsity for cartesian coordinates and for higher dimensionality. In case of the 2D Z-matrix calculation even the dense Hamiltonian is completely required.

These numbers might lead to a misinterpretation: The use of cartesian coordinates is still disadvantageous compared to internal coordinates in most cases. Here, two calculations of the same dimensionality are compared. However, this situation

is not realistic, as a full-dimensional discription in cartesian coordinates requires six DOFs more than in internal coordinates. Also for reduced-dimensional considerations usually more active DOFs are required in cartesian coordinates than in internal coordinates, as explained earlier. In case perfect sparsity would be achieved still the diagonal of the Hamiltonian is needed. The number of entries on the diagonal is the number of total grid points, which scales exponentially with dimensionality. So the curse of dimensionality outweighs the benefits of higher sparsity, if more DOFs have to be included.

3.4.3 Computational Details

Frequency of Coefficient Checks

For the usage of the adaptive basis representation two time propagation schemes have been implemented in the MrPropa program: Symplectic Integrators (see section 2.3.3) and the Taylor expansion (see section 2.3.4). The first is a modern and universal propagation scheme, which has the main drawback that it is not able to propagate in imaginary time. The latter does not have this deficiency, which makes the adaptive basis representation also available for the calculation of stationary states with the relaxation method.

In the Symplectic Integrators scheme the Hamiltonian is applied various times on the wavefunction depending on the order of the used scheme (cf. parameter m in section 2.3.3). Using SI in combination with the adaptive basis representation leads to the question when the coefficients checks are carried out. One possibility is to wait until all m operations of the Hamiltonian on the wavefunction are done, hence the check will be conducted after a complete time step. Alternatively a check could be performed after each operation of $\hat{H}$ on ψ. This would require m coefficient checks and basis adjustments per time step. The first alternative is expected to be faster, while the second should be more precise. It is to be examined whether the accuracy is sufficient when the coefficients are only checked after the complete time step has been performed.

Additionally, the coefficient check frequency may be reduced further. Depending on the system and time step it may be sufficient to monitor the coefficients only after a given number of time steps, for example every second or fourth time step. Fig. 3.2 shows that the impact of the check frequency on the total grid size is surprisingly small. Apprearently the moving speed of the wavepacket and therefore the change of its expansion coefficients is not high enough to require a coefficient check at every time step. However, if the update of active coefficients is not perfomed frequently enough the propagation may fail. Time step and coefficient check frequency have to be in an "equilibrium" in order to achieve numerically stable and fast propagations. So the setup with the highest performance has to be tested system specifically. It has been verified that a coefficient check after every action of the Hamiltonian on the

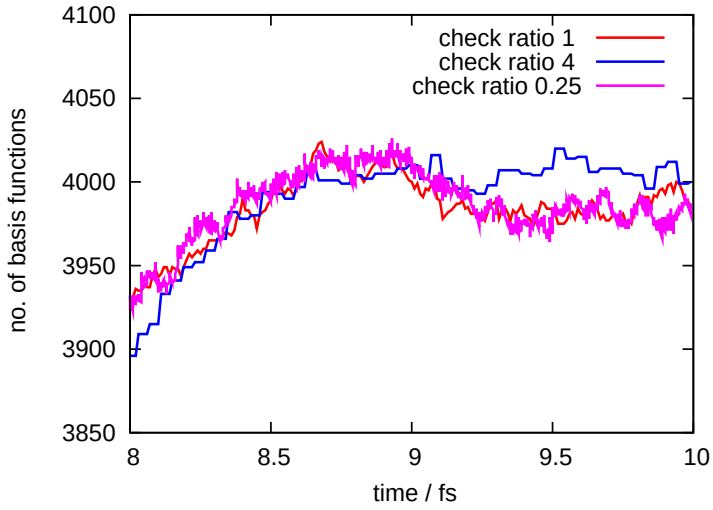

Figure 3.2: Grid size of 2D H_2O test calculation with parameters mentioned in the text. The check ratio is defined as a number of time steps per coefficient check. Grid sizes do not differ significantly, the resulting autocorrelation functions (not shown) do not deviate from each other (visually). However, computational expenses for the calculation can be decreased by performing less frequent coefficient checks: Timings for this calculation on the test machine were 0:48 h for check ratio 4, 1:16 h for check ratio 1 and 3:08 h for check ratio 0.25.

wavefunction is usually not necessary and the additional computational effort cannot be compensated by a larger time step. The current implementation in MrPropa offers the possibilty to perform coefficient checks either most frequently after every SI-iteration, after every time step or after a given number of time steps.

Absorbing Potentials

For the 3D application, the photodissociation of NOCl, a CAP has been employed in the dissociative coordinate. Parts of the wavepacket traveling into a dissociative channel do not experience reflections back to the region of interest whenever the dissociacion channel does not show any sharp bends (kinematically dissociative) and the energy is monotonically approaching a constant value (energetically dissociative). In case of a traditional fixed grid calculation a CAP is also required to avoid unphysical reflections of the wavepacket from the grid boundary. In the adaptive basis representation no such grid boundaries exist, but the grid would be enlarged constantly in the dissociation channel. So it is advisable to use an absorbing potential there for two reasons. First, the used pre-calculated PES is of finite size, which would be exceeded, and second, the larger grid size would increase the numerical effort without gain of new physical information.

In section 2.5 CAPs have been presented for traditional representations. They require the parameter $q^{\max}$, which denotes the end of the grid. As in the adaptive basis representation no such parameter exists, the functional form has to be slightly

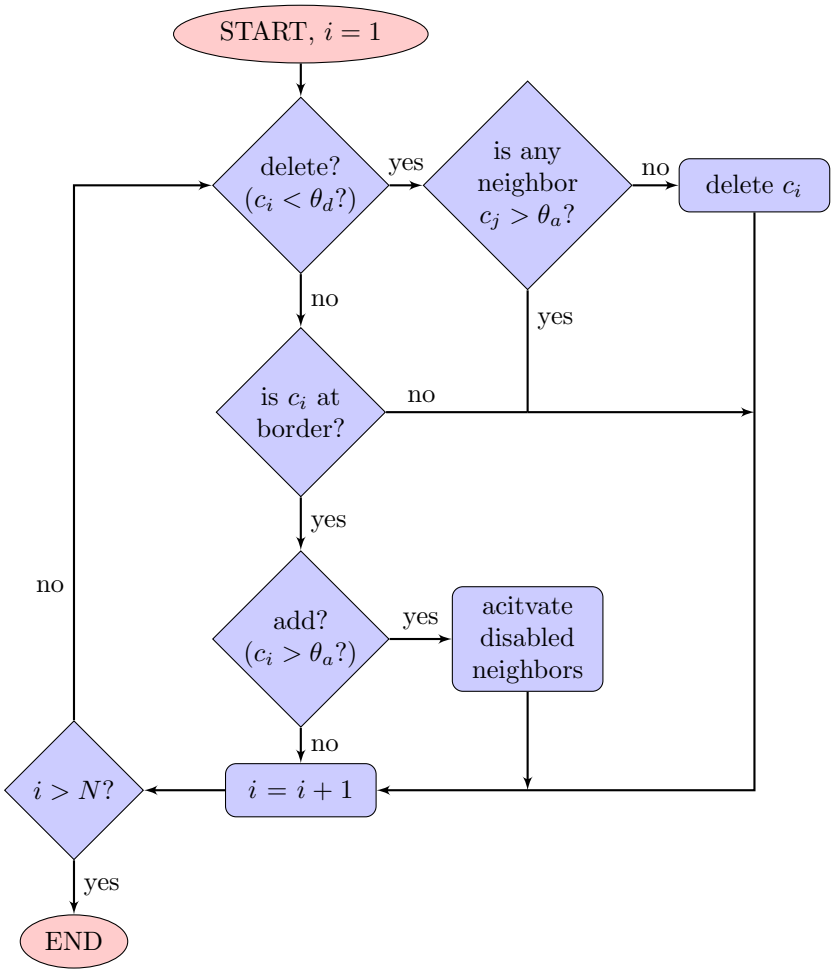

Figure 3.3: Flow chart of PRODG algorithm. c_i denotes the indexed wavefunction expansion coefficient, with a total number of N grid points. θ_a and θ_d mark the thresholds explained in section II of the paper. Basis adaption only occurs if $\theta_d < \theta_a$.

adjusted to this new situation. It has been found that the choice $q^{\max} = q^0 + 20\Delta q$, where q^0 is the starting point of the CAP and Δq is the grid spacing, yields good results. Of course, the arbitrary choice of the CAP's width of 20 grid points can be varied and adjusted system specifically. It corresponds to the strength of the CAP.

Computational Demands

In Fig. 10 of this chapter's publication the time expenses for the PRODG approach were shown. Most of the time is used for the overhead of the new method while only a small fraction of the time is spent on the actual propagation. Of course, here are great possibilities for further enhancement of the method. The flow chart in Fig. 3.3 displays the algorithm used to determine which coefficients are to be activated or deleted in the adaptive basis representation. The most time consuming operation of this part is to check the activation status of neighbor coefficients. This occurs in two situations. First, in case c_i drops below θ_d the size of all active neighbor coefficients

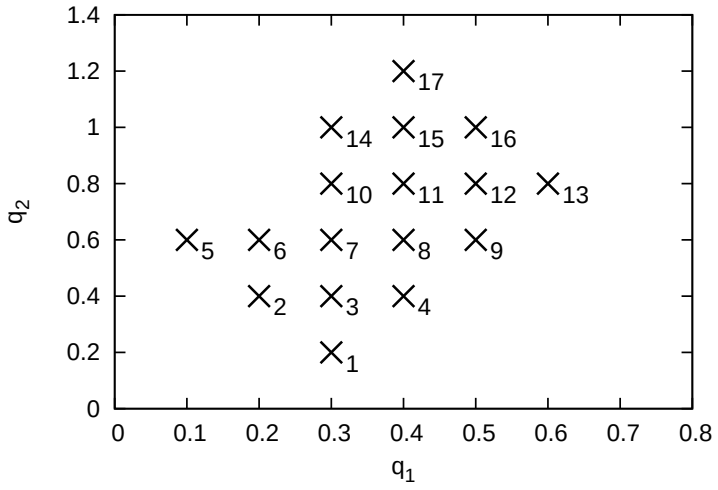

Figure 3.4: Grid of active expansion coefficients exemplifying a two-dimensional wavefunction and indices used in the indexed vector array.

has to be evaluated to check if they are larger than the enlargement threshold θ_a. Second, if c_i rises above θ_a all disabled neighbors of c_i have to be activated. To avoid the neighbor-check for coefficients that are in the "bulk" of the wavefunction a separate array stores the information if a coefficient already has the maximum number of neighbors (two per active dimension) or not. So the neighbor search only has to be performed for coefficients, that are larger than the threshold θ_a and do not yet have all neighbor coefficients activated.

After determination of the required modifications they actually have to be performed: All wavefunction based indexed arrays and the Hamiltonian matrix have to be adjusted. Some entries have to be deleted, new entries have to be calculated and sorted into the existing arrays. Keeping the arrays sorted is essential as the action of the Hamiltonian on the wavefunction is numerically a matrix-vector multiplication. This is only carried out correctly if the order (and therefore the grid point numbering) of the wavefunction coefficients is the same as in the Hamiltonian matrix. Involved in the resizing and reordering process are the Hamiltonian matrix including the new kinetic functions (TNUM) and the PES, the extra potential, the absorbing potential and the "flux box"[1]. The focus of this work was to demonstrate that the extension of the initial idea to higher dimensionality is straightforward in principle. Even in this quite basic implementation the FBR-based PRODG method came close to the traditional FFT method with respect to time and memory requirements. Improvements of the neighbor-check algorithm and data structure (which involves sorting) give rise to larger savings and is highly encouraged for future work.

[1] The flux is calculated by integration of a subspace of the complete configuration space (cf. section III.A of the paper). If a grid point is introduced into this area, also the integration has to include this new grid point.

The most time consuming part of the algorithm in its present implementation is the determination of the indices of neighboring coefficients. This can be understood with the help of the following example. Fig. 3.4 exemplifies the position of active expansion coefficients of a two-dimensional wavefunction. Assuming that coefficient 4 rises above the enlargement threshold θ_a it has to be found out where to activate new coefficients. Considering that a grid point has two direct neighbors per dimension, in this example four points have to be found and checked. The number of neighbors could also be defined differently by including grid points which are located diagonally. It is not expected that this choice makes a big difference. When including the "diagonal" neighbors every grid point in this two-dimensional example may be activated by a maximum number of eight grid points opposed to four grid points when just including two direct neighbors per dimension. As adjacent grid points have similar absolute values, a non-active gridpoint would only be activated by more than one neighbor when the wavepacket is moving. This redundancy would presumably only cause numerical costs without the gain of physically relevant information.

Looking back to the example stated above: Already active neighbors of grid point no. 4 are coefficients 3 and 8. In the current implementation, in order to find out if the neighboring coefficients 3 and 8 are present the coordinates of active coefficients are compared to the (known) real valued coordinates of the neighbor (e. g. (0.3, 0.4) for coefficient 3), which causes high computational cost.

As a second step two new coefficients have to be introduced. One has to be placed to the right of coefficient 1 and one to the right of coefficient 4. Introducing these two coefficients in the indexed wavefunction array changes almost all indices of the old coefficients. Because of the permanent renumbering the information about two neighboring coefficients is lost, e. g. after the introduction of the new coefficient 2 to the right of coefficient 1, coefficients 1 and 3 are no longer direct neighbors, but now no. 1 and 4 are neighbors as the label for the former coefficient 3 changed to 4. In order to keep track of this information the real valued grid coordinates are saved for all active coordinates. They are stored in an array in a characteristic order and, thus, the position of the coordinates in the array points to the index number of the grid point. Similar difficulties arise upon the deletion of coefficients, as the sizes of neighboring coefficients have to be checked before actual deletion (see flowchart Fig. 3.3).

One possible way to avoid saving this information would be to place an imagined indexed maximum grid in the background. Having a fixed number of grid points per dimension allows to determine the index of all neighbors on this imagined grid analytically.

3.5 Outlook

The results presented in the paper are encouraging for larger applications. The current implementation has technical limitations mainly concerning the speed of insertion and deletion of elements, but even in this implementation for 3D calculations a significant speedup compared to traditional FBR is reported and computational costs come even close to FFT. In general, higher-dimensional problems give rise to even larger savings. However, to achieve this numerically, the implementation has to be enhanced. Improvements of the data structure for the Hamiltonian matrix and corresponding the wavefunction-based vectors are developed in a collaboration with E. Steffen and S. Börm (Univ. Kiel). In the framework of a master thesis E. Steffen develops a *tree* data structure, which is optimized for constantly adding and deleting entries and thus offers the perspective for an efficient calculation of larger applications. It is also well-suitable for distributed computing on several CPUs, which gives rise to a substantial speed up of the calculations. As the ongoing work of this collaboration coincided with the work of this thesis the applications of the remaining chapters have not been computed in the novel adaptive basis representation, but have already been carried out before an improved implementation was available. This strategy ensured simultaneous progress in several areas.

The proDG adaptive basis representation offers the possibility to realize *on-the-fly* quantum-dynamical calculations. Beginning with a start wave function no further information is required. Calculation of the potential energy can be performed analytically (if available) or using interfaces to quantum chemistry programs. By propagating the wavepacket fully quantum-dynamically new gridpoints are activated without any other information and all necessary values for the new Hamiltonian matrix elements can be calculated on-the-fly. The potential energy V and the kinetic functions f_1^k and f_2^{kl} (eqs. 2.110 and 2.109) are all solely geometry dependent. Up to this point the current implementation already provides the possibility of on-the-fly wavepacket dynamics. Future extensions could include the analytical evaluation of matrix elements as an analytical integration of the interpolation Gaussian basis functions can easily be done. However, an analytical representation of the PES and the KEO would be necessary. Efficient interpolating schemes allow for the reduction of points where the potential has to be calculated. The imagined background grid is well-suited for standard interpolation schemes because it is equally spaced.

4

Quantum-Dynamical Investigations into Double-Minimum Potentials

4.1 Scope of the Project

In textbooks the energy profile along a "reaction coordinate" traditionally consists of two local minima, reactants and products, which are divided by a local maximum. This maximum is usually narrow, for example close to a Gaussian function and called the transition state. The reaction may also proceed over two transition states separated by a third local minimum, the intermediate, which is higher in energy than the products. In-between cases are usually not considered. However, it has been found that different transition states can exist, that show a plateau-like shape [122–124]. Theories for usual transition states, such as the transition state theory (TST) or its variational extension, fail to describe such systems. Rauhut and coworkers [125] identified the double proton transfer reaction (DPTR) in the pyrazole-guanidine cluster to exhibit such a delocalized transition state structure. To study its characteristics they applied the reaction path Hamiltonian (RPH) [126] using classical mechanics. Von Horsten *et al.* [127, 128] have studied this DPTR quantum-dynamically using reduced-dimensional models with partly analytical model PESs. Other prominent DPTR systems are carboxylic acid dimers, which are well investigated theoretically (e. g. [129, 130]). In general, proton transfer reactions are well-known as they play a key role not only in DNA base pairs [131, 132] but also in many other biochemical reactions [133–137].

In order to exploit the dynamical behavior of such systems with more explicitly treated DOFs and to extend the work of von Horsten *et al.*, PESs have to be calculated for the complete space of active coordinates. As the number of grid points scales exponentially with dimensionality of active coordinates this is a tedious task, for which it is mandatory to develop more intelligent evaluation schemes. Performing lower level quantum-chemical calculations is not a possibility since DPTRs require a high level of quantum chemistry. Otherwise the plateau would not be calculated correctly and would fade to either the standard Eckart or the case with a reactive

intermediate. A close collaboration with G. Rauhut (Univ. Stuttgart) supported by the German Science Foundation (DFG) via joint grant Ha2498/6 – Ra 656/9-1 enabled the link between efficient PES generation and reduced-dimensional quantum dynamics.

The PES of any system can be expanded in a series of many-body contributions. This allows for efficient calculation of high-dimensional (or even full-dimensional) PESs as the series may be truncated after the three-body or four-body terms in many cases. So a minimized number of quantum chemical single point calculations have to be performed, which enables the use of highly accurate methods. Such so-called n-mode representations have been used with different coordinates before and applied for the calculation of static spectra around the minimum structure [105,106, 138–140]. Fitted to a suitable analytical expression the highly accurate PES may be used as input for the quantum-dynamical calculations. This offers the possibility to investigate and compare different reduced-dimensional models with varying active coordinates without the burden of generating a new PES for every calculation.

4.2 Project Objectives

With DPTR and plateau reactions as ultimate goals it is a suitable pre-exercise to deal with regular double-minimum potentials. Acting as model systems the tunneling splitting of H_2O_2 and its isotopologues and the cumulative reaction probability of PHDCl have been studied. The main focus was set on the realization of a highly general and flexible interface between PES generation and quantum dynamics. In contrast to prior work the n-mode expansion is performed around the transition state in order to describe the double-minimum optimally. From the dynamical point of view it has been achieved to use highly accurate PESs by means of a purely analytical evaluation of a polynomial fit to *ab initio* data, which has to be performed only once in advance of the dynamical calculations. So the present publication illustrates the ability to extend the use of n-mode representations away from static spectra which are evaluated around the minimum structure to chemical reactions.

Calculations for other chemical systems including single and double proton transfer reactions have been attempted but were not realized yet. The occurring difficulties will be explained in more detail in the last part of this chapter. The main problem was to find a suitable coordinate system for the molecular systems under investigation. After thoroughly testing and comparing normal mode coordinates with internal Z-matrix coordinates it has been found that calculating the n-mode representation in Z-matrix coordinates is superior to propagation with the Watson-Hamiltonian in normal mode coordinates. Extension to other molecular systems including DPTRs may be a topic of future work.

4.3 Towards Automated Multi-Dimensional Quantum-Dynamical Investigations of Double-Minimum Potentials: Principles and Example Applications

Own contributions presented in the paper:

- Implementation of PES evaluation with polynomial fit data
- Quantum-dynamics calculations of hydrogen-peroxide
- Interpretation of numerical results

Additional work within this project, not presented in the paper:

- Relaxed PESs from fit data
- Normal mode to internal coordinate transformations, tested for various molecules
- Propagation in normal mode coordinates: The Watson-Hamiltonian

Abstract

A multi-coordinate expansion of potential energy surfaces has been used to perform quantum dynamical calculations for reactions showing double-minimum potentials. Starting from the transition state, a fully automated algorithm for exploring the multi-dimensional potential energy surface represented by arbitrary internal or normal coordinates allows for an accurate description of the relevant regions for vibrational dynamics calculations. An interface to our multi-purpose quantum-dynamics program MrPropa enables routine calculations for simple chemical reactions. Illustrative calculations involving potential energy surfaces obtained from explicitly-correlated coupled-cluster calculations, CCSD(T)-F12a, are provided for the tunneling splittings in the isotopologues of hydrogen peroxide and for reaction dynamics based on the enantiomeric inversion of PHDCl.

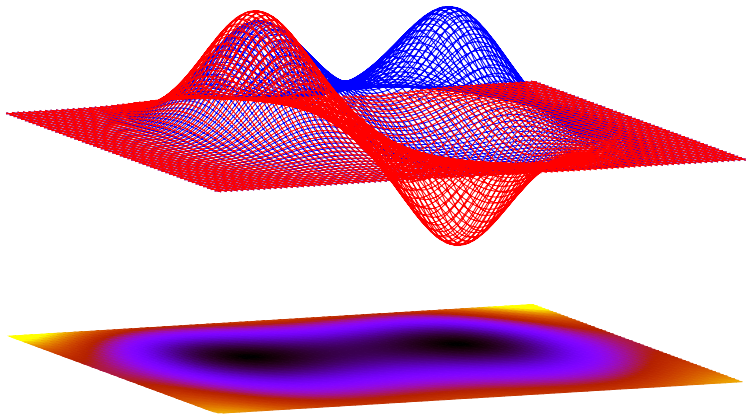

Chemic. Phys., **2010**, in press, corrected proof

Available online June 22, 2010
DOI: 10.1016/j.chemphys.2010.06.018

4.4 Additional Information

4.4.1 Relaxed PESs

As explained in section 2.7.1, for any reduced-dimensional dynamical treatment one has to decide how to handle the inactive DOFs. While the theory of the KEO is getting complicated, there are two simple main approaches for the potential part of the Hamiltonian. Either the inactive coordinates are held fixed at a reference geometry, e. g. a minimum or transition state structure (rigid model, section 2.7.1) or the nuclear coordinates of the remaining DOFs are allowed to relax locally, meaning that a constrained geometry optimization with fixed values for the active coordinates at every grid point (see relaxed model, section 2.7.2) has to be performed. The physical difference between the two models is the following. When performing dynamics on fully relaxed PESs it is assumed implicitly that all other DOFs adjust to the molecular structure changes *instantaneously*, while in the rigid model all inactive nuclei move infinitely slow, hence, do not adjust to the changed molecular structure *at all*. The physical effects of these two models are also included in the discussion of the publication in chapter 5.2, where a relaxed PES is used to describe the photochemical ring-opening reaction of cyclohexadiene. Figure 4.1 shows the differences between one-dimensional cuts through the hydrogen-peroxide PES along the dihedral angle. The presented relaxed and rigid *ab initio* PESs are calculated at two different levels of theory. For the CCSD(T)-F12a-level of theory the rigid barrier height is 4.05 kJ/mol, while the relaxed calculations yield a barrier height of 4.44 kJ/mol. The barrier height increases in the relaxed model as the molecule may relax into the global minimum.

In the previous publication the PESs are calculated by analytical evaluation of polynomial fits to *ab initio* points. For that, only the active coordinates are changed from the reference geometry, corresponding to the rigid model. In order to switch

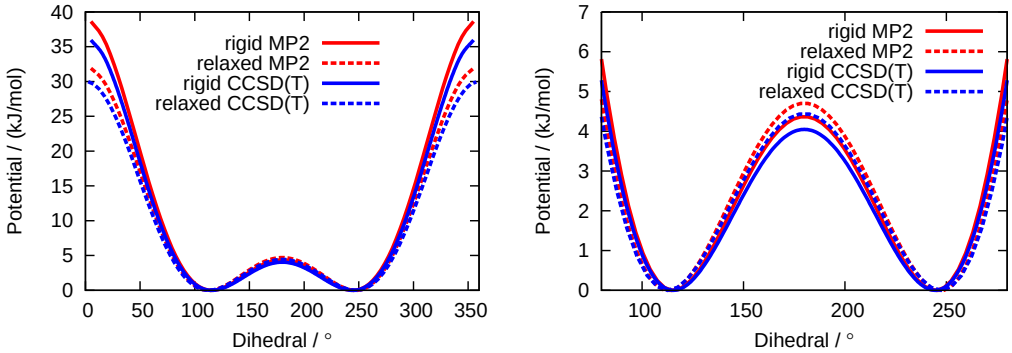

Figure 4.1: Differences between rigid and relaxed model. One-dimensional cut through the H_2O_2 PES along the dihedral angle. All other coordinates are either held fixed at their TS geometry (rigid) or local geometry optimizations were performed (relaxed). The right panel shows an enlargement of the transition state region. Levels of theory: CCSD(T)-F12a/tzvp and MP2/vdz.

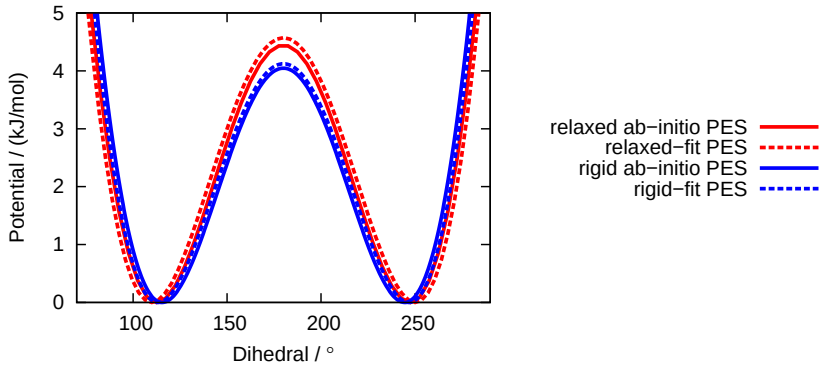

Figure 4.2: Deviations of polynomial fits (dashed lines) from *ab initio* (CCSD(T)-F12a/tzvp) data (solid lines). Cut through relaxed and rigid H_2O_2-PES along dihedral angle.

to the relaxed model local geometry optimizations would have to be performed at every grid point. However, since the set of *ab initio* points is calculated in the full-dimensional configuration space and fitted afterwards it is sufficient to minimize the resulting energy of the analytical polynomial function with respect to the inactive DOFs while the values of the active coordinates are held fixed. This will be refered to as a *relaxed fit* in the following. Since a polynomial features analytic first derivatives minimizations can easily be done with local optimization subroutines from the literature. This enables a very efficient way of obtaining relaxed PESs as local optimizations with the analytic PES are much faster than on any *ab initio* level.

The six lowest eigenstates of a relaxed 1D PES were presented in this chapter's publication. The used PES was calculated by performing 36 constrained quantum chemical geometry optimizations. As stated above, it is also possible and faster to calculate relaxed PESs with local optimizations of the analytic fit data. However, the numerical quality of the relaxed fit has to be checked. Fig. 4.2 compares both relaxed and rigid PESs in a one-dimensional cut through the H_2O_2 PES along the dihedral angle, which are evaluated either by *ab initio* calculations (CCSD(T)-F12a, solid lines) or with the polynomial fit data (dashed lines). The resulting barrier height for the rigid *ab initio* PES is 4.05 kJ/mol (4.12 kJ/mol for the fit). For the relaxed system it increases to 4.44 kJ/mol (4.57 kJ/mol for the fit). Table 4.1 compares the resulting eigenenergies for the relaxed *ab initio* (Table 2 of this chapter's publication) and the relaxed fit PES. The numbers for the relaxed fit are not of sufficient accuracy yet so the quality of the relaxed fit has to be improved. There are two possible error sources: first, the polynomial fit itself can be improved, for example by using more *ab initio* points or enlarging the order of the fit-polynomial. Second, the accuracy of the (constrained) local minimization routine can be enlarged. For higher-dimensional calculations the (constrained) local optimization of the polynomial becomes even

Table 4.1: Torsional spectrum of H_2O_2 in cm^{-1}, relative to the fundamental. The eigenstates are calculated on relaxed PESs in a one-dimensional cut through the H_2O_2 PES along the dihedral angle, which are calculated either by constrained quantum chemical geometry optimizations directly or by using a locally minimized polynomial fit.

ab initio relaxed	relaxed fit
12.8	10.6
250.4	249.8
371.3	365.3
570.2	563.2
777.8	772.5
1002.7	1002.8

more problematic. Since the polynomial fit quality decreases for bigger elongations from the reference structure also the local minimization of the polynomial becomes less stable. Especially if the 3- and 4-mode terms have large contributions the minimization fails to converge as these terms itself tend to diverge near the border of the grid.

4.4.2 Coordinate Transformations

Initially the n-mode representation was implemented using normal mode coordinates. These coordinates describe elongations from a reference geometry along eigenvectors of the Hessian matrix. A normal mode analysis is carried out in every frequency calculation of quantum chemical programs. The MrPropa program (section 2.8) is optimized for the use of cartesian or internal Z-matrix coordinates, though, which offers the use of the interfaced Tnum framework (section 2.6.2) in order to calculate the KEO. Apart from that, normal mode coordinates have found to be inferior for dynamics [72, 73], as they are describing motions of the nuclei at small distortions from the minimum structure only.

As a consequence, the coordinates used for the potential and the kinetic part of the Hamiltonian differ. To overcome this problem there are two strategies. Either a suitable coordinate transformation has to be performed between the two different representations or the coordinate representation of one part of the Hamiltonian has to be changed to match the other one from the beginning. In the first case, at any given grid point the molecular geometry in internal coordinates (used in the kinetic part) has to be converted to normal mode coordinates (used in the potential part) so the potential energy at this grid point can be evaluated. The second strategy requires to synchronize the representation of the Hamiltonian. So either the quantum-dynamical calculations have to be performed in normal mode coordinates or the PES fit has to be supplied in internal coordinates. Changing the kinetic part of the Hamiltonian to normal mode coordinates is possbible with the so-

called Watson-Hamiltonian. However, keeping the KEO in curvilinear coordinates has been found to be superior to all aforementioned approaches and has therefore been used in the publication presented before. Nevertheless, since all strategies were subject of this thesis their advantages and disadvantages will be described and discussed in the following.

Numerical Transformation from Normal Modes to Internal Coordinates

Normal mode coordinates are, in a sense, a special case of cartesian coordinates, hence, in an N-atom molecule every normal mode consists of $3N$ components. Z-matrix coordinates dispose of the information about spacial orientation of the molecule and hence only employ $3N-6$ DOFs. The coordinate transformation from Z-matrix to normal mode coordinates is problematic due to this fact and, in contrast to many other coordinate transformations, it is ambiguous in this direction, but not in the other way around. Using this unambiguous back-transformation it is possible to accomplish the coordinate transformation numerically. This strategy will be described in the next paragraphs.

In case the n-mode expansion

$$\begin{aligned} V(q_1, q_2, \ldots, q_{3N-6}) &= \sum_i V_i(q_i) + \sum_{i<j} V_{ij}(q_i, q_j) \\ &\quad + \sum_{i<j<k} V_{ijk}(q_i, q_j, q_k) + \ldots, \end{aligned} \tag{4.1}$$

and hence the polynomial fit, is done in normal coordinates at every grid point of the propagation the task is to find the coordinates $\mathbf{q} = (q_1, q_2, \ldots, q_{3N-6})^T$ that correspond to a given molecular structure in Z-matrix coordinates. This coordinate transformation can be understood as a high-dimensional root search: Normal mode coordinates refer to specific elongations from a reference structure $\mathbf{X}_0$ in cartesian coordinates. So the aim is to find the amplitudes q_i of the displacements of different normal modes $\mathbf{N}_i$ in order to match the requested molecular structure $\mathbf{Z}_{\text{req}}$. A test geometry $\mathbf{Z}_{\text{test}}$ is determined through

$$\mathbf{X}_0 + \sum_i q_i \mathbf{N}_i = \mathbf{X}_{\text{test}} \rightarrow \mathbf{Z}_{\text{test}}, \tag{4.2}$$

where the coordinate transformation from $\mathbf{X}_{\text{test}}$ to $\mathbf{Z}_{\text{test}}$ is unambiguous in contrast to its back-transformation.

In case the correct displacement vector $\mathbf{q}$ is found the test structure matches the requested structure for the given grid point, so

$$\mathbf{Z}_{\text{req}} - \mathbf{Z}_{\text{test}} = 0. \tag{4.3}$$

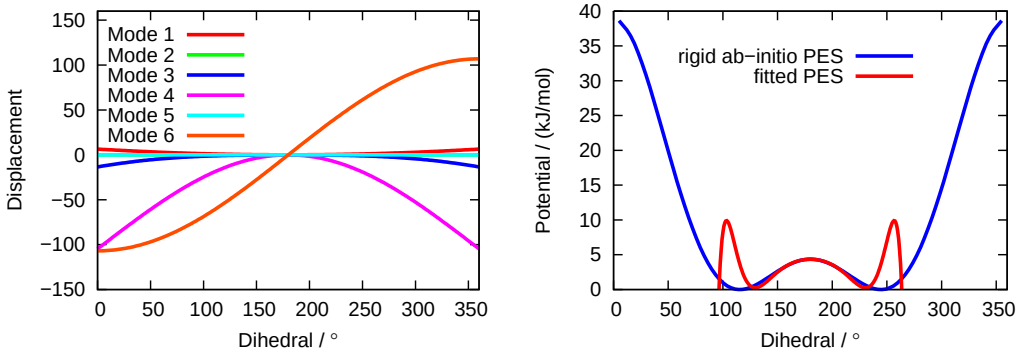

Figure 4.3: a) Normal mode coordinates displacement vectors as a function of the H_2O_2 dihedral angle to describe the one-dimensional PES cut. Modes 4 and 6 strongly dominate. b) Resulting PES demonstrating the poor fit quality at larger elongations from the TS structure. This can possibly be enhanced by a larger fit range, but not as much as needed.

Since $\mathbf{Z}_{\text{test}}$ is a function of $\mathbf{q}$ Eq. (4.3) can be regarded as a $(3N-6)$-dimensional root search. This search may find numerous solutions, which have to be judged manually or by chemical intuition.

Numerical Results for H_2O_2 The displacement vector $\mathbf{q}$ (Eq. (4.2)) for a rigid scan of the dihedral angle is shown in Fig. 4.3 (left). The resulting PES (right) shows substantial deviations from the *ab initio*-PES at larger displacements from the TS. One possible reason for the large deviations is visualized in Fig. 4.4. The picture shows the -20-fold value of the elongation from the reference structure in the "dihedral" mode 6. Clearly, mode 6 contains contributions not only from the HOOH dihedral angle but also from OH stretches. For small elongations, the latter contributions are insignificant, but for larger ones they become intolerably large and have to be compensated by negative elongations in mode 4 (see Fig. 4.3). For example, to reach the rigid PES minimum structure (dihedral $= 112°$) the displacement vector exhibits entries as large as -17.7 for mode 4 and -59.2 for mode 6.

Figure 4.4: Visualizing the inferior role of normal mode coordinates for dynamical calculations. The picture shows the -20-fold value of the elongation from the H_2O_2 transition state structure in mode 6. For displacements as large as this one the so-called dihedral mode also contains OH-stretch contributions, which have to be compensated by negative elongations in mode 4 in order to describe the dihedral angle (see Fig. 4.3).

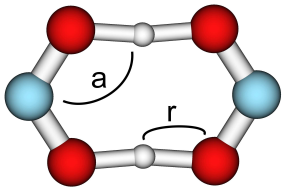

Figure 4.5: Relevant coordinates (r_{OH} and a_{NOH}) for the double proton transfer reaction in the HNO_2 dimer. Color code: O (red), N (blue), H (white).

There is no problem in principle to find the correct displacement vector $\mathbf{q}$ but there are a number of disadvantages appearing. First, a $(3N-6)$-dimensional root search has to be performed for *every* grid point included in the dynamics. The numerical effort per grid point is *not* dependent on the number of active DOFs, so it is not possible to reduce the numerical costs for a given molecular system by freezing or neglecting certain normal modes. Second, the required elongations in regions far away from the transition state are too big in order to perform reliable *ab initio* calculations and to obtain an n-mode expansion which converges within the first few-body contributions.

Numerical Results for other molecules The numerical coordinate transformation has been tested for several different molecular systems, which involve double-minimum potentials or (double) proton transfers. Since reduced-dimensional models are available for the dynamics the size of the system is not of primary interest from this point of view (of course, quantum chemical calculations always scale with the size of the system). All tested systems encounter the same problems. In most cases the displacement vector exhibited entries that are too large for reliable corresponding quantum chemical calculations. Apart from this main difficulty a second problem may occur, which will be described for the HNO_2 dimer (see Fig. 4.5) in the following.

For the double proton transfer reaction in the HNO_2 dimer only few major internal coordinates are involved: two OH-distances with corresponding NOH-angles. Due to symmetry these four internal coordinates can be reduced to just two if each of them is forced to have the same value than the symmetry equivalent one.[1] Again, the PES has been calculated as n-mode representation around the transition state, where the H-atom is equally spaced between the two O-atoms. Before calculating the "full" two-dimensional PES two one-dimensional cuts along both coordinates were considered.

For the one-dimensional cut along the OH-distance the result of the root search was encouraging, since the dominating modes 14, 17 and the imaginary mode 18 (see Fig. 4.6, left) are smooth and their maximal value can be covered by quantum

[1] In MrPropa this can be achieved by the *symmetry matrix*. See the manual (Ref. [61], section `zmatrix.in`) for details.

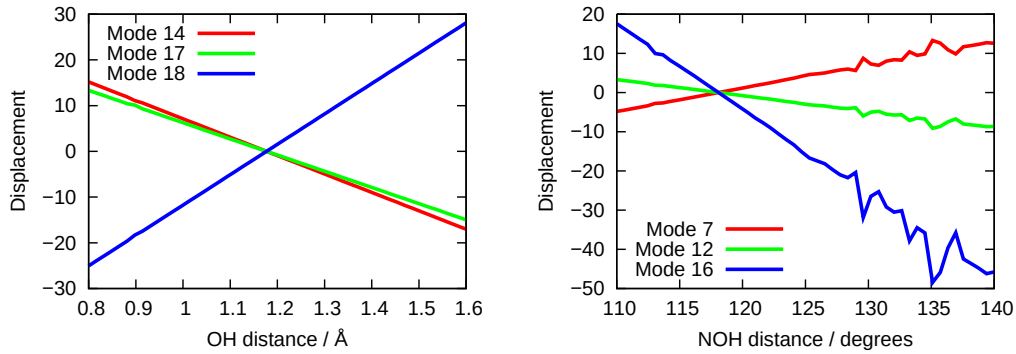

Figure 4.6: Elongations from reference structure in selected normal modes in order to match the rigid Z-matrix scan of the OH-distance (left) and NOH-angle (right). The high-dimensional root search does not yield smooth curves of the displacement vector.

chemistry. The root search for the cut along the NOH angle encountered severe problems, though. It did *not* fail to converge at any point, but as seen in Fig. 4.6 (right panel), it did not yield smooth curves for the displacement vector. There are 18 DOFs in this system, so a 18-dimensional root search has to be performed. Quite commonly many-dimensional root searches yield numerous results. Here, at some grid points the result did not match the results at the neighboring grid points. Of course, all curves have to show a smooth shape and must not have any kinks or sudden steps. For small elongations from the transition state structure the curves are smooth, but problems arise again in outer regions. It may be possible to overcome this problem by using more sophisticated root search algorithms, smarter initial guesses, or even an analytic transformation [141], but this was not topic of this work.

Conclusions: Coordinate Transformations

In order to cover the range necessary for the dynamics calculation the displacement vector exhibits large entries. It was shown that some large displacements caused by certain normal modes have to be compensated by others, which causes difficulties for the quantum chemical PES calculation and the quality of the fit. These problems become more severe when including more active DOFs in the dynamics as the n-mode representation seems not to converge within the first few-body contributions. Also in the current implementation the number of grid points for *ab initio* calculations is limited to 24 per mode, which entails a big grid spacing and hence reduced accuracy if large regions have to be covered.

Furthermore, a $(3N-6)$-dimensional root search has to be performed on *every* grid point. Due to the exponential scaling of grid points with dimensionality this will make this procedure infeasible for systems with more than three active DOFs. A second problem arises from the ambiguous result of the root search. It has to be

checked by chemical intuition if the results are physically meaningful and if smooth displacement vector curves are found throughout the configuration space.

The occurring problems enforce the conclusion that it is superior to change to internal Z-matrix coordinates for the n-mode representation rather than using different coordinate representations for the potential and kinetic part of the Hamiltonian.

4.4.3 KEO in Normal Mode Coordinates: The Watson-Hamiltonian

To avoid any coordinate transformation it is also possible to perform the quantum-dynamical calculations in normal mode coordinates. It has been stated earlier and shown in the previous section that for large displacements normal mode coordinates are not describing internal motion of molecular systems well. In the introduction of Ref. [142] the problems with a Hamiltonian in normal mode coordinates are reviewed. Nevertheless, the theory for the KEO in these coordinates will be introduced shortly in the following section. It is widely used for the theoretical simulation of (static) vibrational spectra, where only small distortions around the minimum structure are necessary to calculate the lowest energy levels and, hece, the normal mode coordinates are of higher quality. It will also be demonstrated how to express the Watson-KEO in a form that is compatible to the TNUM framework. This enables the usage of the KEO in normal mode coordinates without reprogramming major parts of the MRPROPA code.

The KEO for molecular systems in normal mode coordinates was first derived by Watson in 1968 [143]. In its original form it is

$$\hat{T}(\mathbf{q},\partial_{\mathbf{q}}) = \frac{1}{2}\sum_{\alpha\beta}\hat{\pi}_\alpha\mu_{\alpha\beta}\hat{\pi}_\beta - \frac{1}{8}\sum_{\alpha}\mu_{\alpha\alpha} - \frac{1}{2}\sum_{i}^{3N-6}\frac{\partial^2}{\partial q_i^2}, \tag{4.4}$$

with the μ-tensor being the inverse of the corrected moment of inertia tensor $\mathbf{I}'$, $\alpha,\beta \in x,y,z$ and $\hat{\pi}_\alpha$ given as

$$\hat{\pi}_\alpha = -i\sum_{rs}\zeta_{rs}^{\alpha}(\mathbf{q_0})q_r\frac{\partial}{\partial q_s}. \tag{4.5}$$

$\zeta_{rs}^{\alpha}(\mathbf{q_0})$ denote the Coriolis-ζ-constants [144].

Barone [145] showed that the approximation of a constant $\mu_{\alpha\beta} \approx \frac{\delta_{\alpha\beta}}{\mathbf{I}_{\alpha\beta}}$ is valid frequently, which simplifies [144] the expression to

$$\hat{T}(\mathbf{q},\partial_{\mathbf{q}}) = \frac{1}{2}\sum_{\alpha}\frac{1}{\mathbf{I}(\mathbf{q_0})_{\alpha\alpha}}\hat{\pi}_\alpha\hat{\pi}_\alpha - \frac{1}{8}\sum_{\alpha}\left(\mathbf{I}'(\mathbf{q})^{-1}\right)_{\alpha\alpha} - \frac{1}{2}\sum_{i}^{3N-6}\frac{\partial^2}{\partial q_i^2}. \tag{4.6}$$

Here, $\mathbf{I}(\mathbf{q_0})$ is the moment of inertia tensor at the equilibrium geometry $\mathbf{q_0}$, whereas in the second term $\left(\mathbf{I}'(\mathbf{q})^{-1}\right)_{\alpha\alpha}$ is the inverse of the corrected moment of inertia

tensor calculated at the actual geometry $\mathbf{q}$. After inserting $\hat{\pi}$ and applying the product rule one gets:

$$\begin{aligned}\hat{T}(\mathbf{q},\partial_{\mathbf{q}}) = &-\frac{1}{2}\sum_{\alpha}\frac{1}{\mathbf{I}(\mathbf{q_0})_{\alpha\alpha}}\sum_{rstu}^{3N-6}\zeta_{rs}^{\alpha}(\mathbf{q_0})\zeta_{tu}^{\alpha}(\mathbf{q_0})\ q_r\left(\delta_{st}\frac{\partial}{\partial q_u}+q_t\frac{\partial}{\partial q_s}\frac{\partial}{\partial q_u}\right)\\ &-\frac{1}{8}\sum_{\alpha}\left(\mathbf{I}'(\mathbf{q})^{-1}\right)_{\alpha\alpha}-\frac{1}{2}\sum_{i}^{3N-6}\frac{\partial^2}{\partial q_i^2}.\end{aligned} \tag{4.7}$$

It is convenient to rewrite the Watson-Hamiltonian in the form of Eq. (2.107), p. 31, which is compatible to the TNUM format. The first term is expanded and the sums are simplified using the Kronecker delta δ_{st}:

$$\begin{aligned}&-\frac{1}{2}\sum_{\alpha}\frac{1}{\mathbf{I}(\mathbf{q_0})_{\alpha\alpha}}\sum_{rstu}^{3N-6}\zeta_{rs}^{\alpha}(\mathbf{q_0})\zeta_{tu}^{\alpha}(\mathbf{q_0})\ q_r\left(\delta_{st}\frac{\partial}{\partial q_u}+q_t\frac{\partial}{\partial q_s}\frac{\partial}{\partial q_u}\right)\\ =&-\frac{1}{2}\sum_{\alpha}\frac{1}{\mathbf{I}(\mathbf{q_0})_{\alpha\alpha}}\sum_{rsu}^{3N-6}\zeta_{rs}^{\alpha}(\mathbf{q_0})\zeta_{su}^{\alpha}(\mathbf{q_0})\ q_r\frac{\partial}{\partial q_u}\\ &-\frac{1}{2}\sum_{\alpha}\frac{1}{\mathbf{I}(\mathbf{q_0})_{\alpha\alpha}}\sum_{rstu}^{3N-6}\zeta_{rs}^{\alpha}(\mathbf{q_0})\zeta_{tu}^{\alpha}(\mathbf{q_0})\ q_rq_t\frac{\partial}{\partial q_s}\frac{\partial}{\partial q_u}.\end{aligned} \tag{4.8}$$

Hence, the complete KEO (including second and third correction term) can again, and in full analogy to the TNUM format, be written as:

$$\hat{T}(\mathbf{q},\partial_{\mathbf{q}}) = \sum_{i,j=1}^{3N-6} f_2^{ij}(\mathbf{q})\frac{\partial^2}{\partial_{q_i}\partial_{q_j}} + \sum_{i=1}^{3N-6} f_1^{i}(\mathbf{q})\frac{\partial}{\partial_{q_i}} + V_{\mathrm{ep}}(\mathbf{q}) \tag{4.9}$$

with

$$f_2^{ij}(\mathbf{q}) = -\delta_{ij}\frac{1}{2} - \frac{1}{2}\sum_{\alpha}\frac{1}{\mathbf{I}(\mathbf{q_0})_{\alpha\alpha}}\sum_{rt}^{3N-6}\zeta_{ri}^{\alpha}(\mathbf{q_0})\zeta_{tj}^{\alpha}(\mathbf{q_0})\ q_rq_t, \tag{4.10}$$

$$f_1^{i}(\mathbf{q}) = -\frac{1}{2}\sum_{\alpha}\frac{1}{\mathbf{I}(\mathbf{q_0})_{\alpha\alpha}}\sum_{rs}^{3N-6}\zeta_{rs}^{\alpha}(\mathbf{q_0})\zeta_{si}^{\alpha}(\mathbf{q_0})\ q_r \tag{4.11}$$

and

$$V_{\mathrm{ep}}(\mathbf{q}) = -\frac{1}{8}\sum_{\alpha}\left(\mathbf{I}'(\mathbf{q})^{-1}\right)_{\alpha\alpha}. \tag{4.12}$$

In this form the Watson-Hamiltonian is implemented in the MRPROPA-framework. It has not been used for any presented propagations, though, as the deficiencies from normal mode coordinates are still present. However, it enlarges the number of available features in MRPROPA.

4.5 Outlook

This chapter demonstrates the ability to combine algorithms for efficient electronic structure calculations of full-dimensional PESs with reduced- and full-dimensional quantum-dynamical calculations in the framework of the MrPropa program. A polynomial fit of the PES n-mode representation, which has been implemented into the Molpro program package by G. Rauhut (Univ. Stuttgart), serves as an interface to the quantum-chemical program. With this the PES is available analytically, which enables quick evaluation of the potential and therefore offers the ability to dynamically explore the considered systems with xdifferent sets of active coordinates in reduced-dimensional models.

Internal Z-matrix coordinates have been found to be advantageous compared to normal mode coordinates in order to carry out quantum-dynamical calculations. The n-mode representation of the PES was originally implemented in normal mode coordinates. So coordinate transformations between normal mode and internal Z-matrix coordinates were necessary, but the required elongations from the reference structure were found to be too large to achieve numerically accurate results from quantum chemistry. Carrying out the dynamical calculations in normal mode coordinates has also been tested and but was not furher employed. Finally, the PES fit has been provided in Z-matrix coordinates.

After presenting this fundamental work, which is rather a *proof-of-principle* by calculating the tunneling splitting in H_2O_2 and its isotopologues and the cumulative reaction probability of PHDCl, the focus can be set to different molecular systems. As stated in the introduction DPTRs are of high interest here but no restrictions in principle apply to the systems under investigation.

The analytical evaluation of the potential is of great benefit also in combination with the adaptive basis representation scheme presented in chapter 3. As stated above the polynomial fit quality dramatically decreases in outer regions of the PES or, in the relaxed model, the (constrained) local optimization of the PES polynomial even fails to converge completely. In outer regions of the surfaces the value of the potential is high (at least for bound coordinates), so it is unlikely for the wavepacket to travel in such regions. Using the proDG approach avoids the evaluation of the PES at places where the wavepacket is negligibly small. Thus, combining the two approaches leads to efficient quantum-dynamical calculations with analytical, yet highly accurate, PESs.

5 Quantum Dynamics of Molecular Switches

5.1 Scope of the Projects

Photochemical reactions are initiated by interaction of reactants with light rather than by thermal energy. Their exact definition and their dynamics, including non-adiabatic effects, are nicely introduced and reviewed e. g. in Refs. [6, 7, 146, 147]. Absorption of electromagnetic radiation causes promotion of the system from the electronic ground state to an electronically excited state, which can initiate a chemical reaction. Such photochemical reactions may occur on an ultrafast time scales and play an important role in various different fields. Biochemically relevant, for example, is the photochemically induced inversion of the retinal chromophore, which is initiated by exposure of light on the retina of the eye and occurs in about 200 fs. Another example is the ultrafast radiationless deexcitation pathway of nucleic acids, which avoids chemical damages to the DNA by preventing chemical reactions in the excited state [148]. Photophysical processes such as fluorescence or phosphorescence are somewhat slower than this, not getting faster than pico- to nanoseconds. Generally, many inversions, cyclizations or cleavages are caused by photochemical processes.

Fig. 5.1 summarizes different photochemical events. Starting at the reactants R absorption of light transfers the system to upper PESs. According to Kasha's rule deexcitation processes are faster than movements of the nuclei leading to the expectation that the final deexcitation is taking place from the lowest excited state. From there several possibilities are available. The system may evolve to a local minimum R* and deexcite with emission of light back to the ground state PES. Usually, this will not include any chemical reaction, so this part of the figure is labeled "photophysics". Moving to the right of R* leads to a branch which is called adiabatic photochemistry. As the upper and lower PESs are well separated the Born-Oppenheimer approximation remains valid and the complete reaction can be described on the upper PES only. Emission of light transfers the system back to the ground state and depending on its topology product formation (point P) may have

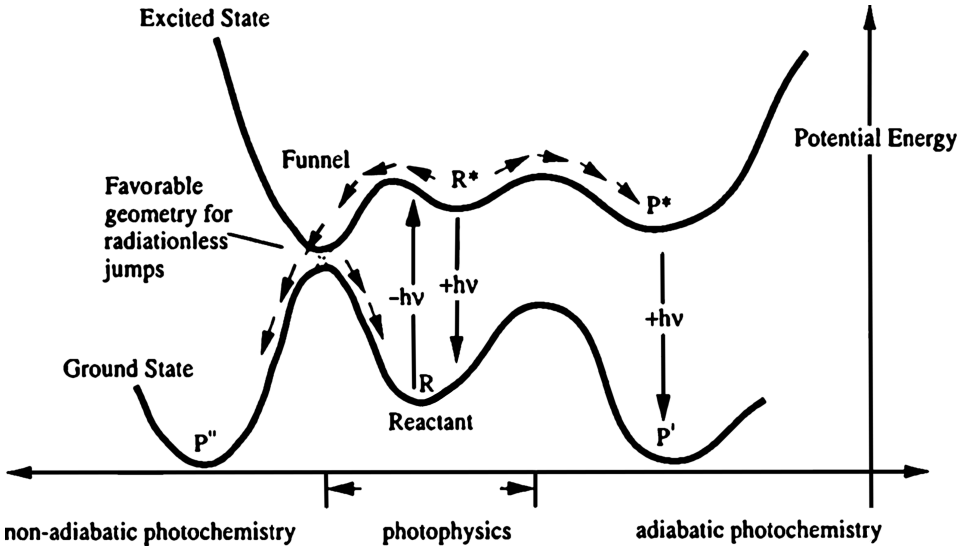

Figure 5.1: Schematic sketch of photochemical and photophysical processes on two potential energy surfaces.

Figure from Ref. [146].

occurred. On the left side of the figure the situation is different. The upper and lower PESs come close to each other so non-adiabatic effects have to be taken into account and the Born-Oppenheimer approximation looses its validity as the non-adiabatic coupling terms are not negligible anymore. After the system has approached the funnel a radiationless deexcitation to the ground state may occur. Again, two possible pathways arise there. Either the reaction goes back to the reactants R to fulfill a photophysical cycle or it evolves to the product minimum P. Reactions proceeding on such radiationless pathways are often faster than the adiabatic or purely physical processes, so competing photochemical and photophysical processes can determine the yield of a reaction. In contrast to what is shown in this figure the product P may also lie higher in energy than the reactants R. This is why photochemical reactions in general give rise to formation of thermally less stable products.

New experimental and theoretical developments made it possible to get insight into the first few femto- to picoseconds of chemical reactions. The noble prize awarded development of femtosecond laser spectroscopy by A. Zewail [149, 150] using pump/probe laser pulse sequences was a major breakthrough in order to experimentally observe ultrashort processes. On the theoretical side molecular dynamics simulations (either quantum mechanically or classically) are dealing with moving nuclei on the same time scale and are hence an adequate tool for studying ultrafast reactions. Calculations are often useful to interpret and support the experimental findings. Classical molecular dynamics calculations have the advantage of a feasible full-dimensional treatment of the molecule, but suffer from the fact that in order to achieve statistically relevant results a large number of trajectories has to be calculated. Most efficient calculations make use of force fields or semi-empirical

methods. *Ab initio* molecular dynamics codes are also available, but usually have the disadvantage of relatively high computational costs for the evaluation of the potential while still treating the movement of the nuclei classically. Furthermore, in the context of photodynamics, classical treatment of nuclei fails in regions with strong non-adiabatic effects requiring further approximations such as the surface-hopping approach. Refs. [151,152] give an introductional overview of non-Born-Oppenheimer molecular dynamics. In contrast to classically treated nuclei, in quantum wavepacket dynamics propagation on several PESs is no problem in principle when non-adiabatic coupling elements are known. In addition, the explicit treatment of interaction with electromagnetic fields (such as laser pulses) is easy to include. Although a full-dimensional treatment is possible in principle, due to the large computational costs caused by the exponential scaling with dimensionality quantum dynamic simulations are limited to few internal movements. In typical photochemical situations this is often justified as ultrafast non-adiabatic effects are mostly focused on the movement of few atoms while other parts of the molecule need more time to follow and can be excluded from the explicit dynamic treatment. Due to the explicit quantum-mechanical treatment only one wavepacket has to be propagated.

The "Collaborative Research Center (SFB) 677—Function by Switching" deals with molecular switches. In three project areas switching processes are investigated as single molecules in solution, on surfaces, and incorporated in solid state materials. Mostly, switching is triggered by irradiation of light. In project A1 the dynamics of prototype molecular switches is studied in close cooperation, experimentally and theoretically. Two main types of switches, azobenzene derivatives [118, 153] and furylfulgides [154], are investigated. Both can be switched from one form to another upon irradiation of light. Well-separated absorption maxima for different switching processes allow for selective switching with different wavelengths. Depending on the thermal stability of the isomers the switches are used for different and numerous technical applications such as molecular memories, photo-control of enzyme activity, photo-modulation of optical materials, photo-induced liquid crystal phase changes, photo-switching of electron and energy transfer processes, or fluorescence modulation. The thermal stability of the thermodynamically less stable isomer is longer for the fulgide systems compared to azobenzene derivatives.

Both types of switches are subject of this work. First, an often used model for fulgide switches is the photochemical ring-opening reaction of cyclohexadiene as the central building unit of fulgides is also a six-membered ring system. Second, bridged azobenzene derivatives have been studied earlier within a diploma thesis in this group [117,118]. That work, using semiclassical surface-hopping dynamics, revealed the most important DOFs for the dynamics. They are used to calculate a relaxed PES, on which quantum-dynamical wavepacket propagtions are the basis to simulate transient absorption spectra. The work will be presented in the second part of this chapter.

5.2 Cyclohexadiene Ring-Opening Reaction

5.2.1 Project Objectives

In Ref. [154] Temps and coworkers investigated into the photo-induced isomerization of the *(E)*-isomer of a photochromic furylfulgide in *n*-hexane using femtosecond time-resolved transient absorption spectroscopy. As Fig. 5.2 demonstrates the investigated furylfulgide has three thermally stable isomers. The central six-membered ring can be switched back and forth between an open *(E)* and a closed *(C)* form by irradiation of visible and UV light, respectively. Furthermore, there is a competing isomerization of the open *(E)*-isomer around a double bond to form a corresponding *(Z)*-conformer.

As the central switching unit for the *(E)* → *(C)* isomerization is a six-membered ring the photochemical ring-opening reaction of cyclohexadiene is often referred to as a model system. In this work, the attention is drawn to exactly this system. Hofmann *et al.* [155, 156] were able to identify the two most important reactive coordinates and performed quantum wavepacket propagations on a two-dimensional PES. This PES was constructed by calculating the energy of orthogonal rigid displacements from the minimum energy path.

In the present work a different approach is followed. The evaluation of the potential is not limited to regions close to the reaction path, but constructed globally over the configuration space, which is spanned by the two most important DOFs. All other coordinates are treated in the adiabatic model, where they geometrically relax. The differences arising from this approach to the former work of Hofmann *et al.* are discussed in the upcoming publication. A quantum-dynamical wavepacket propagation is performed on the 2A PES calculated at a CASSCF level.

The ring-opening reaction of cyclohexadiene is also accessible experimentally [157, 158]. To compare the population on the 2A surface with experimental observations the conical intersection (seam) to the lower 1A state has to be modeled as only one PES is included in the calculation. In order to simulate the transfer from the upper to the lower PES and with this to reduce the population on the 2A PES when the wavepacket enters the CI seam, a purely imaginary absorbing potential (see

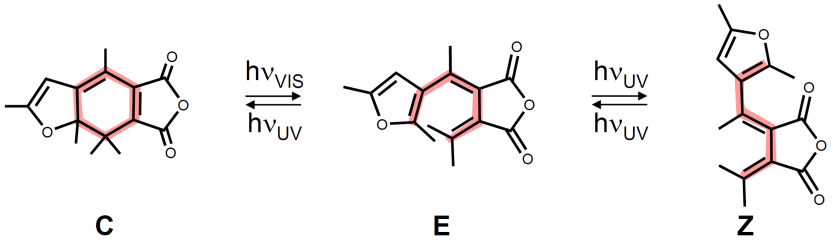

Figure 5.2: Three thermally stable isomers of an experimentally studied [154] furylfulgide that can be switched back and forth photochemically.

section 2.5) is applied. This novel model enables the comparison to experimentally determined time scales, which are well reproduced. The validity of the new model has been verified by one-dimensional model calculations, which are presented in the appendix of the paper.

5.2.2 Photochemical Ring-Opening of Cyclohexadiene: Quantum Wavepacket Dynamics on a Global ab initio Potential Energy Surface

Own contributions presented in the paper:

- All wavepacket dynamics calculations
- Development of irregular shaped absorbing potential to simulate the Conical Intersection seam
- Provided parts of the discussion

Additional work within this project, not presented in the paper:

- Simulation of probe-pulse region
- Thorough tests of various initial parameter sets

Abstract

We have assembled a global CASSCF potential energy surface for the excited 2A state of the cyclohexadiene -hexatriene system, in two degrees of freedom, with full relaxation in all other degrees of freedom. Quantum wavepacket dynamics on this surface yields simple interpretations of recent experimental data on the ultrafast photochemical ring-opening of cyclohexadiene as well as predictions on preferred product configurations. The feasibility of this system as a model for fulgide molecular switches is discussed.

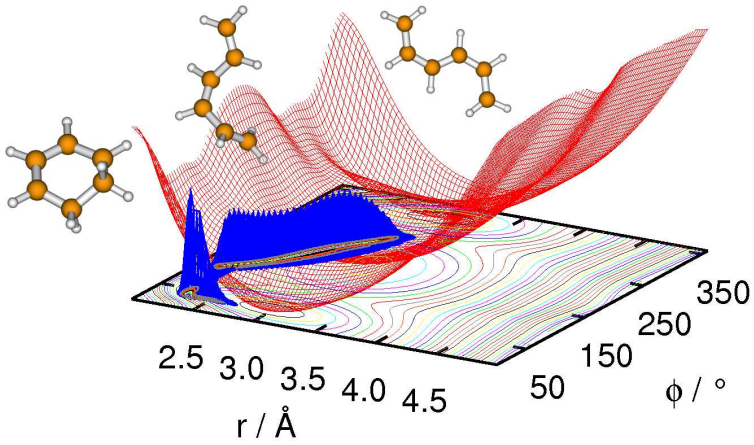

published in J. Chem. Phys. A, **2010**, *114*, 4036

Received September 29, 2009; Revised Manuscript Received: February 6, 2010
First published on the web March 8, 2010
DOI: 10.1021/jp909362c

5.2.3 Additional Information: Variation of Initial Parameters

The ring-opening reaction of cyclohexadiene is initiated by a laser pulse, which transfers a wavepacket from the ground state PES (1A) to the second excited state (1B). Here, "ballistic" motion transfers the wavepacket to the 2A PES through the 1B/2A CI. At this point the current work starts and an initial wavepacket has to be modeled. The optimized 1B/2A-CI is not part of the used 2A surface, as all remaining DOFs are geometrically relaxed. However, the optimized values of the two active coordinates can be taken as initial parameters for the center of the wavefunction but a major amount of uncertainty remains. As mentioned in the paper, initial parameters of the wavepacket and the 2A/1A CI-simulating absorbing potential have been varied in order to verify that modifications to the initial parameters do not change the main characteristics of the propagation.

Variation of Absorbing Potential Strength

Fig. 5.3 shows the norm of the wavepacket on the 2A surface with different absorber strengths. As expected, when the wavepacket first enters the CI seam where the absorbing potential is located it is directly depending on the absorber strength how much of the wavepacket is absorbed. When the remaining wavepacket enters the CI-region the second time less may be absorbed the more has been absorbed at first. Hence, the second step height is smaller the stronger the absorbing potential is.

Furthermore, a calculation with an absorbing potential, which starts at a fixed value of $r^0 = 2.3\,\text{Å}$, is presented. The IAP strength could be adjusted so that the population curve matches the reference (solid red). This shows that the (r, ϕ)-dependent form of the absorbing potential is not essential to cover the main charac-

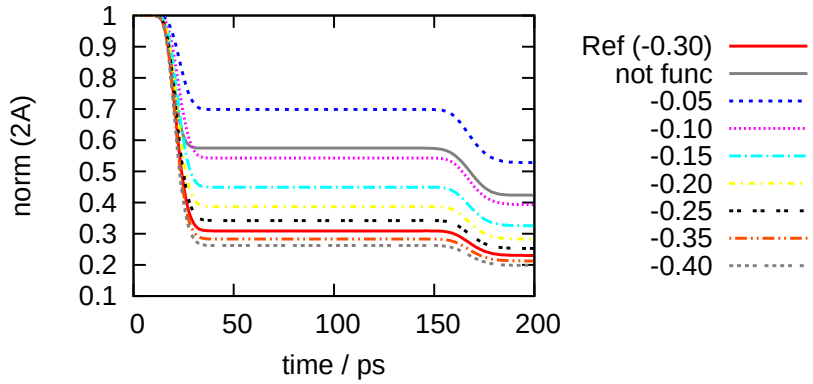

Figure 5.3: Variation of IAP strength. The key shows the prefactor $V_I/E_T^{\max}$ with $E_T^{\max} = 350\,\text{kJ/mol}$ (Equation (2) in the paper) in atomic units. The solid red line is the reference (same as published), all discontinuous lines are variations of the absorber strength, while the solid gray line shows a calculation with an absorbing potential without (r, ϕ) dependency.

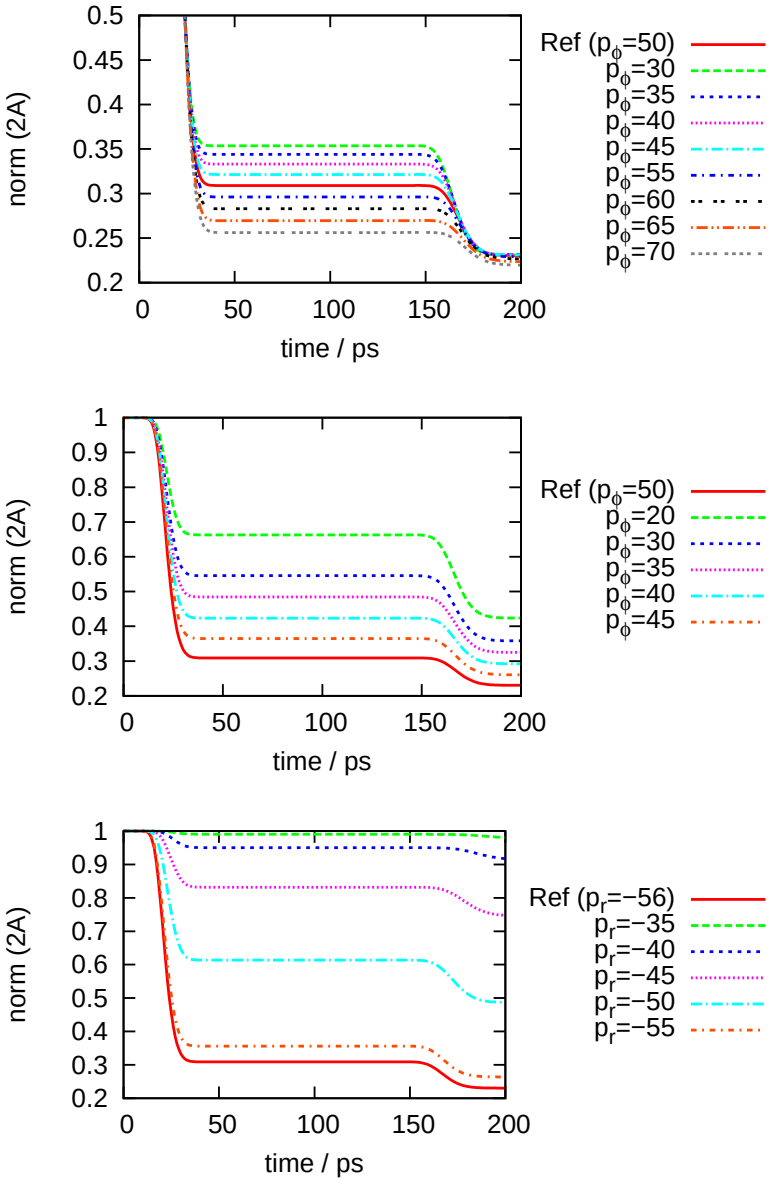

Figure 5.4: Variation of parameters $p_1 = p_r$ and $p_2 = p_\phi$ that control the momentum of initial wavepacket. The solid red line is the reference (as published) Top: Both parameters are changed (p_r not shown in key) to maintain a total energy of about 200 kJ/mol. Center/Bottom: Only the one parameter listed in the key is changed leading to a reduced total energy of the wavepacket. Note different scales.

teristics and times between the steps. However, using it is a substantial improvement as it ensures that no absorption takes place in regions that are not part of the CI seam.

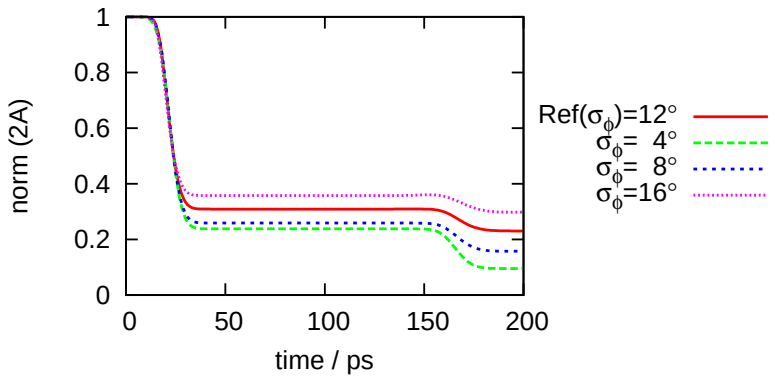

Figure 5.5: Variation of initial wavepacket width. The parameter σ_ϕ is changed, while the second parameter σ_r is changed to maintain a total energy of 200 kJ/mol.

Variation of Initial Momenta

In Fig. 5.4 similar variations of initial parameters are performed. The modified parameter is the initial momentum of the wavepacket. The reference calculation has been set up in order to have an initial total energy of about 200 kJ/mol. Fig. 5.4 (top) shows variation of the initial momenta in both directions, basically maintaining the total energy of 200 kJ/mol (±2 %). To achieve this the initial momentum $p_2 = p_\phi$ is varied between 30 to 70 a.u. and $p_1 = p_r$ is adjusted accordingly (yielding numerical values between −60 and −52 a.u.), while all other parameters are kept at the reference values.

Fig. 5.4 (center and bottom) show calculations where only one of the initial momenta is varied, while the other one is kept at its reference value. This leads to changed total energies. As argued in the paper a total energy higher than 200 kJ/mol does not seem to be physically relevant. Because of this the initial momenta are only changed to smaller values, yielding total energies between 108 and 195 kJ/mol.

Again, only the step heights but not their distances (in time) are changed upon changes of the initial momentum. As a different momentum may vary the velocity and hence the depth of penetration into the absorbing potential the amount of absorbed wavepacket varies. However, the basic movement on the PES and therefore the times when the wavepacket enters the CI seam do not change drastically. In all calculations the general direction of the total initial momentum is directed towards the intersection seam. Calculations with initial momenta pointing into the opposite direction, i. e. away from the intersection seam, have already been presented in the appendix of the publication.

Variation of Initial Width

Fig. 5.5 displays similar variations. Here, the width of the initial wavepacket is modified. As before, a total energy of about 200 kJ/mol (±5 %) is maintained by

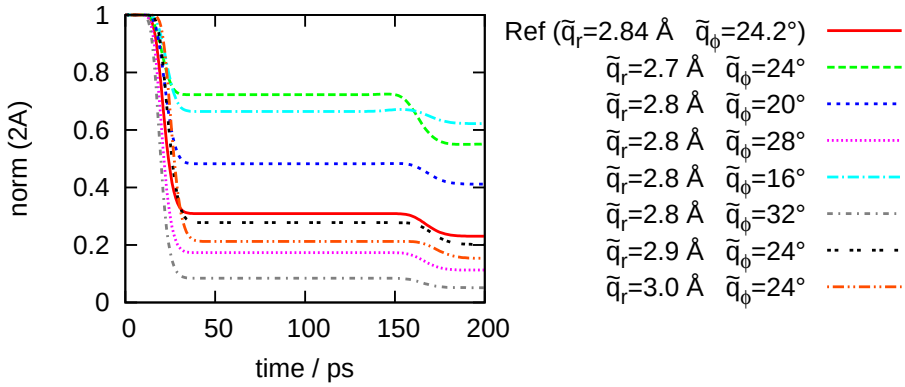

Figure 5.6: Variation the initial wavefunction center. Parameters $\tilde{q}_r$ and $\tilde{q}_\phi$ refer to the center of the initial wavefunction, represented by a two-dimensional Gaussian.

adjusting both parameters of the initial Gaussian wavefunction σ_ϕ (displayed in the key) and σ_r (varying between 0.08 Å and 0.25 Å).

Again, the characteristics of the population curve on the 2A PES does not change. Times between steps are constant, while the step height is effected due to the different energy distributions in the wavepacket. Broader wavepackets hold less kinetic energy than narrow ones leading to a different absorption behavior. Slow parts of wavepackets are known to be absorbed less easily than faster ones.

Variation of Wavepacket Position

The influence of a broad distribution of possible initial wavefunctions is checked by performing various propagations with wavepackets centered at different locations. Fig. 5.6 shows the population on the 2A PES for initial wavepackets centered at different locations. The total energy of the wavepackets vary between 185 and 263 kJ/mol mainly due to changing potential energies at the starting positions.

Conclusion

The essence of all pictures is basically identical. Upon modification of various input parameters the times between two steps of the population decrease do not change. The model is robust against changes of the initial momentum, width and position of the starting wavepacket. Furthermore, also the strength of the absorbing potential only changes the step height but not the times between two absorbing occurrences. This finding is important in order to demonstrate that the main results from the publication do not depend on particular choices of starting conditions (which cannot be deduced exactly from experiment) but are reproduced over a large variety of initial parameters.

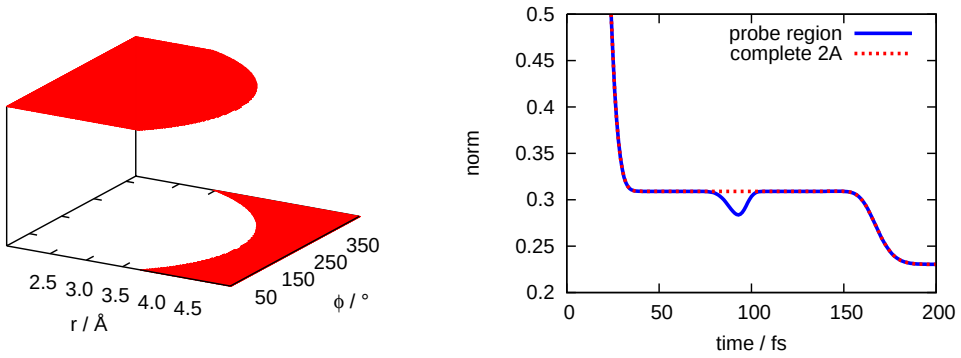

Figure 5.7: Simulated probe pulse region (left) and population within this region (right, solid blue). There is no difference to the reference (right, dashed red) except for a dip, which is caused by the wavepacket leaving and reentering the probe pulse region.

5.2.4 Additional Information: Simulation of Probe-Pulse Region

The simulated populations on the 2A surface do not show slight oscillations as seen in the experiment, but are flat after an absorption event has occurred. This might be caused by the following reason. By comparing the population on the (complete) 2A surface with experimental data it is quietly assumed that the probe pulse in the experiment is equally effective over the whole 2A surface. This is, however, physically not justified in general. The broad probe pulse does not necessarily cover outer regions of the PES, where unlikely molecular geometries are represented. In order to improve the comparability to experiment a distinct probe pulse it is possible to record the norm not on the complete PES but on fractions of it only. For this an (in principle arbitrary) area is defined, which represents the probing region. Differently shaped and sized regions have been tested in this work. Fig. 5.7 shows one example for a simulated probe region, namely a section of a circle (left) with the according norm inside this section (right).

From the picture it can be seen that both curves match except for a small dip, which appears in the solid blue line. This is caused by the wavepacket leaving and reentering the probe pulse region partially. Accordingly, the size of the dip is depending on the size of the simulated probing region. The larger the region, the smaller is the dip, finally completely disappearing, if the probe pulse region covers the whole surface. Unfortunately, the results of this example but also other probing regions did not lead to small and smooth oscillations like the ones seen in Fig. 7 of the present publication, so the approach was not used for the data shown in the paper.

5.2.5 Additional Information: Difficulties from Finite Grids

In the system under investigation the torsional $q_2 = \phi$ coordinate is periodic. By the use of periodic basis functions the periodicity can easily be modeled. If the

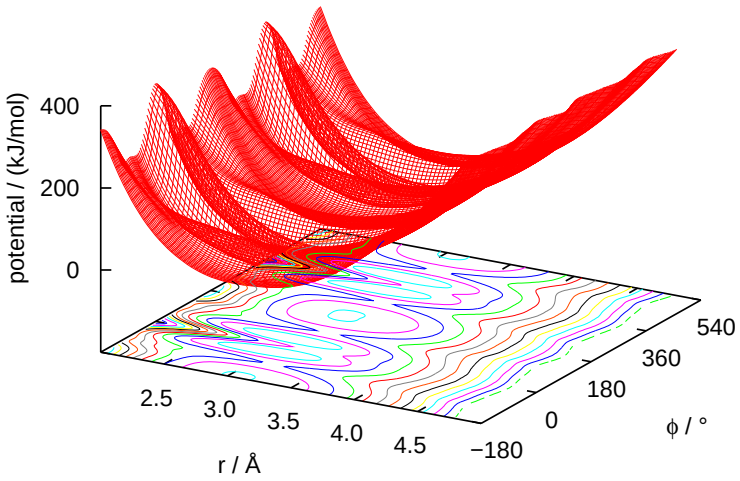

Figure 5.8: Double size PES used for propagations with total propagation times larger than 250 fs.

wavepacket is reaching the border of the grid it may reenter on the opposite side. This is taking periodicity fully into account as the wavepacket may interfere with parts of itself that are (still) present in this region. The FFT method is appropriate for such situations in general.

Unfortunately, numerical difficulties occur in case the KEO is more complicated, meaning that there are non-negligible kinetic functions for first derivatives and "mixed" derivatives (cf. Eqs. (2.109) and (2.110), p. 31). Then, the hermiticity of the Hamiltonian is not guaranteed and if a wavepacket is traveling past the border of a grid it may cause a numerical overflow, which is hard to avoid [159]. This problem is "naturally" avoided for bound coordinates, as they usually have high potential energy in outer grid regions and therefore no parts of the wavepacket ever reach the border. This is not true for periodic coordinates. Here, the wavefunction may be hindered to reach the end of the grid by the use of absorbing potentials. This, however, leads to an unphysical restriction of torsional motion as the wavepacket is not able to re-enter the PES.

In this work the following approximation has been used in order to avoid numerical overflow but still taking periodicity partially into account. The PES has been doubled, i. e. periodically continued in the torsional coordinate. Fig. 5.8 shows the PES, which has actually been used for propagations with total propagation times larger than 250 fs.[1] Hence, it is not only covering the range from 0° to 360° but from −180° to 520°. On all grid borders CAPs ensured that no parts (not even small ones) of the wavepacket reach it and, hence, avoid numerical overflow.

[1] up to 250 fs the wavepacket stays within 360° in the torsional coordinate, so the enlarged PES is not necessary.

Periodic extension of the PES is physically not the same than a true re-entering of the wavepacket on the opposite side of the grid, though. Indeed, the potential energy and hence the effects of it on the wavepacket are identical in both cases, but usually, when re-entering the PES the wavepacket is able to interfere with other parts of itself that are (still) present in this particular area. In the used approach this interference is not possible as the extended region is not populated at first. However, this is not problematic as the initial wavepacket features a momentum in the positive ϕ-direction. So no parts of the wavepacket (at least by visible control) are remaining at small ϕ-values, which means there is no intereference in this area anyway. In conclusion, doubling the PES does take periodic behavior into account with the neglect of interferences caused by periodic re-entering of the wavepacket. These are of minor importance due to the initial conditions of the wavepacket, though.

5.2.6 Outlook

Wavepacket dynamics on a relaxed CASSCF surface of the electronically excited 2A state were performed to investigate into the photochemical ring-opening reaction of cyclohexadiene. Main features of the experimental findings by Fuss *et al.* [157] could be reproduced. Speficially, looking at the population of the 2A state, the times between two steps, are in good agreement. These time steps arise from the wavepacket entering and leaving of the 2A/1A CI-region, where parts of the wavepacket would descend to the lower surface. Effects of the initial conditions of the wavepacket are of minor impact. This is important as the intial conditions cannot be derived from experiment with sufficient accuracy. As the electronic ground state is not included explicitly the CI seam has been modeled by an imaginary potential. The main effects on the wavepacket of an explicitily treated CI and the imaginary model potential could be shown to be in good agreement. This novel model could thus be used in future applications of excited state dynamics, when the explicit simulation of a CI (seam) is not feasible. Especially, the investigation into suitably substituated cyclohexadiene derivatives that either give a better model system for fulgide switches or are better switches by themselves is to be mentioned here.

5.3 Bridged Azobenzene Derivatives

5.3.1 Project Objectives

As a second molecular switch bridged azobenzene derivatives (brAB) are subject of this work. The photoinduced switching process of 5,6-dihydrodibenzo[c,g][1,2]diazocine (see Fig. 5.9) was investigated with semi-empirical surface-hopping molecular dynamics by Carstensen in his diploma thesis [117] and published later on [118]. The well-known photochemical behavior of the regular azobenzene isomerization, as described e. g. in Refs. [160–162], is changed due to the (partially) blocked rotation pathway in brAB.

Experimentally, the photochromic properties of brAB were first investigated by Siewertsen *et al.* [153, 163]. This study revealed brAB as an ideal candidate for an optical molecular switch, as it shows several differences to the unsubstituted parent molecule azobenzene. The separated n$\rightarrow \pi^*$ absorption maxima of the (E) and (Z) isomer and an increased quantum yield are the most prominent features.

In the theoretical work of Carstensen *et al.* the two most important internal degrees of freedom, namely the CNNC dihedral and the CNN angle, were identified. A fully relaxed (adiabatic approximation) semi-empirical PES has been calculated. As an extension to this prior work, in this chapter quantum-dynamical wavepacket calculations are performed on this PES in order to calculate transient absorption spectra. The work presented here is only the first step towards a quantum-dynamical, and hence, inherently more correct description of the system. It is rather a demonstration of the validity and feasibility of the different employed technical methods, namely the reduced-dimensional PES, the quasi-diabatization scheme, the way of calculating the transient absoprtion spectra, than a final description. For this reason only a relatively low qualitative agreement of the spectra with the experimental ones should be expected.

As stated in the theory section, propagation on several PESs is straightforward in principle, but a conversion to the diabatic basis is advantageous. The used semi-empirical program package does not calculate any non-adiabatic coupling terms, hence, it is necessary to apply a diabatization scheme that does not require the coupling terms. In the literature many very simple strategies have been followed. In Refs. [115] the authors use an ad-hoc construction to obtain a mixing angle in order to get smooth diabatic curves in the region where the adiabatic PESs come close to

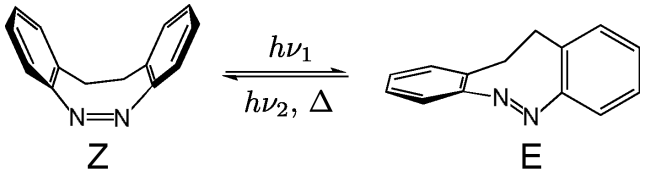

Figure 5.9: Isomerization of 5,6-dihydrodibenzo[c,g][1,2]diazocine.

each other. In outer regions the diabatic PESs should match the adiabatic ones. In Ref. [114] the off-diagonal coupling elements of the Hamiltonian are an analytical ad-hoc construction. Köppel *et al.* [18] proposed the so-called regularized diabatic states that can be obtained in a systematic manner, without recourse to coupling elements. This scheme was followed in this work in order to perform quantum-dynamical wavepacket propagations on the quasi-diabatic PESs and to calculate transient absorption spectra. Those are compared to the theoretically obtained spectra of Carstensen *et al.* and the experimental ones by Siewertsen *et al.*

In section 5.3.2 the quasi-diabatization scheme will be discussed. Also, the theoretical background of calculating transient absorption spectra in a mixed semi-classical quantum-dynamical way will be explained. Section 5.3.3 will finally present the results of the calculations.

5.3.2 Theoretical Background

Regularized Diabatic States

In the picture of semi-classical molecular dynamics, quantum wavepacket calculations represent an infinite number of trajectories. Also, in principle, the full set of coupled electronic states can be included in the dynamics without any further models, such as surface-hopping. As explained in section 2.1.3 all coupling elements between the surfaces have to be known. Depending on the chosen basis (adiabatic or diabatic) they either appear in the kinetic or in the potential part of the Hamiltonian. The basis transformation from adiabatic to diabatic basis is ambiguous, though. In the following, one of the approximate transformations, which does not require non-adiabatic coupling elements, will be presented.

Köppel and coworkers developed the so-called regularized diabatic states, which are constructed by removing the singular derivative couplings in the adiabatic representation [13,17–19]. This can be achieved from the knowledge of the adiabatic PESs alone in many cases. First, the scheme was developed for so-called symmetry-allowed intersections [18] and has been extended to general, fully accidental CIs later [19]. Often symmetry considerations determine the location of a CI. In a subspace of the nuclear coordinates where the investigated electronic states do not interact due to symmetry reasons, coupling only occurs upon distortion of the system along a non-symmetric mode. Intersections occurring for the higher-symmetry conformation are called symmetry-allowed CIs.

For a two-dimensional consideration let one of the coordinates denote an asymmetric coordinate, which leads to an interaction of two states (so-called "coupling mode" q_u). Then, the following working equations can be derived [18, 164] for the

determination of the regularized diabatic potential energy matrix $\mathbf{V}^{(d)_{\mathrm{reg}}}$ from the adiabatic potentials $\mathbf{V}^{(a)}$ alone:

$$\mathbf{V}^{(d)}_{\mathrm{reg}} = \frac{V_1^{(a)} + V_2^{(a)}}{2}\mathbf{1} + \frac{\Delta V}{\sqrt{\frac{\Delta_0^2}{4} + \lambda^2 q_u^2}} \begin{pmatrix} \frac{\Delta V_0}{2} & \lambda q_u \\ \lambda q_u & -\frac{\Delta V_0}{2} \end{pmatrix} \tag{5.1}$$

with $\Delta V = \dfrac{V_1^{(a)} - V_2^{(a)}}{2}$ and $\Delta V_0 = \left.\dfrac{V_1^{(a)} - V_2^{(a)}}{2}\right|_{q_u=0}$.

The parameter λ is determined as

$$\lambda = \left\{ \frac{1}{8}\frac{\partial^2}{\partial q_u^2}[V_2^{(a)}(q_i, q_u) - V_2^{(a)}(q_i, q_u)]^2 \right\}^{\frac{1}{2}}_{q_i,0}, \tag{5.2}$$

where q_i represent the symmetric vibrational mode(s). This expression is a double differentiation with respect to the ith mode in a high-symmetry subspace. The extension to higher dimensionality is straightforward [17].

The given working equations have been implemented in the MrPropa program and used for the calculation of quasi-diabatic brAB potentials from the adiabatic potentials alone. The resulting diabatic PESs and quantum-dynamical wavepacket propagations on these surfaces will be presented in the following.

Transient Absorption Spectra

In this work, transient absorption spectra are calculated in analogy to the semi-classical work presented by Carstensen *et al.* in Refs. [117, 118]. A large number of trajectories is evaluated there. At each point in time, a trajectory is one single point on the (full-dimensional) PES and therefore vertical excitation energies are directly available from the semi-empirical CI calculations. Together with the transition dipole moments, the intensities for every electronic excitation to higher states can be calculated. Averaging over a large number of trajectories leads to the calculated spectra presented in that work.

There is a close relationship between a wavepacket and a set of trajectories. In the limit of infinitely many trajectories statistically they are representing a quantum wavepacket. The strategy for calculating transient absorption (and emission) spectra with a set of trajectories presented by Persico and coworkers [165] and used by Carstensen *et al.* [117, 118] is also applicable for quantum wavepackets if the complete grid supporting the wavefunction is analyzed as follows. For every grid point x_i the excitation energies ($\Delta E_{\mathrm{KL},\, x_i}, \mathrm{K} < \mathrm{L}$) is recorded. The transition probability PA_{x_i} is proportional to the corresponding square transition dipole moment $\mu^2_{\mathrm{KL},\, x_i}$ multiplied with the square of the absolute value of the adiabatic wavefunction on surface K at this grid point $\Psi_K^{(a)}(x_i)$. To produce the function $PA(\Delta E)$ all proba-

bilities are summed with respect to their excitation energy over the complete grid and all possible excitations at given times.

Experimentally, transient absorption spectra are recorded as difference between a static ground state spectrum and the pump-probe experiment. This so-called change in optical density (ΔOD) is graphed with respect to wavelength and different probing times. The static ground state spectrum can also be obtained in the above mentioned quantum wavepacket approach. A wavepacket representing the reference state (e. g. the lowest vibrational eigenfunction of the electronic ground state) is placed on the (relaxed) ground state PES and an absorption spectrum is calculated according to the formerly stated procedure. It is important to mention that in case relaxed PESs are used good results are only produced if the state for geometry optimization is the ground state. In order to enhance comparison to experiment all data are convoluted with a Gaussian with a full width at half maximum (FWHM) which corresponds to the temporal resolution of the experiment (here 20 fs).

A fully quantum way of simulating pump-probe experiments and calculating transient absorption spectra would require the simulation of both laser pulses. Explicit simulation of laser pulses can be achieved by simply adding a time-dependent electric field to the Hamiltonian. However, in this case standard propagation schemes are not applicable anymore. Often short time steps are used in combination with the approximation of time-independent Hamiltonians at every time step. The time dependence only changes the Hamiltonian from one time step to another. Propagation schemes for explicitly time-depentent Hamiltonians are given in Refs. [40, 166], for example. In the approach followed in this work, both, the pump and probe pulse are not explicitly simulated, which is physically interpreted an excitation with a delta pulse (infinitesimally narrow bandwidth). Such pulses transfer the complete wavepacket to the different PESs instantaneously.

5.3.3 Numerical Results

The dihedral angle around the N-N bond ϕ and the CNN angle ψ (see Fig. 5.9) are the two most important internal degrees of freedom for the isomerization process. They were characterized by semi-empirical surface-hopping dynamics calculations within Carstensen's diploma thesis [117]. In his work those two DOFs were used as active coordinates $\mathbf{q} = (\psi, \phi)^T$ to set up reduced-dimensional PESs at the same level of theory. All other DOFs were allowed to relax to their first excited state structure. For this work the PESs have been recalculated covering a larger range of both coordinates. The quality of the reparametrized semi-empirical floating-occupation configuration-interaction FOCI-AM1 calculations has been discussed in Ref. [118] and showed good agreement with CASSCF and CASPT2 calculations.

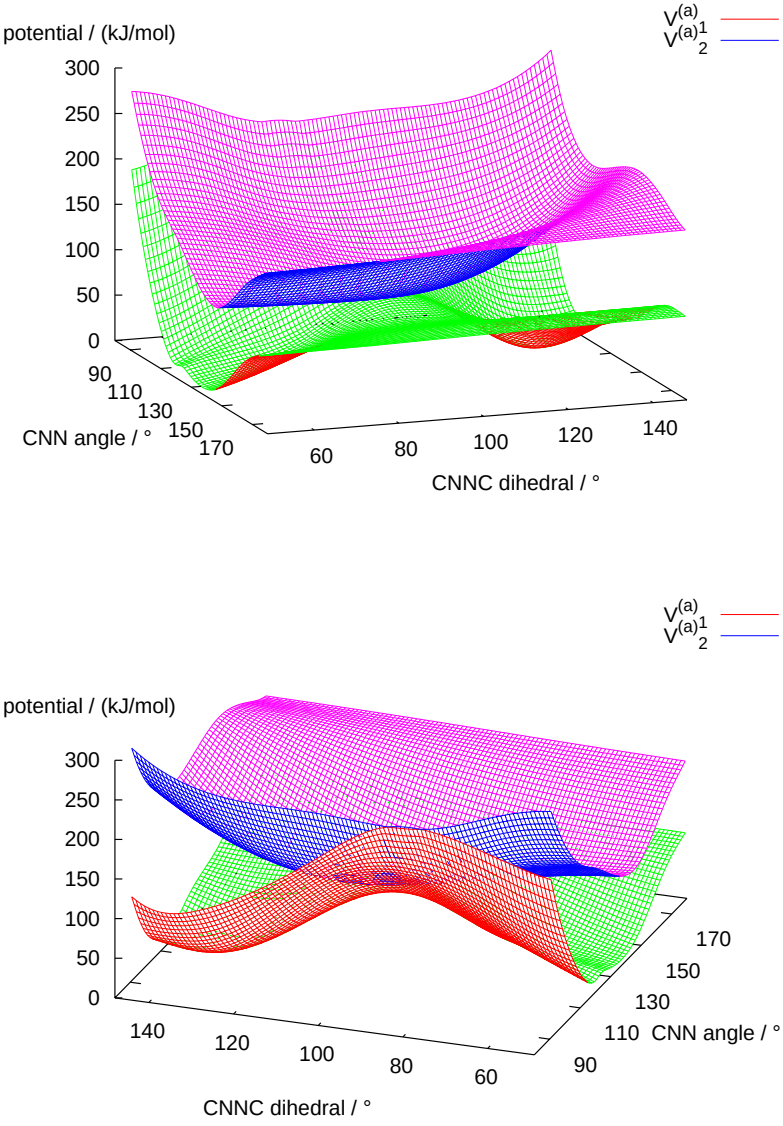

Figure 5.10: Adiabatic PESs (two different views) for the two most important coordinates describing the brAB-inversion. They are considered as active coordinates for the dynamics calculations.

Reduced-Dimensional Quasi-Diabatic PESs

Semi-empirical FOCI-AM1 calculations [167, 168] with parameters re-fitted to the parent compound azobenze [165] are performed on a grid with 46x56 points to evaluate the adiabatic PESs, which are shown in Fig. 5.10. They range from 50° to 150° in the dihedral and 80° to 180° in the NNC-angle coordinate. The calculations were performed with a CAS-CI of 6 electrons in 4 orbitals. Additionally, single excitations from the seven highest occupied to the six lowest unoccupied orbitals have been included, leading to a total of 94 determinants in the CI space. All geometries were allowed to relax to their S_1 structures. The physical interpretation of using fully relaxed PESs is that after the pump pulse the system instantaneously adjusts to the excitation. All inactive DOFs immediately obtain the value of their relaxed excited state structure. Afterwards, when the wavepacket travels around the PESs the inactive coordinates remain at the relaxed S_1 geometries, even if the wavepacket traverses to the electronic ground state. Refs. [117, 118] include further topological descriptions of the PESs and of the optimized CIs. On these surfaces the CI is located at $\mathbf{q} = (32°, 95°)^T$. The ($E$)-isomer minimum is located at $\mathbf{q} = (109°, 138°)^T$. The ($Z$)-isomer is not part of the surfaces, but the channel of this isomer starts at dihedrals smaller than 100°. For all quantum dynamics calculations the calculated points are interpolated with cubic splines.

Fig. 5.11 shows the resulting quasi-diabatic PESs. For their calculation the method by Köppel *et al.* [18] was employed. The ungerade coordinate q_u, which is necessary for the calculation of λ in Eq. (5.2) is the dihedral coordinate, while the remaining CNN angle is considered to be the symmetric one. Although this assumption does not meet the physical symmetry of the system the results for the quasi-diabatic PESs are encouraging. In regions far away from the CI the adiabatic representation and the quasi-diabatic diagonal terms are almost identical. The resulting off-diagonal coupling element is also shown in Fig. 5.11 (bottom). It is exactly zero by construction at the CI. Moving away from this point leads to larger values, which are either positive or negative. At outer regions, where diabatic and adiabatic representation are identical the mixing-angle is close to 0° resp. 90° (see Fig. 5.12). Around the location of the CI the two diabatic PESs are crossing and the mixing angle shows a large step. Here, it is (almost) represented by a step function, which scales down towards the border of the grid, i. e. towards larger or smaller values for the CNN angle. This feature is inherently caused by the applied diabatization scheme.

Two patches are arising, that would merge into the remaining mixing angle surface if mirrored at $\theta = 45°$. Their appearence can be explained as follows. The calculation of the quasi-diabatic states relies on the assumption that in the adiabatic representation there is only one point of degeneracy in the subspace of the two coordinates. However, in this work the adiabatic PES show a larger region of (at least near) degeneracy at angles between 80° and 140° and dihedrals between 80°

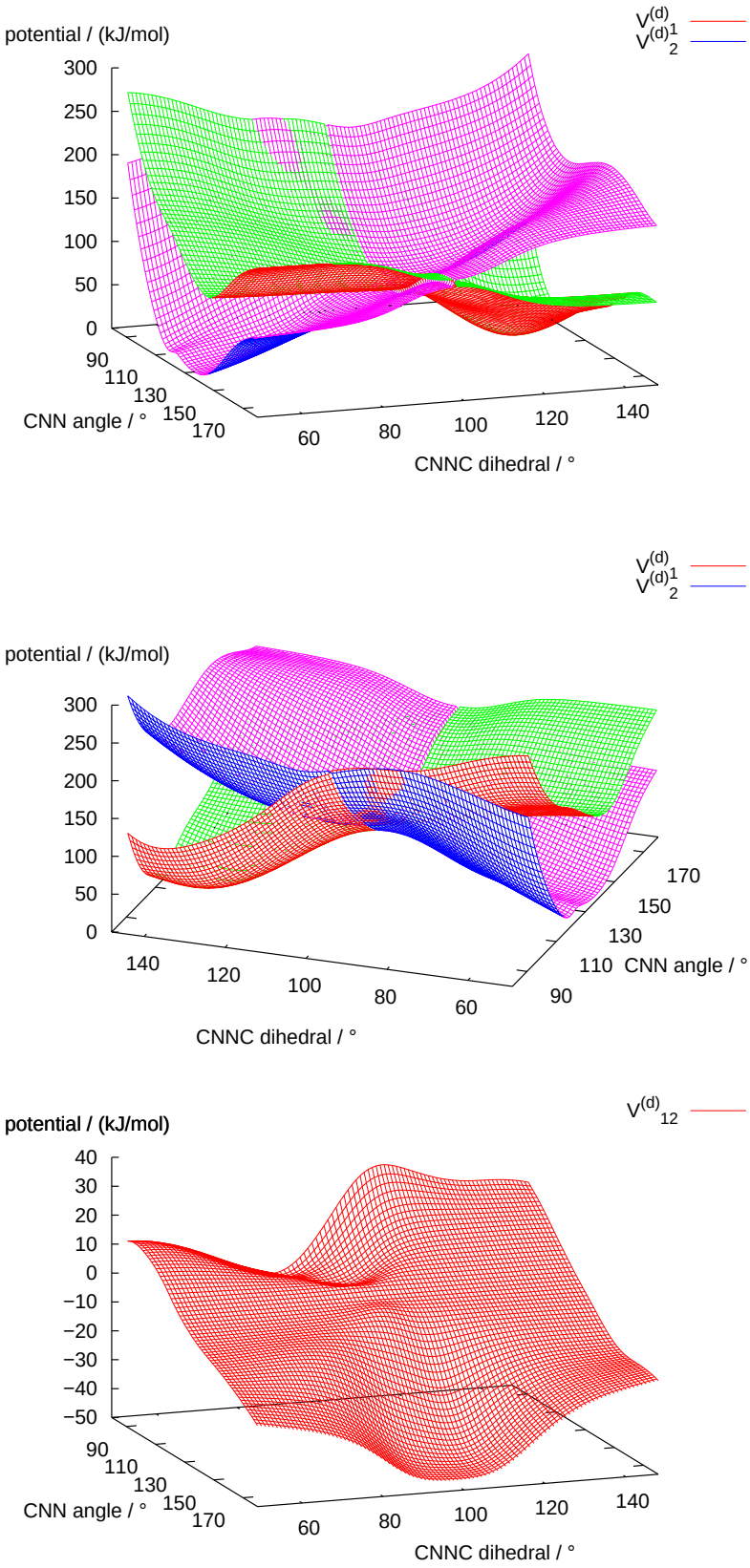

Figure 5.11: Resulting regularized diabatic PESs. The location of the CI was set to $q = (126°, 98°)^T$. Both diagonal terms, i. e. the quasi-diabatic PESs are displayed in two different views (top, middle) and the off-diagonal potential $V_{12}^{(d)}$ (coupling) is shown in the bottom panel.

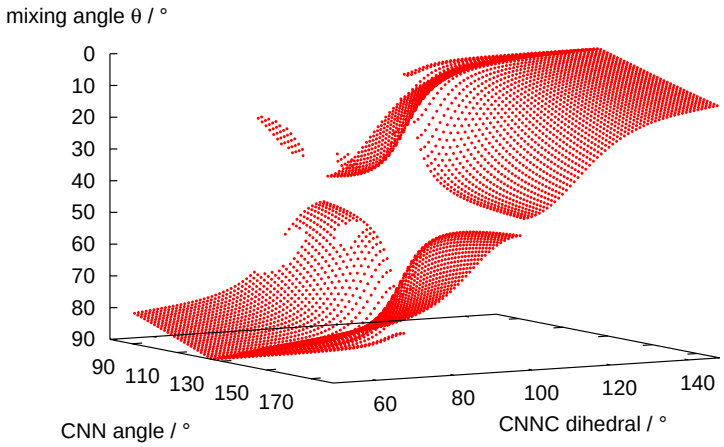

Figure 5.12: Diabatic to adiabatic mixing angle used for basis transformation. The mixing angle shows a step function a the point specified as CI, which is caused by the applied diabatization scheme. Two small patches arise, that would merge into the remaining mixing angle surface if mirrored at $\theta = 45°$. The reason for their appearance is explained in the text.

and 100°. The resulting quasi-diabatic states show an opposed ordering as expected in this region. This can be seen in Fig. 5.11 by the unexpected change from green to purple in the upper panel. In those regions, the diabatic wavepackets have to be transformed "in the other direction", resulting in the discontinuous mixing angle.

Reduced-Dimensional Quantum-Dynamical Calculations

Technically, it has not been possible to extend the PES for angles larger than 180°. Depending on the initial conditions in propagations the wavepacket may hit the border of the grid in this coordinate before or while entering the CI-region. In order to avoid reflections from the grid border absorbing potentials are a popular choice, but here they are not used because the unphysical deletion would lead to results that are hard to interprete. Fast parts of the wavepacket would be absorbed first, which would change the composition of the wavepacket significantly. Instead, the PES has been extended harmonically, which accounts for the higher energy that is expected for larger angles due to the strongly distorted ethylene bridge. Due to the harmonic extension the wavepacket stays compact and returns neither with a changed composition of fast and slow parts nor with unphysical reflections from the grid border. However, it has to be mentioned that extending the surface in this way is just a model approximation and does not include quantum chemical calculations. On all other borders of the grid CAPs (cf. Eqs. (2.103) and (2.104), p. 28) are used to absorb parts of the wavepacket that reach the border.

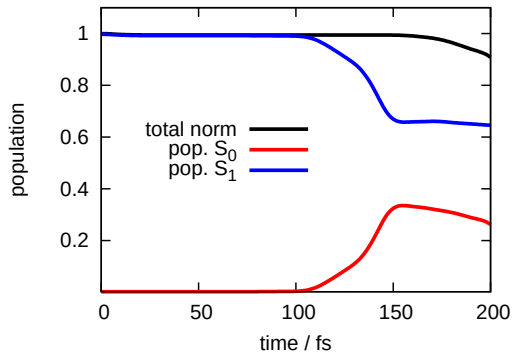

Figure 5.13: Adiabatic population of the wavepacket on the S_0 and S_1 surfaces.

As an initial wavepacket the lowest vibrational eigenstate of the relaxed electronic ground state is placed on the upper (diabatic) PES representing the point of time shortly after a delta-pulse excitation has transferred the ground state population to the S_1 surface. It would be an even better model for an excitation of a molecule in solution at room temperature to calculate a Boltzman distribution of the vibrational eigenstates of the ground state. Taking just the lowest eigenstate as initial wavepacket for the dynamics is an approximation, which is not assumed to have a big effect, though. In experiments the pump pulse lasts for at least 30 to 40 fs. The approach to place the initial wavepacket to the upper PES is a marked approximation. With explicitly simulated excitation pulses the wavepacket would gradually be transferred to the upper PES and evolve downwards the S_1 surface gradient immediately. So after the pulse the wavepacket on the upper PES would rather be broad than a compact ground state eigenfunction. The wavepacket is propagated on a 371x246 grid with symplectic integrators of order 12 (for parameters see Ref. [43]) and a time step of 0.075 fs. At given time steps a back-transformation of the wavepacket to the adiabatic representation is performed in order to record the population on the S_0 and S_1 surface. It is calculated as the adiabatic norm of the wavepacket on each PES, being $\langle \Psi_K^{(a)} | \Psi_K^{(a)} \rangle$.

In Fig. 5.13 the population on the S_0 and S_1 surface is displayed. Starting from a completely populated upper PES the wavepacket travels down the gradient of the surface towards the CI-region. First parts of the wavepacket reach it at about 110 fs. This causes almost 40% of the wavepacket to transfer to the lower PES. Almost all of the transferred parts of the wavepacket are traveling into the (Z)-isomer product channel (at least by visual control). This cannot be viewed as an estimate for the quantum yield of the reaction as the remaining parts of the wavepacket on the S_1 surface may return to the CI-region at times later than the propagation time limit and travel to either side of the ground state. Nevertheless, it can be stated that the total quantum yield cannot be smaller than 40% within this model. Longer propagation times are not available for the used surfaces as the wavepacket reaches the border of the propagation grid towards the (Z)-isomer product channel already

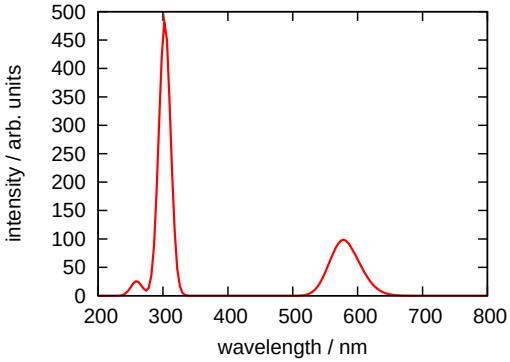

Figure 5.14: Static reference spectrum for calculation of ΔOD. The peak at 590 nm results from the $S_0 \rightarrow S_1$ excitation, while the other peak contains excitations from S_0 to all other included states (S_2, S_3, S_4).

within 200 fs. In this work it is absorbed by a CAP there, which is the reason for the decreasing total norm starting at about 180 fs seen in Fig. 5.13. The (first) transfer of the wavepacket from the upper S_1 to the lower S_0 surface stops at about 150 fs as the wavepacket has traveled past the CI-region. Then, almost all parts are located at dihedral angles smaller than 100°, which is the beginning of the (Z)-isomer channel. A further enlargement of the PES in this direction could prolong the maximal propagation times and include a second appearance of the wavepacket in the CI-region. Since these are only first exploratory calculations, a quantitative analysis of the "branching ratio" is reserved for future work.

Transient Absorption Spectra

Transient absorption spectra are calculated with the method explained above. Apart from the two singlet states on which the propagation is performed further three singlet states are available for excitations. Their energy values and the corresponding transition dipole moments have been calculated by FOCI-AM1. In order to evaluate the change in optical density a static spectrum is required. This is evaluated as follows. The potential is (re-)calculated (in a smaller region around the ground state minimum) with the same parameters as before, but the inactive coordinates are allowed to relax to their ground state instead of their S_1 structures. On this relaxed ground state PES the lowest vibrational eigenfunction is placed as an initial wavepacket. A transient absorption spectrum is calculated, which serves as static ground state reference spectrum for the calculation of the *change* in optical density for all time steps. The calculated static spectrum is shown in Fig. 5.14. It has been folded with a Gaussian with a FWHM of 20 fs in order to simulate experimental resolution and is in good agreement with experimental [163] and other theoretical [117] findings.

Fig. 5.15 shows the transient absorption spectrum for the (E) → (Z) isomerization. In the top panel the change in optical density (ΔOD) is plotted versus

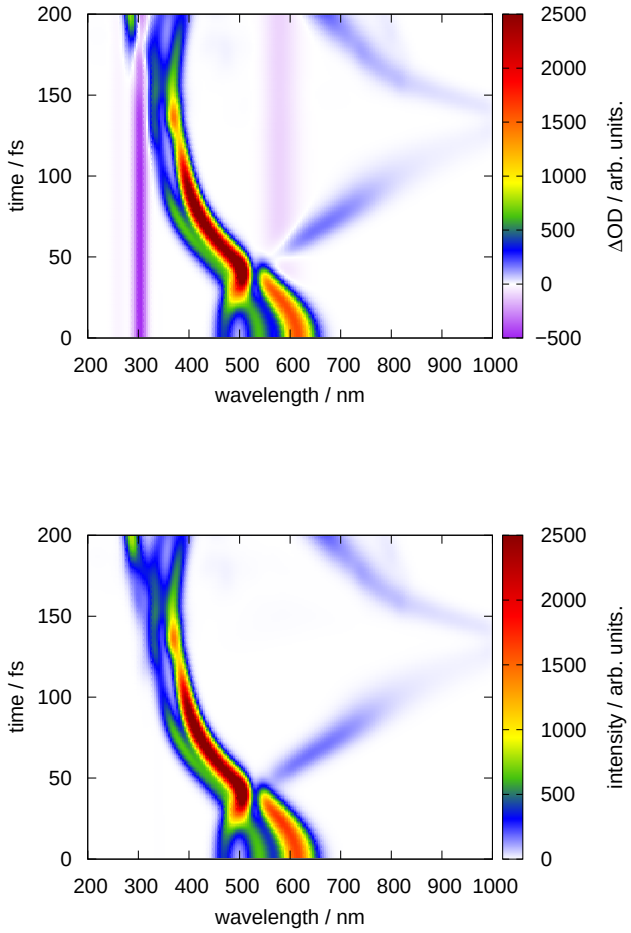

Figure 5.15: Transient absorption spectrum. Top panel: ΔOD, bottom panel: spectrum without subtracting reference. No large differences are present as the static spectrum intensity is about one order of magnitude smaller than the excited state absorption.

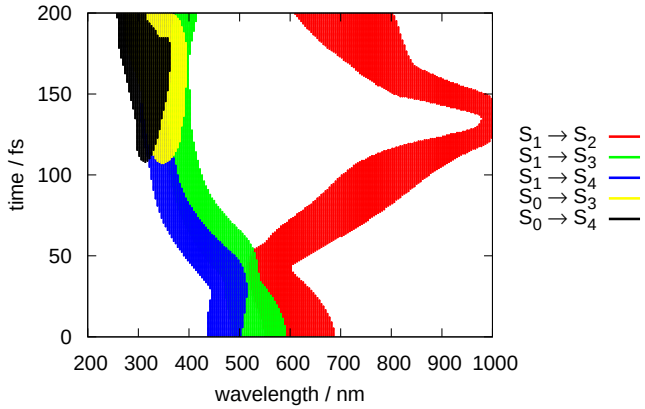

Figure 5.16: Contributions to the transient absorption spectrum of the most important excitations.

wavelength and time, while the lower panel displays the spectrum without subtraction of the static reference. There are only slight deviations, namely light purple bands at 300 nm and 590 nm, as the value of the intensity in the static spectrum is about one order of magnitude smaller than for the excited state absorption. Fig. 5.16 reveals the contributions of the most important excitations to the spectrum. This picture shows that the strong absorption band is caused by the very bright $S_1 \rightarrow S_3$ transition (green). First excitations from the "hot" ground state occur at 130 fs mainly to the S_3 (yellow) and S_4 (black) state. The shift of the main absorption band to lower wavelengths with time can be understood by analyzing the movement of the wavepacket. As the initial wavepacket moves downwards the S_1 surface towards the CI-region the energy difference to higher states increases causing absorptions at lower wavelengths. When the wavepacket transfers to the S_0 state by traveling through the CI the intensity of the $S_1 \rightarrow S_3$ transition decreases, while new "hot" ground state excitations appear.

5.3.4 Discussion

The first results obtained here can be compared to experimentally [163] and theoretically [117,118] obtained transient absorption spectra. The main restriction of the method presented here is the short total propagation time of only 200 fs. Although the isomerization is an ultrafast process on the femtosecond time scale, important characteristics of the reaction occur at times later than 200 fs. As only five electronic states are involved, excited state absorption to higher states cannot be seen in the spectra. Those absorption bands are expected at lower wavelenghts, as the excitation to higher states requires more energy. Nevertheless, the spectra presented here show features that are also seen in the experimental and the semi-classical theoretical work, e. g. the shift of the absorption band to lower wavelengths.

Another difference between the work presented here and the semi-classical trajectories is the number of included DOFs. In semi-classical trajectory calculations all DOFs are included in the dynamics. In this work, only the two most important DOFs were included. However, with only a single wavepacket propagation all quantum effects are accounted for, including the non-local character of quantum-mechanics. Of course, the choice of active coordinates and the type of the employed reduced-dimensional model (cf. section 2.7, p. 32) is essential for reliable results. The selection made here, which was suggested by analysis of semi-classical trajectories, seems to meet the physical conditions as the presented spectra are not contradictory to the experimental and semi-classically obtained ones. Since it is hard to predict what actual changes in the set of active coordinates induce to the final transient absorption spectra it could be helpful to systematically test their influence. This could be performed in a similar way to the analysis of important DOFs in hydrogen peroxide in chapter 4. Also, in comparison with experiment all solvent effects are neglected in the theoretical works. However, especially viscous solvents usually

not only slow down large-amplitude motions, e. g. of the phenyl rings in brAB, but also the molecular motion in general. This in turn leads to transitions between (adiabatic) states focussing more strongly on the innermost CI-region.

5.3.5 Summary and Outlook

First quantum-dynamical wavepacket calculations of brAB are presented in this chapter. A semi-empirical PES has been calculated in a two-dimensional subspace, which was suggested by the preliminary work of Carstensen *et al.* [117,118]. Transition dipole moments and a total of five singlet surfaces have been used to generate transient absorption spectra of this reduced-dimensional system.

A number of approximations had to be made. First, using a semi-empirical method always begs the question if employed parameters are also valid for the system under investigation. This has been answered in the positive by Ref. [118]. Although the calculation of regularized diabatic states, following the method of Köppel and coworkers [18], requires symmetry-allowed CIs, the main characteristics of the regularized quasi-diabatic PESs calculated here suggest the validity of the approach for this system. The diabatic states lie on top of the adiabatic ones in the outer regions, while they cross each other in the CI-region. To calculate transient absorption spectra, instantaneous excitation by a delta laser pulse has been assumed by placing the initial wavepacket on the S_1 surface. Also the way of calculating the intensity of excitations to higher states at given time steps with the transition dipole moments incorporates instantaneous and complete transfer of the wavepacket to the higher states.

The resulting transient absorption spectra have been compared to experimental spectra and hold the additional information from where the different absorption bands arise. The main absorption takes place from the S_1 to the S_3 surface. After a propagation time of 150 fs the wavepacket traverses to the ground state and $S_0 \rightarrow S_3$ and $S_0 \rightarrow S_4$ excitations dominate the spectrum.

The used methodology is encouraging for future work. First of all, analysis of the back-isomerization from the (Z)- to the (E)-isomer is possible with the same models. The underlying characterization of the important DOFs and the calculation of a small PESs has also already be performed in Refs. [117,118].

The adaptive basis representation (chapter 3) is, in principle, also available for non-adiabatic propagations on several PESs. The employed diabatization scheme by Köppel *et al.* can be used *on-the-fly* once the CI location has been evaluated. Also, the *on-the-fly* calculation of the potential is feasible, particularly because of the minor computational cost for semi-empirical data points even for geometry optimizations. An inherent advantage of the adaptive basis representation is that the potential does not even have to be calculated in outer regions of the PES where calculations often fail to converge as the wavepacket does not travel there. This

is also true for the present system, however, technical problems will still occur at CNN angles larger than 180° (here the used Z-matrix is not defined and has to be reordered) and at CNNC-dihedrals smaller than 80° as the semi-empirical calculations also fail to converge into the correct minimum. Nevertheless, a combination of the adaptive basis representation with the regularized diabatic states seems to be a quite powerful extension for future work.

6

Summary and Outlook

This thesis deals with development and application of theoretical methods for quantum-mechanical reaction dynamics. Three main topics were presented: the further development of the proDG-algorithm for a sparse and adaptive wavefunction representation, an automated interface towards an efficient, yet accurate, potential energy evaluation and the photochemistry of the two molecular switches cyclohexadiene and a bridged azobenzene derivative. The developed new methods were implemented into the MrPropa code [61].

Traditional wavefunction representations on grids suffer from the exponential scaling with dimensionality. In chapter 3 the adaptive basis representation proDG is extended from a proof-of-principle implementation towards a production code for higher-dimensional applications. The collaboration partner F. Krüger of the Schneider group (Univ. Kiel, now TU Berlin) developed a novel kind of basis function that satisfies the needs for the proDG method. In combination with the collocation method a sparse and efficient wavefunction representation has been implemented in the MrPropa code.

The method relies on the fact that it is sufficient to store the wavefunction only on grid points where it has a non-negligible value. In most chemical real-life situations the wavepacket does not spread out over the complete coordinate space. Here, no points are stored that do not contribute to the total wavefunction significantly, which results in reduced memory requirements. Application examples in two and three dimensions demonstrate the huge memory savings compared to traditional FBR. The computational demands can even compete with the fast and efficient FFT method. For higher-dimensional applications the potential savings are assumed to be even larger.

A more efficient implementation and a suitable tree-data structure is currently developed by the cooperation partner E. Steffen of the Börm group (Univ. Kiel) setting a focus on distributed computing on several CPUs. The current implementation is already the first step towards efficient *on-the-fly* quantum dynamics. The potential energy is only calculated at points where the wavefunction actually is present.

This way convergence problems of quantum-chemical calculations in outer regions of the PES can be avoided. Future implementation of intelligent interpolation schemes can further reduce the number of quantum-chemical calculations. In priciple, the proDG-scheme also allows for diabatic propagations on several PESs.

For many chemical systems a multi-dimensional treatment is essential. In this case, not only the demands for the quantum-dynamical calculations, but also for the PES generation by quantum-chemical methods are computationally challenging. The system requirements for high-level calculations are very large and it is not affordable to cover a complete direct product grid. A many-mode representation for the PES was developed by the collaboration partner G. Rauhut (Univ. Stuttgart). The representation is combined with an intelligent and efficient interpolation scheme, which reduces the number of required *ab initio* calculations. The resulting points are fitted analytically and interfaced to the MrPropa program. This offers the possibility of a fast, yet accurate, PES evaluation for quantum-dynamical calculations.

Thorough testing of different coordinate systems and their suitability for reactive systems has been performed and presented in chapter 4. First, it was tried to perform the analytic PES evaluation in normal mode coordinates, while the propagations were performed in Z-matrix coordinates. This required a coordinate transformation from Z-matrix to normal mode coordinates in order to evaluate the polynomial PES fit. It was also tried to perform the quantum-dynamical calculations in normal mode coordinates. However, in accordance to earlier findings in the literature, they fail to correctly describe large amplitute motions. As a consequence, the PES fit has been perfomed in Z-matrix coordinates, as well as the quantum-dynamical propagations.

The automated scheme was tested with systems featuring a double-minimum potential. The tunneling splittings of hydrogen-peroxide and its isotopologues have been evaluated. By using reduced-dimensional models and including a different number of DOFs in a set of quantum-dynamical calculuations it has been analyzed that the OO-bond is a spectator mode, which does not couple significantly to the other DOFs. In contrast, all five remaining coordinates are reaction-promoting and contribute to the tunneling splitting in the dihedral coordinate. Our cooperation partner F. von Horsten (Univ. Oxford) calculated the cumulative reaction probability of the compound PHDCl.

The automated PES generation with a reduced number of *ab initio* calculations interfaced to the MrPropa code makes high-level potentials available for quantum-chemical propagations at low computational effort. After demonstrating the validity of the approach future applications may focus on other reactive systems. Investigations into so-called plateau-reactions, which exhibit a plateau of almost constant energy in the region of transition state, should be mentioned in the first place.

The “Collaborative Research Center (SFB) 677—Function by Switching” at the University of Kiel deals with molecular switching processes. In chapter 5 applications towards the interpretation of two photochemical reactions are presented: the ring-

opening reaction of cyclohexadiene and the isomerization around the NN-bond in a bridged azobenzene derivative.

Quantum-dynamical wavepacket propagations were performed on the fully relaxed 2A surface of cyclohexadiene. The PES was calculated in our group by B. Schönborn. It is spanned by the two most important DOFs describing the ring-opening reaction. To include non-adiabatic effects the 2A/1A CI-seam was simulated by a purely imaginary potential. This simulated the transmission of the 2A wavepacket to the 1A surface without explicitly inculding the lower PES. The relative delay times of the observed steps that result from the wavepacket travelling in and out of the CI-region are in good agreement with experimental data.

Cyclohexadiene is not a particulary good model system for the experimentally interesting fulgides. As the open form hexatriene is very flexible, it is not easy to switch from the ring to the open structure back and forth. Also, excitation has to be performed in the UV. Future work may involve suitably substituted cyclohexadienes, which serve as a better model or are better switches even by themselves. Also, the investiagtion into the experimentally examined fulgides with quantum-chemical methods at a lower level of theory is currently performed [169].

As a second molecular switch, an ethylene-bridged azobenzene derivative, which has already been examined experimentally [153, 154] and theoretically [117, 118] within SFB 677, has been investigated in the last section of chapter 5. It exhibits improved switching properties compared to its parent compound azobenzene as the absorption maxima for the $(E) \rightarrow (Z)$ and its back-isomerization are well separated and the thermal life-time is increased.

The chapter demonstrates a mixed quantum-semiclassical way of calculating transient absorption spectra from wavepacket propagations. They are performed in a diabatic basis, which was constructed employing the regularized diabatic states model by Köppel *et al.* The results presented are a first step towards simulation of transient absorption spectra for this system, which involve a number of approximations. The validity of the regularized diabatic states cannot finally be judged as brAB does not fulfill some of the physical assumptions of the model. Furthermore, the PESs had to be extended harmonically in order to avoid early deletion by an absorbing potential. Unfortunately, the propagation times were limited to about 200 fs anyhow, as the border of the PES in the (Z)-isomer channel was hit. Nevertheless, these first results show the general possibility of calculating transient absorption spectra from reduced-dimensional wavepacket propagations without explicit simulation of the pump or probe pulses. An analysis of the most important DOFs is essential for the set-up of the correct reduced-dimensional PES. As the very basic interpretation of the transient absorption spectrum is not contradictory to spectra obtained from experiment and from semi-classical trajectories this is an indication that the choice of active coordinates for the reduced-dimensional model is reasonable.

Summarizing, all theoretical concepts used and developed within the three main topics of this work have been implemented into the MrPropa program suite [61]. Hereby, the universal and user-friendly character of the program has been preserved. Accordingly, future extensions and applications of this program could also benefit from a combination of the three rather independent topics of this work. In principle, the proDG method is not restricted to certain procedures. The adaptive basis could be combined with most theoretical concepts in quantum dynamics, in particular with reduced-dimensional PES representations and dynamical models, and also with propagations on multiple coupled surfaces. This offers the possibility of efficient quantum dynamics calculations with the ease of a user-friendly computer program.

Bibliography

[1] I. N. Levine, *Quantum Chemistry*, Prentice Hall, 1999.

[2] A. Szabo and N. S. Ostlund, *Modern Quantum Chemistry*, McGraw-Hill, New York, 1989.

[3] F. Jensen, *Introduction to Computational Chemistry*, John Wiley & Sons, Chichester, 1999.

[4] R. Schinke, *Photodissociation Dynamics*, Cambridge University Press, 1993.

[5] B. Hartke, *Introduction to Quantum Dynamics*, Lecture at Univ. Kiel, 2008.

[6] W. Domcke, D. R. Yarkony, and H. Köppel, editors, *Conical Intersections: Electronic Structure, Dynamics and Spectroscopy*, volume 15 of *Advanced Series in Physical Chemistry*, World Scientific, 2004.

[7] S. Matsika, Conical Intersections in Molecular Systems, in *Reviews in Computational Chemistry*, edited by K. B. Lipkowitz and T. R. Cundari, volume 23, pp. 83–124, Wiley-VCH, 2007.

[8] D. J. Tannor, *Introduction to Quantum Mechanics: A Time-Dependent Perspective*, University Science Books, Sausalito, California, 2007.

[9] H. F. von Horsten, *Quantum dynamics of larger molecules with reduced-dimensional models*, PhD thesis, University of Kiel, 2008.

[10] M. Nest, *Chemical Physics Letters* **472**, 171 (2009).

[11] M. Born and R. Oppenheimer, *Ann. d. Phys.* **84**, 457 (1927).

[12] S. E. Braslavsky, *Pure Appl. Chem.* **79**, 293 (2007).

[13] H. Köppel, *Diabatic Representation: Methods for the Construction of Diabatic Electronic States*, volume 15 of *Advanced Series in Physical Chemistry*, pp. 175–204, World Scientific, 2004.

[14] T. Pacher, L. S. Cederbaum, and H. Köppel, *Adv. Chem. Phys.* **84**, 293 (1993).

[15] C. A. Mead and D. G. Truhlar, *J. Chem. Phys.* **77**, 6090 (1982).

[16] H. Köppel, W. Domcke, and L. S. Cederbaum, *Adv. Chem. Phys.* **57**, 59 (1984).

[17] H. Köppel, *Faraday Discuss.* **127**, 35 (2004).

[18] H. Köppel, J. Gronki, and S. Mahapatra, *J. Chem. Phys.* **115**, 2377 (2001).

[19] H. Köppel and B. Schubert, *Mol. Phys.* **104**, 1069 (2006).

[20] W. H. Miller, *J. Chem. Soc., Faraday Trans.* **93**, 685 (1997).

[21] S. Goedecker, *Wavelets and their application for the solution of partial differential equations in physics*, Presses Polytechniques et Universitaires Romandes, Lausanne, 1998.

[22] S. Goedecker, *Multiscale Simulation Methods in Molecular Sciences*, volume 42 of *Publication Series of the John von Neumann Institute for Computing (NIC)*, chapter Wavelets and Their Application for the Solution of Poisson's and Schrödinger's Equation, pp. 507–534, Institute for Advanced Simulation, Forschungszentrum Jülich, 2009.

[23] R. A. Friesner, *J. Chem. Phys.* **85**, 1462 (1986).

[24] W. Yang and A. C. Peet, *Chem. Phys. Lett.* **153**, 98 (1988).

[25] A. S. Dickinson and P. R. Certain, *J. Chem. Phys.* **49**, 4209 (1968).

[26] D. O. Harris, G. G. Engerholm, and W. D. Gwinn, *J. Chem. Phys.* **43**, 1515 (1965).

[27] J. C. Light, I. P. Hamilton, and J. V. Lill, *J. Chem. Phys.* **82**, 1400 (1985).

[28] J. C. Light and T. Carrington, Jr., *Adv. Chem. Phys.* **114**, 263 (2000).

[29] M. D. Feit, J. A. Fleck, Jr., and A. Steiger, *J. Comput. Phys.* **47**, 412 (1982).

[30] M. D. Feit and J. A. Fleck, Jr., *J. Chem. Phys.* **80**, 2578 (1984).

[31] M. D. Feit and J. A. Fleck, Jr., *J. Chem. Phys.* **78**, 301 (1983).

[32] D. Kosloff and R. Kosloff, *J. Comput. Phys.* **52**, 35 (1983).

[33] R. Kosloff and D. Kosloff, *J. Chem. Phys.* **79**, 1823 (1983).

[34] R. Kosloff, *J. Phys. Chem.* **92**, 2087 (1988).

[35] R. Kosloff, *The Fourier Method*, volume 412 of *NATO ASI Series C*, pp. 175–194, Kluwer, Dordrecht, 1993.

[36] H. D. Meyer, U. Manthe, and L. S. Cederbaum, *Chem. Phys. Lett.* **165**, 73 (1990).

[37] H.-D. Meyer and G. A. Worth, *Theor. Chem. Acc.* **109**, 251 (2003).

[38] M. H. Beck, A. Jackle, G. A. Worth, and H. D. Meyer, *Phys. Rep.* **324**, 1 (2000).

[39] C. Leforestier, R. H. Bisseling, C. Cerjan, M. D. Feit, R. Friesner, A. Guldberg, A. Hammerich, G. Jolicard, W. Karrlein, H.-D.

Meyer, N. Lipkin, O. Roncero, and R. Kosloff, *J. Comput. Phys.* **94**, 59 (1991).

[40] D. Lauvergnat, S. Blasco, X. Chapuisat, and A. Nauts, *J. Chem. Phys.* **126**, 204103 (2007).

[41] A. Askar and A. S. Cakamak, *J. Chem. Phys.* **68**, 2794 (1978).

[42] U. Manthe and H. Köppel, *J. Chem. Phys.* **93**, 345 (1990).

[43] S. K. Gray and D. E. Manolopoulos, *J. Chem. Phys.* **104**, 7099 (1996).

[44] H. Tal-Ezer and R. Kosloff, *J. Chem. Phys.* **81**, 3967 (1984).

[45] T. J. Park and J. C. Light, *J. Chem. Phys.* **85**, 5870 (1986).

[46] R. Kosloff and H. Tal-Ezer, *Chem. Phys. Lett.* **127**, 223 (1986).

[47] J. Muga, J. Palao, B. Navarro, and I. Egusquiza, *Phys. Rep.* **395**, 357 (2004).

[48] D. Manolopoulos, Talk at the Charles Coulson Summer School in Theoretical Chemistry, Oxford, 1996.

[49] J.-Y. Ge and J. Z. H. Zhang, *J. Chem. Phys.* **108**, 1429 (1998).

[50] R. D. Woods and D. S. Saxon, *Phys. Rev.* **95**, 577 (1954).

[51] C. Leforestier and R. E. Wyatt, *J. Chem. Phys.* **78**, 2334 (1983).

[52] J. M. Bowman, *J. Phys. Chem.* **95**, 4960 (1991).

[53] S. M. Colwell and N. C. Handy, *Mol. Phys.* **92**, 317 (1997).

[54] A. Nauts and X. Chapuisat, *Mol. Phys.* **55**, 1287 (1985).

[55] X. Chapuisat, A. Belafhal, and A. Nauts, *J. Mol. Spectrosc.* **149**, 274 (1991).

[56] B. Podolsky, *Phys. Rev.* **32**, 812 (1928).

[57] D. Lauvergnat and A. Nauts, *J. Chem. Phys.* **116**, 8560 (2002).

[58] D. Sölter, H.-J. Werner, M. von Dirke, A. Untch, A. Vegiri, and R. Schinke, *J. Chem. Phys.* **97**, 3357 (1992).

[59] R. T. Pack and G. A. Parker, *J. Chem. Phys.* **87**, 3888 (1987).

[60] Y. Shi and D. J. Tannor, *J. Chem. Phys.* **92**, 2517 (1990).

[61] H. F. von Horsten, J. Sielk, and B. Hartke, MrPropa – A Quantum Dynamical Wavepacket Propagation Program, see http://www.mrpropa.de.

[62] E. B. Wilson Jr., J. C. Decius, and P. C. Cross, *Molecular Vibrations*, McGraw-Hill, New York, 1955.

[63] F. Gatti, Y. Justum, M. Menou, A. Nauts, and X. Chapuisat, *J. Mol. Spectrosc.* **181**, 403 (1997).

[64] J. T. Hougen, P. R. Bunker, and J. W. C. Johns, *J. Mol. Spectrosc.* **34**, 136 (1970).

[65] M. Mladenović and Z. Bačić, *J. Chem. Phys.* **94**, 4988 (1991).

[66] M. L. Senent, *Chem. Phys. Lett.* **296**, 299 (1998).

[67] R. Meyer, *J. Mol. Spectrosc.* **76**, 266 (1979).

[68] J. Makarewicz, *J. Mol. Spectrosc.* **176**, 169 (1996).

[69] S. Blasco and D. Lauvergnat, *Chem. Phys. Lett.* **373**, 344 (2003).

[70] D. Lauvergnat and A. Nauts, *Chem. Phys.* **305**, 105 (2004).

[71] D. Lauvergnat, A. Nauts, Y. Justum, and X. Chapuisat, *J. Chem. Phys.* **114**, 6592 (2001).

[72] R. H. Bisseling, R. Kosloff, J. Manz, F. Mrugala, J. Römelt, and G. Weichselbaumer, *J. Chem. Phys.* **86**, 2626 (1987).

[73] B. Hartke, A. E. Janza, W. Karrlein, J. Manz, V. Mohan, and H.-J. Schreier, *J. Chem. Phys.* **96**, 3569 (1992).

[74] S. Heislbetz, P. Schwerdtfeger, and G. Rauhut, *Mol. Phys.* **105**, 1385 (2007).

[75] O. Christiansen and J. M. Luis, *Int. J. Quantum Chem.* **104**, 667 (2005).

[76] E. Baloïtcha, B. Lasorne, D. Lauvergnat, G. Dive, Y. Justum, and M. Desouter-Lecomte, *J. Chem. Phys.* **117**, 727 (2002).

[77] D. Luckhaus, *J. Chem. Phys.* **113**, 1329 (2000).

[78] B. Hartke and H.-J. Werner, *Chem. Phys. Lett.* **280**, 430 (1997).

[79] V. Aquilanti and S. Cavalli, *J. Chem. Phys.* **85**, 1355 (1986).

[80] M. Ragni, A. C. P. Bitencourt, and V. Aquilanti, *Int. J. Quantum Chem.* **107**, 2870 (2007).

[81] M. Mladenović, *J. Chem. Phys.* **112**, 1082 (2000).

[82] O. Vendrell, F. Gatti, D. Lauvergnat, and H.-D. Meyer, *J. Chem. Phys.* **127**, 184302 (2007).

[83] O. Vendrell, F. Gatti, and H.-D. Meyer, *J. Chem. Phys.* **127**, 184303 (2007).

[84] G. Avila and T. Carrington, Jr., *J. Chem. Phys.* **131**, 174103 (2009).

[85] X.-G. Wang and T. Carrington, Jr., *J. Chem. Phys.* **128**, 194109 (2008).

[86] J. Cooper and T. Carrington, Jr., *J. Chem. Phys.* **130**, 214110 (2009).

[87] C. L. Lopreore and R. E. Wyatt, *Phys. Rev. Lett.* **82**, 5190 (1999).

[88] R. E. Wyatt, *J. Chem. Phys.* **117**, 9569 (2002).

[89] L. R. Pettey and R. E. Wyatt, *Chem. Phys. Lett.* **424**, 443 (2006).

[90] L. R. Pettey and R. E. Wyatt, *Int. J. Quantum Chem.* **107**, 1566 (2007).

[91] H.-D. Meyer, F. Gatti, and G. Worth, editors, *Multidimensional Quantum Dynamics*, Wiley-VCH, 2009.

[92] R. B. Gerber, V. Buch, and M. A. Ratner, *J. Chem. Phys.* **77**, 3022 (1982).

[93] R. H. Bisseling, R. Kosloff, R. B. Gerber, M. A. Ratner, L. Gibson, and C. Cerjan, *J. Chem. Phys.* **87**, 2760 (1987).

[94] M. Thoss and H. Wang, *Chem. Phys.* **322**, 210 (2006).

[95] H. Wang and M. Thoss, *J. Chem. Phys.* **119**, 1289 (2003).

[96] M. Parrinello and W. Andreoni, CPMD consortium, see http://www.cpmd.org/.

[97] E. J. Heller, *J. Chem. Phys.* **62**, 1544 (1975).

[98] T. J. Martinez, M. Ben-Nun, and G. Ashkenazi, *J. Chem. Phys.* **104**, 2847 (1996).

[99] T. J. Martinez, *Chem. Phys. Lett.* **272**, 139 (1997).

[100] M. Ben-Nun and T. J. Martinez, *J. Chem. Phys.* **112**, 6113 (2000).

[101] I. Burghardt, H.-D. Meyer, and L. S. Cederbaum, *J. Chem. Phys.* **111**, 2927 (1999).

[102] S. S. Iyengar and J. Jakowski, *J. Chem. Phys.* **122**, 114105 (2005).

[103] J. Jakowski, I. Sumner, and S. S. Iyengar, *J. Chem. Theory Comput.* **2**, 1203 (2006).

[104] H. Rabitz and O. F. Alis, *J. Math. Chem.* **25**, 197 (1999).

[105] S. Carter, S. J. Culik, and J. M. Bowman, *J. Chem. Phys.* **107**, 10459 (1997).

[106] S. Carter, J. M. Bowman, and L. B. Harding, *Spectrochim. Acta A* **53**, 1179 (1997).

[107] C. R. Evenhuis and U. Manthe, *J. Chem. Phys.* **129**, 024104 (2008).

[108] K. Yagi, T. Taketsugu, K. Hirao, and M. S. Gordon, *J. Chem. Phys.* **113**, 1005 (2000).

[109] M. A. Collins, *Theor. Chem. Acc.* **108**, 313 (2002).

[110] O. Godsi, M. A. Collins, and U. Peskin, *J. Chem. Phys.* **132**, 124106 (2010).

[111] R. G. Sadygov and D. R. Yarkony, *J. Chem. Phys.* **109**, 20 (1998).

[112] R. Abrol and A. Kuppermann, *J. Chem. Phys.* **116**, 1035 (2002).

[113] T. Pacher, L. S. Cederbaum, and H. Köppel, *J. Chem. Phys.* **89**, 7367 (1988).

[114] K. Piechowska-Strumik, D. Lauvergnat, M.-C. Bacchus-Montabonel, and M. Desouter-Lecomte, *Chem. Phys. Lett.* **425**, 16 (2006).

[115] T. Rozgonyi and L. González, *J. Phys. Chem. A* **112**, 5573 (2008).

[116] B. Hartke, *Phys. Chem. Chem. Phys.* **8**, 3627 (2006).

[117] O. Carstensen, *Photodynamics of a Bridged Azobenzene Derivative*, Master's thesis, Univ. Kiel, 2009.

[118] O. Carstensen, J. Sielk, J. B. Schönborn, G. Granucci, and B. Hartke, *J. Chem. Phys.* , in press (2010).

[119] G. Rauhut, G. Knizia, and H.-J. Werner, *J. Chem. Phys.* **130**, 54105 (2009).

[120] G. Rauhut and B. Hartke, *J. Chem. Phys.* **131**, 14108 (2009).

[121] R. Kosloff, *Quantum molecular dynamics on grids*, p. 185, Marcel Dekker Inc., New York, 1996.

[122] S. Schweiger and G. Rauhut, *J. Phys. Chem. A* **107**, 9668 (2003).

[123] P. Li and Y. Bu, *J. Phys. Chem. A* **108**, 10288 (2004).

[124] C. Raynaud, J. P. Daudey, L. Maron, and F. Jolibois, *J. Phys. Chem. A* **109**, 9646 (2005).

[125] S. Schweiger, B. Hartkeb, and G. Rauhut, *Phys. Chem. Chem. Phys.* **6**, 3341 (2004).

[126] W. H. Miller, N. C. Handy, and J. E. Adams, *J. Chem. Phys.* **72**, 99 (1980).

[127] H. F. von Horsten, G. Rauhut, and B. Hartke, *J. Phys. Chem. A* **110**, 13014 (2006).

[128] H. F. von Horsten and B. Hartke, *Chem. Phys.* **338**, 160 (2007).

[129] D. Luckhaus, *Phys. Chem. Chem. Phys.* **12**, 8357 (2010).

[130] D. Luckhaus, *J. Phys. Chem. A* **110**, 3151 (2006).

[131] J. Bertran, A. Oliva, L. Rodriguez-Santiago, and M. Sodupe, *J. Am. Chem. Soc.* **120**, 8159 (1998).

[132] A. L. Sobolewski and W. Domcke, *Phys. Chem. Chem. Phys.* **6**, 2763 (2004).

[133] E. F. Caldin and V. Gold, *Proton Transfer Reactions*, Chapman and Hall, 1975.

[134] W.-I. Shiau, E. N. Duesler, I. C. Paul, D. Y. Curtin, W. G. Blann, and C. A. Fyfe, *J. Am. Chem. Soc.* **102**, 4546 (1980).

[135] J. R. de la Vega, J. H. Bisch, J. H. Schauble, K. L. Kunze, and B. E. Haggert, *J. Am. Chem. Soc.* **104**, 3295 (1982).

[136] E. Nir, K. Kleinermanns, and M. S. de Vries, *Nature* **408**, 949 (2000).

[137] M. Meuwly, *Fut. Generations Comput. Systems* **21**, 1285 (2005).

[138] Y. Wang and J. M. Bowman, *J. Chem. Phys.* **129**, 121103 (2008).

[139] Y. Wang, B. J. Braams, J. M. Bowman, S. Carter, and D. P. Tew, *J. Chem. Phys.* **128**, 224314 (2008).

[140] E. Kamarchik, Y. Wang, and J. Bowman, *J. Phys. Chem. A* **113**, 7556 (2009).

[141] A. R. Hoy, I. M. Mills, and G. Strey, *Mol. Phys.* **24**, 1265 (1972).

[142] D. Lauvergnat and A. Nauts, *Phys. Chem. Chem. Phys.* **12**, 8405 (2010).

[143] J. K. G. Watson, *Mol. Phys.* **15**, 479 (1968).

[144] G. Rauhut and T. Hrenar, *Chem. Phys.* **346**, 160 (2008).

[145] V. Barone, *J. Chem. Phys.* **122**, 014108 (2005).

[146] M. Robb, M. Olivucci, and F. Bernardi, Photochemistry, in *Encyclopedia of Computational Chemistry*, pp. 2056–2063, John Wiley & Sons, 1998.

[147] G. A. Worth and L. S. Cederbaum, *Annu. Rev. Phys. Chem.* **55**, 127 (2004).

[148] C. E. Crespo-Hernández, B. Cohen, P. M. Hare, and B. Kohler, *Chem. Rev.* **104**, 1977 (2004).

[149] M. Dantus, M. J. Rosker, and A. H. Zewail, *J. Chem. Phys.* **87**, 2395 (1987).

[150] A. H. Zewail, *J. Phys. Chem. A* **104**, 5660 (2000).

[151] A. W. Jasper, C. Zhu, S. Nangia, and D. G. Truhlar, *Faraday Discuss.* **127**, 1 (2004).

[152] A. W. Jasper, S. Nangia, C. Zhu, and D. G. Truhlar, *Acc. Chem. Res.* **39**, 101 (2006).

[153] R. Siewertsen, H. Neumann, B. Buchheim-Stehn, R. Herges, C. Näther, F. Renth, and F. Temps, *J. Am. Chem. Soc.* **131**, 15594 (2009).

[154] R. Siewertsen, F. Renth, F. Temps, and F. Sonnichsen, *Phys. Chem. Chem. Phys.* **11**, 5952 (2009).

[155] A. Hofmann and R. de Vivie-Riedle, *Chem. Phys. Lett.* **346**, 299 (2001).

[156] A. Hofmann and R. de Vivie-Riedle, *J. Chem. Phys.* **112**, 5054 (2000).

[157] W. Fuss, W. E. Schmid, and S. A. Trushin, *J. Chem. Phys.* **112**, 8347 (2000).

[158] K. Kosma, S. A. Trushin, W. Fuss, and W. E. Schmid, *Phys. Chem. Chem. Phys.* **11**, 172 (2009).

[159] D. Lauvergnat, Personal Communication.

[160] H. Satzger, C. Root, and M. Braun, *J. Phys. Chem. A* **108**, 6265 (2004).

[161] I. K. Lednev, T. Q. Ye, P. Matousek, M. Towrie, P. Foggi, F. V. R. Neuwahl, S. Umapathy, R. E. Hester, and J. N. Moore, *Chem. Phys. Lett.* **290**, 68 (1998).

[162] T. Nägele, R. Hoche, W. Zinth, and J. Wachtveitl, *Chem. Phys. Lett.* **272**, 489 (1997).

[163] R. Siewertsen, Schönborn, B. Hartke, F. Renth, and F. Temps, *Phys. Chem. Chem. Phys.* , submitted 2010.

[164] A. Thiel and H. Köppel, *J. Chem. Phys.* **110**, 9371 (1999).

[165] C. Ciminelli, G. Granucci, and M. Persico, *Chem. Eur. J.* **10**, 2327 (2004).

[166] M. Ndong, H. Tal-Ezer, R. Kosloff, and C. P. Koch, *J. Chem. Phys.* **132**, 064105 (2010).

[167] G. Granucci, M. Persico, and A. Toniolo, *J. Chem. Phys.* **114**, 10608 (2001).

[168] G. Granucci and A. Toniolo, *Chem. Phys. Lett.* **325**, 79 (2000).

[169] B. Schönborn, Current work within the framework of a PhD thesis, Univ. Kiel, 2010.

Declaration

Hereby, I declare that the work presented in thesis was done by me, under the supervision of Prof. Bernd Hartke with no other help than the referenced sources in the text.

This is my first dissertation and the work has never been used in any other dissertation attempts.

The dissertation complies to the good scienticfic practice rules as proposed by the Germand Resarch Foundation (DFG).

Kiel, 27/7/2010

Jan Sielk

Acknowledgements

First and foremost, I would like to thank my advisor Prof. B. Hartke for the assignement of my work and his everlasting willingness for detailed discussions. I really appreciate his "open-door policy" which always gave me the feeling of a warm and direct support.

I would particularly like to thank Frank von Horsten for spending endless hours of introducing me to quantum-dynamics in general, and his computer program in special. I appreciate the patience he has shown in answering my questions which I bombarded him with and thank him for proof-reading this manuscript. It was a pleasure for me to receive his trust and to become a member of the MrPropa developer team. Without his help this work would not have been possible.

I am grateful for all sucessful collaborations with other groups, in particular with Guntram Rauhut from the University of Stuttgart. He supplied me with high-level potential energy surfaces. Also, thanks go to the German Research Foundation for funding parts of my work and giving me the opportunity of attending conferences via joint grant Ha2498/6 – Ra656/9-1 and via SFB 677.

I would also like to thank *all* members of the Hartke-group, both past and present ones, for a very special working atmosphere. Especially, I thank my roommates Boyke Schönborn and Ole Carstensen for many endless and enlightening discussions, both on work and other issues.

Finally, thanks to my family and close friends who have always supported me throughout my studies in Aachen and the time of this thesis in Kiel.